THE OVERLOOKED MODULATING ROLE OF NITROUS OXIDE FOR CORRINOID-DEPENDENT MICROBIAL PROCESSES

A Dissertation Presented for the
Doctor of Philosophy
Degree
The University of Tennessee, Knoxville

Yongchao Yin
December 2019

Copyright © 2019 by Yongchao Yin.
All rights reserved.

ACKNOWLEDGEMENTS

This work would not have been possible without the great support, help and encouragement of many people over the past five years. I want to express my sincere thanks to all the people I met along my PhD and my life journey.

First and foremost, I would like to thank my advisor, Dr. Frank Löffler. I am truly grateful for all of your patience, support, advice, discussions and guidance. Your passion and enthusiasm towards science, your rigorous attitude towards research kept inspiring and motivating me over the years. Working with you has been a true gift to me. Thank you!

I would also like to thank my committee members Dr. Alison Buchan, Dr. Gary Sayler and Dr. Qiang He for giving me countless helpful advices and suggestions throughout the course of my research. Your services on my committee means a great deal to me, and I hope for continued discussions, collaborations, and to keep in touch as I continue to pursue a career in academia. I would like to thank Drs. Jun Yan, Gao Chen, Fadime and Robert Murdoch, and Amanda Lee for their contributions to research support and advice over the years. Thank you to Cindy Swift, who helped a lot for the lab rules and safety trainings. Thanks to graduate students in Löffler lab, Yongchao Xie, Yanchen Sun, Briana Mcdowell and Laurel Seus. Thank you for the helps, the scientific discussions and also the inspiring lunch talks. Thank you to all my friends for your encouragement and friendship during these challenging years.

Thank you to my beloved wife Danxia Wang for being my side along the way, for your continued love, support and hugs. You are the best lover and friend. Weison and Eliora, thank you for being my children. You two let me know the feeling of purest love. Special thanks to my parents. Thank you for always being there for me, for being more familiar with Knoxville weather than I do, even you are in the other side the world. This dissertation could not have been completed without your encouragement, unconditional love and support. Thank you all!

ABSTRACT

Nitrous oxide (N_2O) is a potent ozone-depleting greenhouse gas that is primarily produced by microbial denitrification and nitrification in terrestrial and aquatic systems. N_2O interferes with cobalt(I)-containing corrinoids, an essential enzyme cofactor in biology facilitating carbon skeleton rearrangements, methyl group transfer and reductive dehalogenation. With increasing N_2O emissions and elevated concentrations in air-soil-water systems due to human perturbations of the N cycle, the impacts of N_2O on microbial processes that depend on corrinoid-dependent enzyme systems must be elucidated. Methanogenic archaea (methanogens) and organohalide-respiring bacteria (OHRB) play key roles in carbon cycling and both microbial groups rely on the Co(I) supernucleophile in their energy metabolism. This dissertation work investigates the impact of N_2O on these two groups of organisms and explores potential strategies to relieve N_2O toxicity. Experimental evidences presented demonstrate that micromolar levels of N_2O inhibit CH_4 production by methanogens as well as reductive dechlorination of chlorinated compounds by OHRB. Detailed kinetic analyses determined the inhibitory constants (K_I) of N_2O for CH_4 production from different methanogenic substrates (i.e., acetate, hydrogen and CO_2, methanol) and key steps of bacterial tetrachloroethene (PCE) reductive dechlorination, corroborated that N_2O serves as a potent inhibitor of corrinoid-dependent microbial processes. Further 16S rRNA gene-based community composition analyses, as well as qPCR and RT-qPCR assays revealed that N_2O affects growth yields and community compositions of methanogen populations. Metabolomic analyses using dechlorinating consortium SDC-9 demonstrated that N_2O affects corrinoids and metabolic profiles of dechlorinating communities. The introduction of N_2O reducers to N_2O-inhibited OHRB cultures restored dechlorination activity, suggesting reversibility of N_2O inhibition and highlighting a potentially unrecognized detoxification role for phylogenetically diverse bacteria reducing N_2O to dinitrogen gas (N_2). Together, the findings of this work reveal an

overlooked negative feedback of N_2O on corrinoid-dependent microbial processes, including methanogenesis and reductive dechlorination, and provide new information for implementing successful contaminated-site cleanup and enriching Earth System Models with more accurate predictions of greenhouse gas emissions.

TABLE OF CONTENTS

CHAPTER ONE: INTRODUCTION 1
1.1 Summary 2
1.2 Background 4
1.3 Microbial sources and sinks of N_2O 6
1.4 Introduction to corrinoid and corrinoid-dependent enzymatic processes 8
1.4.1 Corrinoid structure and functions 8
1.4.2 Corrinoid-dependent enzyme systems 9
1.4.3 Corrinoid-dependent methyltransferases 10
1.4.4 Corrinoid-dependent reductive dehalogenation 11
1.5 The toxicity of N_2O for corrinoid-dependent enzymes 12
1.6 Rationale, hypotheses and research objectives 15
1.7 References 18
1.8 Appendix 27
CHAPTER TWO: NITROUS OXIDE IS A POTENT INHIBITOR OF BACTERIAL REDUCTIVE DECHLORINATION 29
2.1 Abstract 30
2.2 Introduction 32
2.3 Materials and Methods 34
2.3.1 Chemicals. 34
2.3.2 Bacterial strains and growth conditions. 34
2.3.3 Inhibition experiments. 35
2.3.4 Whole cell suspension dechlorination assays. 36
2.3.5 Analytical procedures. 38
2.3.6 Dechlorination kinetics and inhibition models. 39
2.4 Results 41
2.4.1 N_2O affects reductive dechlorination performance in *Geobacter lovleyi* strain SZ cultures. 41
2.4.2 N_2O affects *c*DCE and VC reductive dechlorination performance in *Dhc* strain BAV1 cultures. 43
2.4.3 Quantification of N_2O inhibition in whole cell suspension dechlorination assays. 45
2.4.4 Kinetic parameters reveal pronounced N_2O inhibition. 46
2.5 Discussion 48
2.5.1 Effects of N_2O on corrinoid-dependent processes. 48
2.5.2 OHRB as a model to study the effects of N_2O inhibition. 49
2.5.3 Elevated groundwater N_2O and kinetic parameters. 51
2.5.4 Implications for *in situ* bioremediation. 54
2.6 Acknowledgments 55
2.7 References 56
2.8 Appendix 63

CHAPTER THREE: THE OVERLOOKED NEGATIVE FEEDBACK OF NITROUS OXIDE ON METHANOGENESIS 71
3.1 Abstract 72
3.2 Introduction 74
3.3 Materials and Methods 76
3.3.1 Methanogenic isolates, consortia, and growth conditions. 76
3.3.2 Inhibition experiments. 77
3.3.3 Whole cell suspension assays. 78
3.3.4 Kinetics of methane generation and inhibition models. 80
3.3.5 DNA isolation and 16S rRNA gene amplicon sequencing 81
3.3.6 81
3.3.7 Growth yield calculations 83
3.4 Results 83
3.4.1 N_2O inhibits CH_4 production and growth yields of *Ms barkeri* 83
3.4.2 N_2O affects CH_4 production and community composition of methanogenic enrichment cultures 86
3.4.3 Kinetic characterization of N_2O inhibition on methanogenesis 88
3.5 Discussion 91
3.6 Acknowledgement 97
3.7 References 98
3.7 Appendix 103
CHAPTER FOUR: ORGANOHALIDE RESPIRATION OF CHLORINATED ETHENES UNDER NITROUS OXIDE INHIBITION: METABOLIC RESPONSES AND POTENTIAL MITIGATITION STRATEGIES 109
4.1 Abstract 110
4.2 Introduction 112
4.3 Materials and Methods 115
4.3.1 Chemicals 115
4.3.2 Cultures and growth condition 115
4.3.3 N_2O inhibition and recovery experiments 116
4.3.4 Corrinoid extraction and analysis 117
4.3.5 Metabolite extraction 118
4.3.6 Ultra-performance liquid chromatography high-resolution mass spectrometry 119
4.3.7 DNA and RNA isolation and cDNA synthesis 120
4.3.8 Primer design and qPCR 121
4.4 Results 124
4.4.1 N_2O affects dechlorination performance and corrinoid profile of consortium SDC-9 124
4.4.2 N_2O modulates the metabolome profile of the SDC-9 culture 126
4.4.3 N_2O affects the expression of genes involved in corrinoid metabolism 128
4.4.4 Recovery of dechlorination activity in N_2O-inhibited organohalide-respiring cultures 129

4.5 Discussion 132
4.5.1 N_2O toxicity and corrinoid metabolism in SDC-9 132
4.5.2 N_2O toxicity and metabolic responses of the SDC-9 consortium 136
4.5.3 Mitigation strategies and recovery of dechlorination activities 137
4.6 Acknowledgement 140
4.7 References 141
4.7 Appendix 148
CHAPTER FIVE: SUMMARY AND CONCLUSION 155
VITA 160

CHAPTER ONE:
INTRODUCTION

1.1 Summary

The massive worldwide production and application of N fertilizers has enabled humans to greatly increase food and biofuel production, but these activities resulted in massive disturbances of the global nitrogen (N) cycle. One major consequence is the intensified production of nitrous oxide (N_2O), a powerful ozone-depleting greenhouse gas. Although the major sources and sinks of N_2O have been identified, knowledge about the impacts of increasing environmental N_2O on microbial communities and associated biogeochemical element cycles are largely lacking. N_2O is known to oxidize and inactivate cobalt(I)- (Co(I))- corrinoid enzymes that are vital to organisms in all domains of life. Therefore, the accumulation of N_2O in the environment has the potential to negatively impact a wide range of corrinoid-dependent enzymatic steps, particularly organisms that rely on Co(I) corrinoids for central metabolisms and/or energy conservation. This chapter outlines the major sources and sinks of N_2O, the mechanism of N_2O toxicity, the microbial processes that lead to N_2O formation, as well as the role of organisms harboring distinct N_2O reductases (i.e., clade I versus clade II NosZ) in addressing the negative effect of N_2O. The available findings highlight the potential negative feedback of N_2O for organisms that rely on corrinoid-dependent enzyme systems in central metabolism, including methanogenic archaea and organohalide-respiring bacteria. Although the sources of N_2O in environmental system are fairly well characterized, the responses and feedback loops of elevated N_2O concentrations are unknown. A

major aim of this study was to investigate the impacts of increasing environmental N_2O on corrinoid-dependent methanogenic archaea and organohalide-respiring bacteria.

1.2 Background

Nitrogen (N) is a fundamental element for all life forms on Earth and the main nutrient limiting primary production [1-3]. To increase N supply and boost agricultural yields, humans introduce around 140 Tg reactive N (N_r) annually into the environment, which is produced via the industrial Haber-Bosch process (N_2 + 3 H_2 → 2 NH_3) [2,4,5]. In excess N_r entering the environment dramatically alters the N cycle and leads to a cascade of unprecedented environmental problems, including eutrophication, biodiversity loss, as well as increased inventories of nitrous oxide (N_2O) [6-8]. The continuous increase of N_2O budget in the environment is of particular concern as N_2O is a powerful greenhouse gas and a major ozone-depleting substance [9,10]. The worldwide overuse of N fertilizers is the largest anthropogenic source of N_2O, and accounts for about 30% of the global N_2O budget [11-15]. In addition to causing significant increases in N_2O emission, the excess N inputs also lead to widespread inorganic N (mainly as nitrate, NO_3^-) contamination and elevated concentrations of dissolved N_2O in groundwater aquifers and watersheds [15,16]. In many watersheds affected by agricultural activities, dissolved groundwater N_2O concentrations have reached over 140 µM, higher than air-equilibrated water (~ 7 nM at 20 °C) by 5 orders of magnitudes [17,18]. Given the increasing fertilizer demand for food, feed and biofuel production, the N_2O concentrations in the atmosphere and in watersheds will continue to increase in the coming decades.

Systematic studies investigating the microbial N_2O cycling networks have improved our understanding of N_2O dynamics in the environment. This work has unraveled novel processes, characterized the underlying biochemistry, and identified microbial taxa [19,20] Considerably less emphasis has been placed on understanding the negative impacts of N_2O on microorganisms in the environment, particularly organisms that are involved in carbon (C) cycling and bioremediation, and how these microbes manage to address the negative impacts of elevated N_2O concentrations. N_2O is known to oxidize Co(I) corrinoid, an enzyme cofactor used in biology to catalyze essential biochemical reactions such as methyl group transfer, carbon skeleton rearrangement and reductive dehalogenation [21-23]. Therefore, the accumulation of N_2O in the environment has the potential to negatively impact a wide range of corrinoid-dependent processes, particularly in organisms that strictly rely on Co(I) corrinoids in energy conservation pathways.

The dissertation work focuses on investigating the negative impact of N_2O on corrinoid-dependent organohalide-respiring bacteria (OHRB) and methanogens, and explores the possible strategies for combating the inhibitory effects of N_2O. OHRB serve as the keystone organisms for reductive dechlorination of widespread toxic and carcinogenic chlorinated contaminants [24], while methanogens are responsible for global CH_4 emissions [25]. Both OHRB and methanogens have strict requirements for Co (I) corrinoids in their energy metabolism, and thus have the potential to be affected by N_2O [26-29]. This chapter

provides a brief summary of the major biotic/abiotic processes and pathways controlling N_2O fluxes in the environment, the major corrinoid-dependent enzymes and organisms that may be subject to N_2O toxicity, as well as the overall hypothesis and objectives of this dissertation. Further detailed background is provided within the appropriate chapters.

1.3 Microbial sources and sinks of N_2O

Bioavailable N in form of organic (e.g., nucleic acids, pyrimidines, purines, proteins, amino acids, urea) and inorganic (e.g., NO_3^-, NH_4^+) nitrogenous compounds entering the biosphere undergoes dynamic transformation reactions mediated by predominantly biotic (enzymes) but also some abiotic (dissolved metals or reactive mineral phases) catalysts[7]. Ultimately, these reactions convert N to N_2O and N_2, and N is recycled back to the atmosphere [3,4,30]. Many N cycle intermediates can be interconverted; however, with the formation of N_2O, the cycle enters a one-way street leading to loss of N to the atmosphere [3,4,30]. The processes leading to N_2O formation are illustrated (**Figure 1**). Almost all microorganisms and processes involved in N cycle have the potential to produce N_2O, and many of these processes are interrelated to each other sharing intermediates or products [4,31]. The key pathways for N_2O production include denitrification [32], nitrification [33], respiratory ammonification (DNRA) [34,35], fungal denitrification [36-38], and chemo-denitrification [39]. Although the major process responsible for N_2O production varies in different ecosystems, microbial

denitrification represents the main drivers for N_2O production and accumulation under anoxic conditions [9]; however, over 30% well-characterized denitrifiers (i.e., with functional *nirK* or *nirS* genes), such as *Agrobacterium tumefaciens* and strains of the genus *Thauera*, lack of *nosZ* genes, and thus cannot further reduce N_2O to N_2 [45]. In addition, molecular studies with denitrifiers showed that the expression of *nosZ* is more sensitive to redox condition and pH changes than other denitrifying genes, indicating that changing environmental conditions favor the net production of N_2O [47]. Other environmental factors such as water content, temperature, availability of copper (the essential metal for synthesizing functional NosZ), as well as the C/N ratio, are also known to influence the efficiency and extend of denitrification and contribute to N_2O production. Ultimately, with the ever-increasing amounts of N_r being introduced into the environment, the fraction of N lost into groundwater and other aquatic systems via runoff and leaching is also on the increase, which will fuel the formation and accumulation of N_2O in the environment [48].

Although multiple sources of N_2O exist, the only known sink for N_2O in environmental systems is the enzymatic reduction to N_2 by organisms possessing *nos* operons and expressing N_2O reductase, NosZ [32]. This enzyme has traditionally been assigned to bacteria and archaea performing complete denitrification (i.e., $NO_3^-/NO_2^- \rightarrow N_2$) [32,49]. A few non-denitrifying bacteria, including *Wolinella succinogenes*, *Bacillus vireti* and *Anaeromyxobacter dehalogenans*, were reported to grow with N_2O as electron acceptor [50-53], but

non-denitrifiers were generally not considered major contributors to N_2O reduction [54]. The increasing number of sequenced microbial genomes from a range of taxa substantially increased the diversity of both denitrifying and non-denitrifying microorganisms with the genetic capacity for N_2O reduction [55-57]. A relevant discovery was that two distinct *nos* clusters (i.e., clade I and II) exist [55,56]. Physiological studies revealed that organisms with clade II *nos* operons exhibit higher growth yields [55,58] and show different kinetic properties than their clade I counterparts. Bacteria expressing clade II NosZ have higher affinity to N_2O, suggesting that microbes with clade II *nos* operons consume N_2O at lower concentrations [58,59].

1.4 Introduction to corrinoid and corrinoid-dependent enzymatic processes

1.4.1 Corrinoid structure and functions

Corrinoids in complete forms (i.e., cobamides) consist of a central cobalt-containing corrin ring and two axial ligands (i.e., an upper Co*β* ligand and a lower Co*α* base) [23]. For example, cyanocobalamin (also known as vitamin B_{12}) features a cyano upper ligand and a 5,6-dimethylbenzimidazole (DMB) lower base [60] (**Figure 1.2**). Depending on the numbers of axial ligands coordinated to the cobalt center, the redox state of a corrinoid can be Co(I), (II), or (III) [61]. With both axial ligands coordinated, the Co(III) state is achieved. Accordingly, with one or no ligand coordination, corrinoid can exists in Co(II) or Co(I) state, respectively [21]. Variations of corrinoids are mainly determined by the structurally diverse lower

bases and upper ligands [28,62]. To date, 17 naturally occurring corrinoids with one of the three major classes of lower ligands (i.e., benzimidazole, purine, and phenol derivatives) have been identified [60,63]. Functional cobamides in biology use a methyl group or a 5'–deoxyadenosyl moiety as the upper ligand and attach one of 17 identified lower bases to the nucleotide loop [64]. Although the lower base is not assigned a direct role in catalysis or electron transfer for maintaining the reactive Co(I) state, the structural features of the lower bases have been shown have important roles in determining the function of the corrinoid cofactor in corrinoid-dependent enzymes [28].

1.4.2 Corrinoid-dependent enzyme systems

Corrinoids are essential enzyme cofactors in biology for catalyzing vital biochemical processes, including isomerization, methyl group transfer and reductive dehalogenation [21,65]. The 5'-deoxyadenosyl cobalamin-(Ado-Cba)-dependent isomerases (*e.g.,* methylmalonyl CoA mutase) represent only a small branch of the corrinoid-dependent enzymes and the central Co atom has been demonstrated fluctuate between Co(III) and Co(II) oxidation states [66]. In contrast, both corrinoid-dependent reductive dehalogenases (RDases) and the diverse corrinoid-dependent methyltransferases (MTases) require the involvement of Co(I) corrinoid for function. Both RDases and MTases have received extensive attention because of their critical roles in catalyzing contaminants detoxification and mediating C cycling, respectively [21,67].

1.4.3 Corrinoid-dependent methyltransferases

Although only one corrinoid-dependent MTase, methionine synthase (MetH), exists in Eukarya, a wide variety of corrinoid-dependent MTases play central roles in the metabolism in Prokarya and Archaea, particularly in organisms that live in anoxic conditions [23]. Many bacteria and archaea employ the Wood-Ljungdahl pathway (WLP) for central metabolism, which requires at least one corrinoid-dependent MTase for methyl group shuttling [25,29]. Generally, with the reducing power provided by H_2, enzymes in the Methyl branch of the WLP catalyze the reduction of CO_2 to form a methyl group that is initially bound to tetrahydrofolate or tetrahydropterin. Next, a MTase I from the MTase complex (corrinoid containing protein, CP) binds and transfers the methyl group onto Co(I) of the super-reduced cofactor bound to CP, resulting a methyl-Co(III)-CP. From there, a MTase II transfers and combines the methyl group to the [CO] produced by the CODH/Acetyl-CoA synthase complex in the Carbonyl branch of the WLP, producing acetyl-CoA and cycling Co(III)-CP back to Co(I) state [68].

Methanogenic archaea (i.e., methanogens) are capable of converting the methyl groups generated in the methyl branch of the WLP into methane (CH_4) with the assistance of a membrane anchored coenzyme M MTase complex (CoM MTases) [69,70]. Similar to the CP mentioned above, the corrinoid cofactor in CoM MTases cycles between Co(III) and Co(I) oxidation states to produce methyl-CoM, which is then reduced to CH_4 by CoM reductase complex [21]. Some methanogens, such as strains of *Methanosarcina*, can also grow with acetate

and methylated compounds such as MeOH by either reversing the CODH/Acetyl-CoA synthase reaction or directly catalyzing CH_4 formation with the help of substrate specific MTases [29,71,72]. Despite that multiple different corrinoid-dependent MTases have been identified in nature, a common feature of these MTases is that they must cycle the cobalt in corrinoid cofactor between Co(I) and Co(III) oxidation states for function [69,70].

1.4.4 Corrinoid-dependent reductive dehalogenation

Reductive dehalogenation performed by OHRB is a respiratory process in which OHRB use organohalogens as terminal electron acceptors. The breakage of the carbon-halogen bond is coupled with energy conservation, a process known as organohalide respiration [24]. OHRB are of environmental importance as they catalyze the reduction of anthropogenic halogenated compounds, such as PCE and trichloroethene (TCE), many of which are significant contaminants in groundwater systems threatening human and environmental health [73]. OHRB capable of dechlorinating PCE or TCE to *cis*-1,2-dichloroethene (*c*DCE) have been identified from diverse bacterial genera distributed among the phyla Chloroflexi, Firmicutes and Proteobacteria, including the genera *Geobacter*, *Desulfitobacterium*, *Sulfurospirillum* , *Dehalobacter*, *Dehalogenimonas* and *Dehalococcoides* [74,75]. However, only several strains of the species *Dehalococcoides mccartyi* (*Dhc*)[73] and *Candidatus Dehalogenimonas*

etheniformans (*Dhgm*)[76] (both of which belong to Chloroflexi phyla) are capable of reducing *c*DCE and vinyl chloride (VC) to environmentally benign ethene [73].

The key enzyme systems responsible for catalyzing organohalide respiration are RDases [24]. All but possibly one RDase (the 3-chlorobenzoate RDase of *Desulfomonile tiedjei* strain DCB-1) strictly require the involvement of a corrinoid cofactor for initiating reductive dechlorination in OHRB. Different to the typical carbon rearrangement or methyl group transfer reactions by corrinoid-dependent enzymes, several catalytic mechanisms have been suggested for the elimination reaction catalyzed by RDases. Based on these differences, RDases have been assigned to a distinct subgroup of corrinoid-dependent enzymes [77]. Functional and structural analyses demonstrated that OHRB share conserved domains and motifs of RDase genes, regardless of their phylogenetically diverse origin [78,79]. Typically, OHRB contains at least a reductive dehalogenase (r*dhA*) gene, encoding the catalytical subunit RdhA, and a *rdhB* gene, encoding a putative membrane-anchoring protein RdhB [27]. Although obligate organohalide-respiring *Dhc* strains such as *Dhc* strain BAV1 cannot *de novo* synthesize corrinoid[73,80], the Co(I) supernucleophile is crucial for RDases to initiate the cleavage of carbon-chlorine bonds.[26,27,81]

1.5 The toxicity of N_2O for corrinoid-dependent enzymes

N_2O is generally considered chemically inert without toxicity to microorganisms, and is either released to the atmosphere or consumed (i.e.,

reduced to innocuous N_2) by microorganisms with *nos* operons and expressing NosZ; however, research conducted in the 1960s demonstrated that N_2O abiotically reacts with certain transition metal complexes including super-reduced Co(I)corrinoids [82,83]. Mechanistic studies demonstrated that N_2O readily mediates a one-electron oxidation of Co(I)corrinoid, which is associated with the generation of a highly reactive hydroxyl radical (HO•) and subsequent inactivation of the corrinoid-dependent enzyme [84] (**equation 1**) [85-87]. For example, N_2O has been shown inhibit the function of corrinoid-dependent methionine synthase (MetH), a critical enzyme system involved in the synthesis of thymidine and DNA [88].

Enzyme-Co(I)corrinoid + N_2O+ H^+→ Enzyme-Co(II)corrinoid + HO• + N_2 (1)

Corrinoid-dependent enzyme systems play key roles in biology, and are essential in the majority of living organisms, including humans [23,66]. More than 70% of organisms in all domains of life contain corrinoid-dependent enzymes, yet only a small portion of Archaea and Bacteria possess the complete corrinoid biosynthetic pathways [61,89]. Corrinoid-auxotrophic organisms, including all mammals, must salvage and modify corrinoids from their environment or rely on exogeneous corrinoid supply. Exposure to N_2O therefore poses a threat to the cellular metabolism of a wide range of organisms in Prokarya and Eukarya due to the critical role(s) of Co(I)corrinoid-dependent enzymatic processes for central metabolisms and/or energy conservation [21,64,90,91]. For example, the hydrogenotrophic methanogen *Methanobacterium bryantii* strain Bab1 strictly

relies on the corrinoid-dependent methyl transfer steps in its WL pathway for energy conservation [29]. N_2O induced inhibition of the Co(I)-corrinoid cofactor therefore would block the energy metabolism of this organism and severely affect its growth. Indeed, the presence of 95 µM N_2O has been showed completely inhibit methanogenesis and growth of *Mb.* strain Bab1 [92]. To compensate the functional loss of corrinoid-dependent enzyme systems caused by N_2O, organisms developed diverse defense strategies. Acetogenic bacteria such as *Acetobacterium woodii* employ an activating enzyme to catalyze the reduction of Co(II) back to catalytically active Co(I)-corrinoids at the expense of ATP [93]. Organisms such as *Paracoccus denitrificans* strain PD1222 and *Escherichia coli* up-regulate MetE (i.e., corrinoid-independent methionine synthase) to circumvent the inhibitory effect of N_2O on MetH, a corrinoid-dependent methionine synthase [21,94]. About 15% of all Bacteria and Archaea harbor *metE*. Functional MetE allows these organisms to synthesize required methionine under conditions where the corrinoid-dependent *metH* pathway is not operational. Recently, phylogenetically diverse non-denitrifying organisms possessing functional *nos* operons (mainly clade II *nosZ*) have been found widely distributed in nature [95], suggesting a possible detoxification role of NosZ in addition to energy conservation. In view of the vital roles of enzyme systems with corrinoid prosthetic groups for central metabolism, microorganisms without alternative pathway(s) to bypass (e.g., MetE) or combat (e.g., NosZ) N_2O toxicity will

potentially be greatly affected by the increasing N_2O concentrations in the environment.

1.6 Rationale, hypotheses and research objectives

N is a fundamental element for all life forms on Earth and an essential macronutrient for the biosynthesis of cellular components (e.g., nucleic acids, proteins) [1-3]. The availability of bio-accessible N depends on diverse N transforming reactions that are eventually controlled by complex networks of metabolically versatile microorganisms [31]. Thus, active N cycling is an inherent feature of active microbial communities in any terrestrial, freshwater and marine environment. As an important component of the N cycle, N_2O can arise from nearly all of the known biological N cycling pathways [31,44]. Therefore, the intensive N fertilizers application as well as fossil fuel combustion on a global scale will continue to amplify the formation of N_2O and result in elevated N_2O concentrations in the environment. The produced N_2O is either directly released into the atmosphere or accumulated at subsurface and further reduced by microbes possessing NosZ. In essence, N cycling and N_2O formation is an inherent feature of any active microbial community. Considering that the N input to the environment will continue to intensify on a global scale to fulfill the food, feed and biofuel crops demands of a burgeoning human population [96], N_2O concentrations will also increase in watersheds and groundwater resources in many regions of the world [44]. As a result, microorganisms experience increasing

N_2O concentrations under most environmental conditions; however, only a fraction of bacteria and archaea have alternate, corrinoid-independent central metabolism pathways (e.g., for methionine biosynthesis), suggesting that many microbial groups will be impacted by N_2O. Therefore, knowledge about the effects of N_2O on biogeochemical cycling will expand our understanding of the dynamics and the interactions of key nutrient cycles in soils, sediments, watersheds, and aquifers.

Triggered by the observation that N_2O exhibits selective inhibition on enzymatic reactions that rely on Co(I) supernucleophile for function, the overarching goal of this dissertation is to assess the effects of N_2O on corrinoid-dependent biochemical processes such as methanogenesis and bacterial reductive dechlorination. The specific goals of this dissertation are: (i) to demonstrate that environmentally relevant N_2O concentrations negatively impact corrinoid-dependent methanogenesis and bacterial reductive dechlorination, (ii) to investigate the impact of N_2O on corrinoid-dependent microbial metabolisms and profiles of microbial communities, and (iii) to explore if bacteria expressing high affinity N_2O reductases might protect (i.e., rescue) corrinoid-dependent biochemical processes from N_2O toxicity.

The current research is based on the following hypotheses:

Hypothesis 1: N_2O is a relevant modulator of corrinoid-dependent microbial processes and directly disrupts C and Cl cycling processes including methanogenesis and organohalide respiration.

Hypothesis 2: The N_2O-reducing bacteria harboring Clade I or Clade II N_2O reductase have a detoxification role in microbial communities.

Hypothesis 3: Exposure of natural microbial assemblages to N_2O induces functional responses observable at molecular level.

The research objectives, based on the hypotheses, are as follows:

Objective 1: Demonstrate the impact of N_2O on methanogenesis and bacterial reductive dechlorination and determine the inhibitory constants (K_I) of N_2O for major methanogenic pathways and key dechlorination steps.

Objective 2: Explore reversibility of N_2O inhibition and the role of bacteria expressing N_2O reductases to protect corrinoid-dependent processes from N_2O toxicity.

Objective 3: Explore the metabolic responses of microbial communities to N_2O exposure and demonstrate the impact of N_2O on corrinoid yields and profiles.

1.7 References

(1) Stein, L. Y.; Klotz, M. G., The nitrogen cycle. *Curr Biol* **2016,** *26* (3), R94-8.

(2) Fowler, D.; Coyle, M.; Skiba, U.; Sutton, M. A.; Cape, J. N.; Reis, S.; Sheppard, L. J.; Jenkins, A.; Grizzetti, B.; Galloway, J. N.; Vitousek, P.; Leach, A.; Bouwman, A. F.; Butterbach-Bahl, K.; Dentener, F.; Stevenson, D.; Amann, M.; Voss, M., The global nitrogen cycle in the twenty-first century. *Philos Trans R Soc Lond B Biol Sci* **2013,** *368* (1621), 20130164.

(3) Gruber, N.; Galloway, J. N., An Earth-system perspective of the global nitrogen cycle. *Nature* **2008,** *451* (7176), 293-6.

(4) Canfield, D. E.; Glazer, A. N.; Falkowski, P. G., The Evolution and Future of Earth's Nitrogen Cycle. *Science* **2010,** *330* (6001), 192-196.

(5) Smil, V., *Enriching the earth: Fritz Haber, Carl Bosch, and the transformation of world food production*. MIT press: 2004.

(6) Jones, C. M.; Spor, A.; Brennan, F. P.; Breuil, M. C.; Bru, D.; Lemanceau, P.; Griffiths, B.; Hallin, S.; Philippot, L., Recently identified microbial guild mediates soil N_2O sink capacity. *Nat Clim Chang* **2014,** *4* (9), 801-805.

(7) Richardson, D.; Felgate, H.; Watmough, N.; Thomson, A.; Baggs, E., Mitigating release of the potent greenhouse gas N(2)O from the nitrogen cycle - could enzymic regulation hold the key? *Trends Biotechnol* **2009,** *27* (7), 388-97.

(8) Erisman, J. W.; Galloway, J. N.; Seitzinger, S.; Bleeker, A.; Dise, N. B.; Petrescu, A. M.; Leach, A. M.; de Vries, W., Consequences of human modification of the global nitrogen cycle. *Philos Trans R Soc Lond B Biol Sci* **2013,** *368* (1621), 20130116.

(9) Ravishankara, A. R.; Daniel, J. S.; Portmann, R. W., Nitrous Oxide (N_2O): The dominant ozone-depleting substance emitted in the 21st Century. *Science* **2009,** *326* (5949), 123-125.

(10) Thomson, A. J.; Giannopoulos, G.; Pretty, J.; Baggs, E. M.; Richardson, D. J., Biological sources and sinks of nitrous oxide and strategies to mitigate emissions. *Philos Trans R Soc Lond B Biol Sci* **2012,** *367* (1593), 1157-1168.

(11) Reay, D. S.; Davidson, E. A.; Smith, K. A.; Smith, P.; Melillo, J. M.; Dentener, F.; Crutzen, P. J., Global agriculture and nitrous oxide emissions. *Nature Climate Change* **2012,** *2*, 410-416.

(12) IPCC, *Climate Change 2013: The Physical Science Basis. Contribution of Working Group I to the Fifth Assessment Report of the Intergovernmental Panel on Climate Change*. Cambridge University Press: Cambridge, United Kingdom and New York, NY, USA, 2013; p 1535.

(13) Tian, H.; Yang, J.; Xu, R.; Lu, C.; Canadell, J. G.; Davidson, E. A.; Jackson, R. B.; Arneth, A.; Chang, J.; Ciais, P.; Gerber, S.; Ito, A.; Joos, F.; Lienert, S.; Messina, P.; Olin, S.; Pan, S.; Peng, C.; Saikawa, E.; Thompson, R. L.; Vuichard, N.; Winiwarter, W.; Zaehle, S.; Zhang, B., Global soil nitrous oxide emissions since the preindustrial era estimated by an ensemble of terrestrial biosphere models: Magnitude, attribution, and uncertainty. *Glob Chang Biol* **2018**.

(14) IPCC, IPCC Climate Change 2014: Mitigation of climate change (eds Edenhofer, O. et al.) (Cambridge Univ. Press, 2014). **2014**.

(15) Shcherbak, I.; Millar, N.; Robertson, G. P., Global metaanalysis of the nonlinear response of soil nitrous oxide (N_2O) emissions to fertilizer nitrogen. *Proc Natl Acad Sci USA* **2014,** *111* (25), 9199-9204.

(16) Reay, D. S.; Davidson, E. A.; Smith, K. A.; Smith, P.; Melillo, J. M.; Dentener, F.; Crutzen, P. J., Global agriculture and nitrous oxide emissions. *Nat Clim Change* **2012,** *2* (6), 410-416.

(17) Jurado, A.; Borges, A. V.; Brouyere, S., Dynamics and emissions of N_2O in groundwater: A review. *Sci Total Environ* **2017,** *584*, 207-218.

(18) Priscu, J. C.; Christner, B. C.; Dore, J. E.; Popp, B. N.; Casciotti, K. L.; Lyons, W. B., Supersaturated N2O in a perennially ice-covered Antarctic lake: Molecular and stable isotopic evidence for a biogeochemical relict. *Limnol Oceanogr* **2008,** *53* (6), 2439-2450.

(19) Pauleta, S. R.; Carepo, M. S. P.; Moura, I., Source and reduction of nitrous oxide. *Coord Chem Rev* **2019,** *387*, 436-449.

(20) Hallin, S.; Philippot, L.; Löffler, F. E.; Sanford, R. A.; Jones, C. M., Genomics and Ecology of Novel N2O-Reducing Microorganisms. *Trends Microbiol* **2018,** *26* (1), 43-55.

(21) Matthews, R. G., Cobalamin- and corrinoid-dependent enzymes. *Met Ions Life Sci* **2009,** *6*, 53-114.

(22) Weimann, J., Toxicity of nitrous oxide. *Best Prac Res Clin Anaesthesiol* **2003,** *17* (1), 47-61.

(23) Banerjee, R.; Ragsdale, S. W., The many faces of vitamin B_{12}: catalysis by cobalamin-dependent enzymes. *Annu Rev Biochem* **2003,** *72*, 209-247.

(24) Adrian, L.; Löffler, F. E., *Organohalide-respiring bacteria*. Springer: Berlin Heidelberg: 2016.

(25) Thauer, R. K.; Kaster, A. K.; Seedorf, H.; Buckel, W.; Hedderich, R., Methanogenic archaea: ecologically relevant differences in energy conservation. *Nat Rev Microbiol* **2008,** *6* (8), 579-591.

(26) Bommer, M.; Kunze, C.; Fesseler, J.; Schubert, T.; Diekert, G.; Dobbek, H., Structural basis for organohalide respiration. *Science* **2014,** *346* (6208), 455-458.

(27) Payne, K. A.; Quezada, C. P.; Fisher, K.; Dunstan, M. S.; Collins, F. A.; Sjuts, H.; Levy, C.; Hay, S.; Rigby, S. E.; Leys, D., Reductive dehalogenase structure suggests a mechanism for B_{12}-dependent dehalogenation. *Nature* **2015,** *517* (7535), 513-516.

(28) Yan, J.; Bi, M.; Bourdon, A. K.; Farmer, A. T.; Wang, P. H.; Molenda, O.; Quaile, A. T.; Jiang, N.; Yang, Y.; Yin, Y.; Şimşir, B.; Campagna, S. R.; Edwards, E. A.; Löffler, F. E., Purinyl-cobamide is a native prosthetic group of reductive dehalogenases. *Nat Chem Biol* **2018,** *14* (1), 8-14.

(29) Ferry, J. G., Fundamentals of methanogenic pathways that are key to the biomethanation of complex biomass. *Curr Opin Struct Biol* **2011,** *22* (3), 351-357.

(30) Thamdrup, B., New pathways and processes in the global nitrogen cycle. *Annual Review of Ecology, Evolution, and Systematics, Vol 43* **2012,** *43*, 407-428.

(31) Kuypers, M. M. M.; Marchant, H. K.; Kartal, B., The microbial nitrogen-cycling network. *Nat Rev Microbiol* **2018,** *16* (5), 263-276.

(32) Zumft, W. G., Cell biology and molecular basis of denitrification. *Microbiology and Molecular Biology Reviews* **1997,** *61* (4), 533-616.

(33) Zhu, X.; Burger, M.; Doane, T. A.; Horwath, W. R., Ammonia oxidation pathways and nitrifier denitrification are significant sources of N_2O and NO under low oxygen availability. *Proceedings of the National Academy of Sciences* **2013,** *110* (16), 6328-6333.

(34) Rütting, T.; Boeckx, P.; Müller, C.; Klemedtsson, L., Assessment of the importance of dissimilatory nitrate reduction to ammonium for the terrestrial nitrogen cycle. *Biogeosciences* **2011,** *8* (7), 1779-1791.

(35) Sun, Y.; De Vos, P.; Heylen, K., Nitrous oxide emission by the non-denitrifying, nitrate ammonifier *Bacillus licheniformis*. *BMC Genomics* **2016,** *17* (1), 68.

(36) Higgins, S. A.; Welsh, A.; Orellana, L. H.; Konstantinidis, K. T.; Chee-Sanford, J. C.; Sanford, R. A.; Schadt, C. W.; Löffler, F. E., Detection and diversity of fungal nitric oxide reductase genes (*p450nor*) in agricultural soils. *Applied and Environmental Microbiology* **2016,** *82* (10), 2919-2928.

(37) Higgins, S. A.; Schadt, C. W.; Matheny, P. B.; Löffler, F. E., Phylogenomics reveal the dynamic evolution of fungal nitric oxide reductases and their relationship to secondary metabolism. *Genome biology and evolution* **2018,** *10* (9), 2474-2489.

(38) Wankel, S. D.; Ziebis, W.; Buchwald, C.; Charoenpong, C.; de Beer, D.; Dentinger, J.; Xu, Z.; Zengler, K., Evidence for fungal and chemodenitrification based N_2O flux from nitrogen impacted coastal sediments. *Nature Communications* **2017,** *8*, 15595.

(39) Onley, J. R.; Ahsan, S.; Sanford, R. A.; Löffler, F. E., Denitrification by *Anaeromyxobacter dehalogenans*, a common soil bacterium lacking the nitrite reductase genes *nirS* and *nirK*. *Applied and Environmental Microbiology* **2018,** *84*, e01985-17.

(40) Conrad, R., Soil microorganisms as controllers of atmospheric trace gases (H_2, CO, CH_4, OCS, N_2O, and NO). *Microbiol Rev* **1996,** *60* (4), 609-640.

(41) Philippot, L.; Andert, J.; Jones, C. M.; Bru, D.; Hallin, S., Importance of denitrifiers lacking the genes encoding the nitrous oxide reductase for N_2O emissions from soil. *Glob Chang Biol* **2011,** *17* (3), 1497-1504.

(42) Jones, C. M.; Welsh, A.; Throback, I. N.; Dorsch, P.; Bakken, L. R.; Hallin, S., Phenotypic and genotypic heterogeneity among closely related soil-borne N2 - and N2 O-producing Bacillus isolates harboring the nosZ gene. *FEMS Microbiol Ecol* **2011,** *76* (3), 541-52.

(43) Jones, C. M.; Graf, D. R.; Bru, D.; Philippot, L.; Hallin, S., The unaccounted yet abundant nitrous oxide-reducing microbial community: a potential nitrous oxide sink. *ISME J* **2013,** *7* (2), 417-26.

(44) Hu, H. W.; Chen, D.; He, J. Z., Microbial regulation of terrestrial nitrous oxide formation: understanding the biological pathways for prediction of emission rates. *FEMS Microbiol Rev* **2015,** *39* (5), 729-49.

(45) Bakken, L. R.; Bergaust, L.; Liu, B.; Frostegard, A., Regulation of denitrification at the cellular level: a clue to the understanding of N_2O emissions from soils. *Philos Trans R Soc Lond B Biol Sci* **2012,** *367* (1593), 1226-34.

(46) Weymann, D.; Well, R.; Flessa, H.; Von der Heide, C.; Deurer, M.; Meyer, K.; Konrad, C.; Walther, W., Groundwater N_2O emission factors of nitrate-

contaminated aquifers as derived from denitrification progress and N_2O accumulation. **2008**.

(47) Chapuis-Lardy, L.; Wrage, N.; Metay, A.; Chotte, J.-L.; Bernoux, M., Soils, a sink for N_2O ? A review. *Glob Chang Biol* **2007,** *13* (1), 1-17.

(48) Davidson, E. A., The contribution of manure and fertilizer nitrogen to atmospheric nitrous oxide since 1860. *Nat Geosci* **2009,** *2* (9), 659-662.

(49) Philippot, L., Denitrifying genes in bacterial and archaeal genomes. *Biochimica et Biophysica Acta (BBA) - Gene Structure and Expression* **2002,** *1577* (3), 355-376.

(50) Payne, W. J.; Grant, M. A.; Shapleigh, J.; Hoffman, P., Nitrogen oxide reduction in *Wolinella succinogenes* and *Campylobacter* species. *Journal of Bacteriology* **1982,** *152* (2), 915-918.

(51) Sanford, R. A.; Cole, J. R.; Tiedje, J. M., Characterization and description of *Anaeromyxobacter dehalogenans* gen. nov., sp. nov., an aryl-halorespiring facultative anaerobic myxobacterium. *Applied and Environmental Microbiology* **2002,** *68* (2), 893-900.

(52) Simon, J.; Einsle, O.; Kroneck, P. M. H.; Zumft, W. G., The unprecedented *nos* gene cluster of *Wolinella succinogenes* encodes a novel respiratory electron transfer pathway to cytochrome *c* nitrous oxide reductase. *FEBS Letters* **2004,** *569* (1), 7-12.

(53) Mania, D.; Heylen, K.; van Spanning, R. J. M.; Frostegård, Å., The nitrate-ammonifying and nosZ-carrying bacterium *Bacillus vireti* is a potent source and sink for nitric and nitrous oxide under high nitrate conditions. *Environmental Microbiology* **2014,** *16* (10), 3196-3210.

(54) Onley, J. R.; Ahsan, S.; Sanford, R. A.; Löffler, F. E., Denitrification by *Anaeromyxobacter dehalogenans*, a common soil bacterium lacking the nitrite reductase genes *nirS* and *nirK*. *Appl Environ Microbiol* **2018,** *84* (4), e01985-17.

(55) Sanford, R. A.; Wagner, D. D.; Wu, Q. Z.; Chee-Sanford, J. C.; Thomas, S. H.; Cruz-Garcia, C.; Rodriguez, G.; Massol-Deya, A.; Krishnani, K. K.; Ritalahti, K. M.; Nissen, S.; Konstantinidis, K. T.; Löffler, F. E., Unexpected nondenitrifier nitrous oxide reductase gene diversity and abundance in soils. *Proceedings of the National Academy of Sciences of the United States of America* **2012,** *109* (48), 19709-19714.

(56) Jones, C. M.; Graf, D. R. H.; Bru, D.; Philippot, L.; Hallin, S., The unaccounted yet abundant nitrous oxide-reducing microbial community: a potential nitrous oxide sink. *ISME Journal* **2013,** *7* (2), 417-426.

(57) Hallin, S.; Philippot, L.; Löffler, F. E.; Sanford, R. A.; Jones, C. M., Genomics and ecology of novel N_2O-reducing microorganisms. *Trends in Microbiology* **2018,** *26* (1), 43-55.

(58) Yoon, S.; Nissen, S.; Park, D.; Sanford, R. A.; Löffler, F. E., Nitrous oxide reduction kinetics distinguish bacteria harboring Clade I NosZ from those harboring Clade II NosZ. *Applied and Environmental Microbiology* **2016,** *82* (13), 3793-3800.

(59) Suenaga, T.; Riya, S.; Hosomi, M.; Terada, A., Biokinetic characterization and activities of N_2O-reducing bacteria in response to various oxygen levels. *Frontiers in Microbiology* **2018,** *9* (697).

(60) Shelton, A. N.; Seth, E. C.; Mok, K. C.; Han, A. W.; Jackson, S. N.; Haft, D. R.; Taga, M. E., Uneven distribution of cobamide biosynthesis and dependence in bacteria predicted by comparative genomics. *ISME J* **2018,** *DOI.org/10.1038/s41396-018-0304-9*.

(61) Randaccio, L.; Geremia, S.; Demitri, N.; Wuerges, J., Vitamin B_{12}: unique metalorganic compounds and the most complex vitamins. *Molecules* **2010,** *15* (5), 3228-3259.

(62) Kräutler, B.; Fieber, W.; Ostermann, S.; Fasching, M.; Ongania, K.-H.; Gruber, K.; Kratky, C.; Mikl, C.; Siebert, A.; Diekert, G., The Cofactor of tetrachloroethene reductive dehalogenase of *Dehalospirillum multivorans* is Norpseudo-B_{12}, a new type of a natural corrinoid. *Helv Chim Acta* **2003,** *86* (11), 3698-3716.

(63) Banerjee, R., *Chemistry and Biochemistry of B_{12}*. John Wiley & Sons: New York, 1999.

(64) Yan, J.; Im, J.; Yang, Y.; Löffler, F. E., Guided cobalamin biosynthesis supports *Dehalococcoides mccartyi* reductive dechlorination activity. *Philos Trans R Soc Lond B Biol Sci* **2013,** *368* (1616), 20120320.

(65) Giedyk, M.; Goliszewska, K.; Gryko, D., Vitamin B_{12} catalysed reactions. *Chem Soc Rev* **2015,** *44* (11), 3391-3404.

(66) Gruber, K.; Puffer, B.; Krautler, B., Vitamin B12-derivatives-enzyme cofactors and ligands of proteins and nucleic acids. *Chem Soc Rev* **2011,** *40* (8), 4346-63.

(67) Marsh, E. N. G., Coenzyme B12 (cobalamin)- dependent enzymes. *Essays Biochem* **1999,** *34*, 139-154.

(68) Richter, N.; Zepeck, F.; Kroutil, W., Cobalamin-dependent enzymatic O-, N-, and S-demethylation. *Trends Biotechnol* **2015,** *33* (7), 371-3.

(69) Hippler, B.; Thauer, R. K., The energy conserving methyltetrahydromethanopterin:coenzyme M methyltransferase complex from methanogenic archaea: function of the subunit MtrH. *FEBS Lett* **1999,** *449* (2), 165-168.

(70) Thauer, R. K.; Kaster, A. K.; Goenrich, M.; Schick, M.; Hiromoto, T.; Shima, S., Hydrogenases from methanogenic archaea, nickel, a novel cofactor, and H2 storage. *Annu Rev Biochem* **2010,** *79*, 507-36.

(71) Matthews, R. G.; Koutmos, M.; Datta, S., Cobalamin-dependent and cobamide-dependent methyltransferases. *Curr Opin Struct Biol* **2008,** *18* (6), 658-66.

(72) Fischer, R.; Thauer, R. K., Methanogenesis from acetate in cell extracts of *Methanosarcina barkeri*: isotope exchange between CO_2 and the carbonyl group of acetyl-CoA, and the role of H_2. *Arch Microbiol* **1990,** *153* (2), 156-162.

(73) Löffler, F. E.; Yan, J.; Ritalahti, K. M.; Adrian, L.; Edwards, E. A.; Konstantinidis, K. T.; Müller, J. A.; Fullerton, H.; Zinder, S. H.; Spormann, A. M., *Dehalococcoides mccartyi gen. nov., sp. nov.*, obligately organohalide-respiring anaerobic bacteria relevant to halogen cycling and bioremediation, belong to a novel bacterial class, *Dehalococcoidia classis nov.*, order *Dehalococcoidales ord. nov.* and family *Dehalococcoidaceae fam. nov*., within the phylum *Chloroflexi*. *Int J Syst Evol Microbiol* **2013,** *63* (2), 625-635.

(74) Hug, L. A.; Edwards, E. A., Diversity of reductive dehalogenase genes from environmental samples and enrichment cultures identified with degenerate primer PCR screens. *Front Microbiol* **2013,** *4*, 1-16.

(75) Schubert, T.; Adrian, L.; Sawers, R. G.; Diekert, G., Organohalide respiratory chains: composition, topology and key enzymes. *FEMS Microbiol Ecol* **2018,** *94* (4), fiy035.

(76) Yang, Y.; Higgins, S. A.; Yan, J.; Simsir, B.; Chourey, K.; Iyer, R.; Hettich, R. L.; Baldwin, B.; Ogles, D. M.; Löffler, F. E., Grape pomace compost harbors organohalide-respiring Dehalogenimonas species with novel reductive dehalogenase genes. *ISME J* **2017,** *11* (12), 2767-2780.

(77) Jugder, B. E.; Ertan, H.; Lee, M.; Manefield, M.; Marquis, C. P., Reductive dehalogenases come of age in biological destruction of organohalides. *Trends Biotechnol* **2015,** *33* (10), 595-610.

(78) Tang, S.; Chan, W. W. M.; Fletcher, K. E.; Seifert, J.; Liang, X.; Löffler, F. E.; Edwards, E. A.; Adrian, L., Functional characterization of reductive dehalogenases by using blue native polyacrylamide gel electrophoresis. *Appl Environ Microbiol* **2013,** *79* (3), 974-981.

(79) Hug, L. A.; Maphosa, F.; Leys, D.; Löffler, F. E.; Smidt, H.; Edwards, E. A.; Adrian, L., Overview of organohalide-respiring bacteria and a proposal for a classification system for reductive dehalogenases. *Philos Trans R Soc Lond B Biol Sci* **2013,** *368* (1616), 20120322.

(80) Seshadri, R.; Adrian, L.; Fouts, D. E.; Eisen, J. A.; Phillippy, A. M.; Methe, B. A.; Ward, N. L.; Nelson, W. C.; Deboy, R. T.; Khouri, H. M.; Kolonay, J. F.; Dodson, R. J.; Daugherty, S. C.; Brinkac, L. M.; Sullivan, S. A.; Madupu, R.; Nelson, K. E.; Kang, K. H.; Impraim, M.; Tran, K.; Robinson, J. M.; Forberger, H. A.; Fraser, C. M.; Zinder, S. H.; Heidelberg, J. F., Genome sequence of the PCE-dechlorinating bacterium *Dehalococcoides ethenogenes*. *Science* **2005,** *307* (5706), 105-108.

(81) Fincker, M.; Spormann, A. M., Biochemistry of catabolic reductive dehalogenation. *Annu Rev Biochem* **2017,** *86*, 357-386.

(82) Banks, R. G. S.; Henderson, R. J.; Pratt, J. M., Reactions of gases in solution. Part III. Some reactions of nitrous oxide with transition-metal complexes. *Journal of the Chemical Society A: Inorganic, Physical, Theoretical* **1968,** (0), 2886-2889.

(83) Blackburn, R.; Kyaw, M.; Swallow, A. J., Reaction of cob(I)alamin with nitrous oxide and cob(III)alamin. *Journal of the Chemical Society, Faraday Transactions 1: Physical Chemistry in Condensed Phases* **1977,** *73* (0), 250-255.

(84) Drummond, J. T.; Matthews, R. G., Nitrous oxide degradation by cobalamin-dependent methionine synthase: characterization of the reactants and products in the inactivation reaction. *Biochemistry* **1994,** *33* (12), 3732-3741.

(85) Blackburn, R.; Kyaw, M.; Swallow, A. J., Reaction of cob(I)alamin with nitrous oxide and cob(III)alamin. *J Chem Soc, Faraday Trans I* **1977,** *73* (0), 250-255.

(86) Balderston, W. L.; Payne, W. J., Inhibition of methanogenesis in salt marsh sediments and whole-cell suspensions of methanogenic bacteria by nitrogen oxides. *Appl Environ Microbiol* **1976,** *32* (2), 264-269.

(87) Banks, R. G. S.; Henderson, R. J.; Pratt, J. M., Reactions of gases in solution. Part III. Some reactions of nitrous oxide with transition-metal complexes. *J Chem Soc Sec A* **1968,** (0), 2886-2889.

(88) Nunn, J. F., Clinical aspects of the interaction between nitrous oxide and vitamin B_{12}. *British Journal of Anaesthesia* **1987,** *59* (1), 3-13.

(89) Ragsdale, S. W., Catalysis of Methyl Group Transfers Involving Tetrahydrofolate and B12. **2008,** *79*, 293-324.

(90) Men, Y.; Seth, E. C.; Yi, S.; Crofts, T. S.; Allen, R. H.; Taga, M. E.; Alvarez-Cohen, L., Identification of specific corrinoids reveals corrinoid modification in dechlorinating microbial communities. *Environ Microbiol* **2014,** *17* (12), 4873-4884.

(91) Yan, J.; Şimşir, B.; Farmer, A. T.; Bi, M.; Yang, Y.; Campagna, S. R.; Löffler, F. E., The corrinoid cofactor of reductive dehalogenases affects dechlorination rates and extents in organohalide-respiring *Dehalococcoides mccartyi*. *ISME J* **2016,** *10* (5), 1092-1101.

(92) Klüber, H. D.; Conrad, R., Inhibitory effects of nitrate, nitrite, NO and N_2O on methanogenesis by *methanosarcina barkeri* and *Methanobacterium bryantii*. *FEMS Microbiol Ecol* **1998,** *25*, 331-339.

(93) Farnberger, J. E.; Richter, N.; Hiebler, K.; Bierbaumer, S.; Pickl, M.; Skibar, W.; Zepeck, F.; Kroutil, W., Biocatalytic methylation and demethylation via a shuttle catalysis concept involving corrinoid proteins. *Commun Chem* **2018,** *1* (1), 82.

(94) Sullivan, M. J.; Gates, A. J.; Appia-Ayme, C.; Rowley, G.; Richardson, D. J., Copper control of bacterial nitrous oxide emission and its impact on vitamin B_{12}-dependent metabolism. *Proc Natl Acad Sci USA* **2013,** *110* (49), 19926-19931.

(95) Sanford, R. A.; Wagner, D. D.; Wu, Q.; Chee-Sanford, J. C.; Thomas, S. H.; Cruz-Garcia, C.; Rodriguez, G.; Massol-Deya, A.; Krishnani, K. K.; Ritalahti, K. M.; Nissen, S.; Konstantinidis, K. T.; Loffler, F. E., Unexpected nondenitrifier nitrous oxide reductase gene diversity and abundance in soils. *Proc Natl Acad Sci USA* **2012,** *109* (48), 19709-19714.

(96) UNEP, Emerging issues of environmental concern. *United Nations Environment Programme, Nairobi* **2019**.

1.8 Appendix

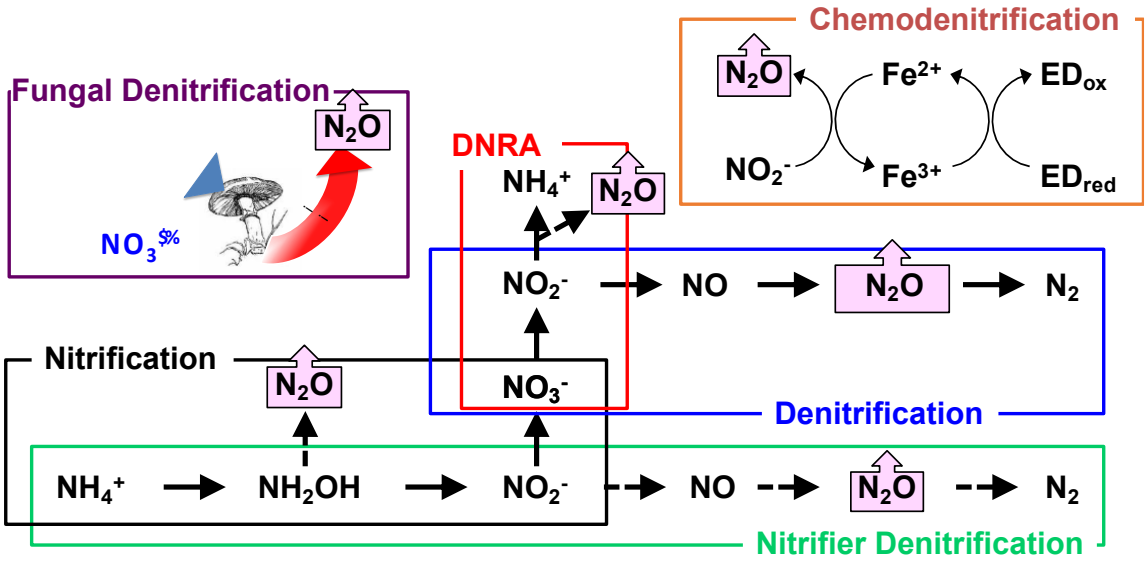


Figure 1. Simplified schematic representations of the major biotic and abiotic pathways for N_2O production (Figure adopted from Dr. Frank Löffler with permission).

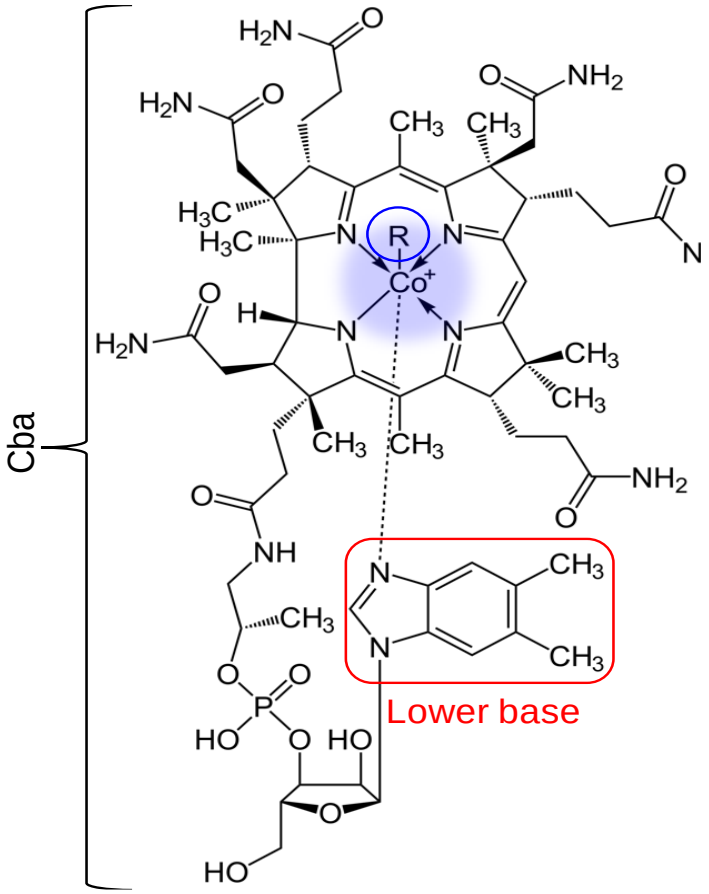


Figure 2. Corrinoid structure. The structure of cobalamin is shown as the example. In the case of cobalamin, the lower base in cobalamin is 5, 6-dimethylbenzimidazole (DMB). The R group (i.e., upper ligand) in functional cobalamin can be the methyl or the adenosyl group. If the upper ligand is cyanide the structure is known as cyanocobalamin or vitamin B_{12}.

CHAPTER TWO:
NITROUS OXIDE IS A POTENT INHIBITOR OF BACTERIAL REDUCTIVE DECHLORINATION

The following chapter is modified from a manuscript published in 2018 in the journal Environmental Science & Technology, volume 53, issue 2, pages 692-701.

2.1 Abstract

Organohalide-respiring bacteria are key players for the turnover of naturally occurring and anthropogenic organohalogens. At sites impacted with chlorinated ethenes, biostimulation alone or combined with bioaugmentation accelerates reductive dechlorination rates; however, stoichiometric conversion of chlorinated ethenes to environmentally benign ethene does not always occur. The experiments demonstrate that nitrous oxide (N_2O), a compound commonly present in groundwater, is a potent inhibitor of organohalide respiration. N_2O concentrations in the low micromolar range decreased dechlorination rates and resulted in incomplete dechlorination of tetrachloroethene (PCE) in *Geobacter lovleyi* strain SZ and of *cis*-1,2-dichloroethene (*c*DCE) and vinyl chloride (VC) in *Dehalococcoides mccartyi* strain BAV1 axenic cultures. Presumably, N_2O interferes with reductive dechlorination by reacting with super-reduced Co(I)-corrinoids of reductive dehalogenases, which is supported by the finding that N_2O did not inhibit corrinoid-independent fumarate to succinate reduction in strain SZ cultures. Kinetic analyses of N_2O effects revealed a best fit to the noncompetitive Michaelis-Menten inhibition model, and determined N_2O inhibitory constants, K_I, for PCE and *c*DCE dechlorination of 40.8 $\pm$ 3.8 µM and 21.2 $\pm$ 3.5 µM in strain SZ and strain BAV1 cultures, respectively. The lowest K_I value of 9.6 $\pm$ 0.4 µM was determined for VC to ethene reductive dechlorination

in strain BAV1 cultures, suggesting that this crucial dechlorination step for achieving detoxification is most susceptible to N_2O inhibition. Groundwater N_2O concentrations exceeding 100 µM are not uncommon, especially in watersheds impacted by agricultural activities and associated nitrate run-off. Thus, dissolved N_2O measurements can inform about *c*DCE and VC stalls at sites impacted with chlorinated ethenes.

2.2 Introduction

Chlorinated solvents such as chlorinated ethenes are widespread groundwater contaminants of concern due to their adverse impact on human and ecosystem health.[1] The discovery of organohalide-respiring bacteria (OHRB) triggered the development of enhanced bioremediation treatment at sites impacted with chlorinated ethenes.[1,2] *Geobacter lovleyi* (*Geo*) strain SZ[3] reductively dechlorinates tetrachloroethene (PCE) via trichloroethene (TCE) to *cis*-1,2-dichloroethene (*c*DCE), and several strains of the species *Dehalococcoides mccartyi* (*Dhc*)[4] and *Candidatus* Dehalogenimonas etheniformans (*Dhgm*)[5] reduce *c*DCE and vinyl chloride (VC) to environmentally benign ethene. Reductive dechlorination is an electron-consuming process and biostimulation with fermentable substrates to increase the flux of hydrogen is a commonly applied approach to enhance *in situ* contaminant detoxification.[2,6] Biostimulation alone or combined with bioaugmentation has been applied at many sites impacted with chlorinated ethenes and substantial reductions in total organic chlorine are generally achieved; however, declining PCE and TCE concentrations are often associated with increasing trends in *c*DCE and VC concentrations.[7-10] Stalled reductive dechlorination may be due to a lack of electron donor (i.e., hydrogen) or unfavorable geochemical conditions such as the presence of competing electron acceptors (e.g., sulfate),[11,12] the presence of oxygen,[13] low pH conditions,[14] or the absence of organohalide-respiring Dehalococcoidia (i.e., *Dhc* and *Dhgm*).[2,15]

Interestingly, a data mining prediction model applied to geochemical and microbial groundwater monitoring data sets collected from sites impacted with chlorinated ethenes ranked nitrate and nitrite concentrations as the most relevant predictors for *in situ* reductive dechlorination and detoxification potential.[16] Microcosm studies have attributed nitrate inhibition of PCE to *c*DCE reductive dechlorination to elevated redox potential in the presence of nitrate;[7,11] however, nitrate had no inhibitory effect on PCE or TCE dechlorination in axenic cultures of *Geo* strain SZ and *Dhc* strain FL2.[3,17] These contrasting observations can be reconciled if a nitrate transformation product exerts an inhibitory effect on reductive dechlorination. Nitrous oxide (N_2O) is a known metabolite of microbial nitrogen metabolism including nitrate reduction or ammonium oxidation,[18-21] and inhibitory effects of N_2O on methanogenesis,[22-24] and in one case on PCE reductive dechlorination,[11] have been reported. Although detailed mechanistic studies are lacking, a likely explanation is the reaction of N_2O with cob(I)amides[25,26] and the ensuing inhibition of corrinoid-dependent enzyme systems involved in methanogenesis.[27] The reductive dehalogenase (RDase) enzyme systems catalyzing carbon-chlorine bond cleavage require a cobamide prosthetic group for function;[28-30] however, the effects of N_2O on reductive dechlorination by OHRB are largely unclear.

As global fertilizer usage continuous to increase and elevated concentrations N_2O occur in groundwater,[31] detailed understanding of the impact of N_2O on relevant microbial processes, including organohalide respiration, is

needed. This study explored the impact of N_2O on microbial reductive dechlorination and determined inhibitory constants (K_I values) of N_2O on reductive dechlorination of PCE in *Geobacter lovleyi* strain SZ and of *c*DCE and VC in *Dhc* strain BAV1.

2.3 Materials and Methods

2.3.1 Chemicals.

PCE, *c*DCE (both ≥99.5%), VC (≥99.5%), ethene (≥99.9%), Vitamin B_{12} (≥98%), sodium fumarate (≥98%) and N_2O (≥99%) were purchased from Sigma-Aldrich (St Louis, MO, USA). All other chemicals used in this study were reagent grade or higher.

2.3.2 Bacterial strains and growth conditions.

The impact of N_2O on reductive dechlorination was investigated using two organohalide-respiring isolates. *Geo* strain SZ, a corrinoid-prototroph capable of dechlorinating PCE and TCE to *c*DCE,[3,32] and *Dhc* strain BAV1, a corrinoid-auxotroph capable of dechlorinating *c*DCE and VC to non-toxic ethene.[4,33] Both cultures were grown in 160 mL serum bottles containing a CO_2/N_2 (20/80, vol/vol) headspace and 100 mL of synthetic, bicarbonate-buffered (30 mM, pH 7.3), and reduced (0.2 mM Na_2S and 0.2 mM L-cysteine) mineral salt medium as described.[30,34] Strain SZ cultures received 5 mM acetate as electron donor and 0.28 mM PCE (38 µmoles/bottle), 10 mM fumarate, or both PCE and fumarate as

electron acceptors, respectively, and a vitamin B_{12}-free Wolin vitamin solution.[35] *Dhc* strain BAV1 culture vessels received 10 mL of hydrogen, 0.8 mM (90 µmoles/bottle) *c*DCE or 0.25 mM (40 µmoles/bottle) VC, and 5 mM acetate as electron donor, electron acceptor, and carbon source, respectively. *Dhc* strain BAV1 culture vessels received the Wolin vitamin stock solution containing vitamin B_{12} to achieve a final concentration of 25 µg L^{-1}. For inoculation, culture vessels received 3% (vol/vol) inocula from actively dechlorinating cultures maintained under the same conditions. All experiments used triplicate culture vessels, and culture bottles without N_2O and without inoculum served as positive and negative controls, respectively. Culture vessels were incubated without agitation at 30°C in the dark with the stoppers facing up.

2.3.3 Inhibition experiments.

For *Geo* strain SZ cultures, undiluted N_2O gas was directly added to incubation vessels using plastic syringes (BD, Franklin Lakes, NJ, USA) to achieve final aqueous N_2O concentrations of 9.5, 19.1 and 57.3 µM in PCE-amended cultures, of 191.4 µM and of 10 mM in fumarate-amended cultures, and of 191.4 µM in cultures grown with both PCE and fumarate. For *Dhc* strain BAV1 cultures, undiluted or 10-fold diluted (with N_2) N_2O gas was added with plastic syringes to achieve final aqueous phase N_2O concentrations of 9.5, 19.1 and 57.3 µM in *c*DCE-amended vessels, and of 2.9, 5.7 and 19.1 µM in VC-amended vessels. The aqueous phase concentrations (in µM) of N_2O in all medium bottles

were calculated from the headspace concentrations using a dimensionless Henry's constant of 1.94 for N_2O at 30°C[36] according to $C_{aq} = \frac{C_g}{H_{cc}}$, where C_{aq}, C_g, and H_{cc} are the aqueous concentration (in µM), the headspace concentration (in µmoles L^{-1}) and the dimensionless Henry's constant, respectively. Average dechlorination rates were calculated based on the continuous accumulation of dechlorination products (i.e., before stable product concentrations were observed). Since each reductive dechlorination step is associated with the release of one chloride ion (Cl^-), the average dechlorination rates determined in growth experiments are reported as the total amount of Cl^- released per volume per unit time (i.e., µmoles Cl^- L^{-1} d^{-1}).

2.3.4 Whole cell suspension dechlorination assays.

Biomass for whole cell suspension assays was harvested by centrifugation at 10,000 x *g* at 4°C for 30 minutes from 1.6 L *Geo* strain SZ and *Dhc* strain BAV1 cultures that had dechlorinated three feedings of PCE and *c*DCE, respectively. Inside an anoxic chamber (Coy Laboratory Products Inc., MI, USA), the supernatants were decanted, and the pellets were suspended in 8 – 10 mL reduced mineral salts medium. For protein quantification, triplicate 0.2 mL (strain SZ) and 1.0 mL (strain BAV1) concentrated cell suspensions were transferred to 2-mL screw cap tubes containing 20 mg of 0.1 mm diameter glass beads, and cells were broken at room temperature using a Bead Ruptor (OMNI, GA, USA) at speed of 6.0 m s^{-1} for three 10-min cycles with 2-min breaks. After centrifugation

at 13,000 x *g* for 2 minutes to remove cell debris, protein content in the supernatants was estimated using the Bradford assay[37] on a plate reader (BioTek Instruments, VT, USA). To ensure consistency between replicate experiments, cell suspensions of both isolates were freshly prepared following identical procedures.

Dechlorination assays for rate determinations were performed in 8-mL glass vials sealed with Teflon-lined butyl rubber septa held in place with aluminum crimps. Each vial contained 3.80 – 4.86 mL of reduced basal salts medium with 5 mM acetate and a N_2/CO_2 (80/20, vol/vol) headspace for *Geo* strain SZ and a H_2/CO_2 (80/20, vol/vol) headspace for *Dhc* strain BAV1. Electron donor was provided in at least 40-fold excess of the theoretical demand to ensure that reductive dechlorination was not electron donor limited. For *Geo* strain SZ cell suspensions, 36 – 1,100 µL of an aqueous 1 mM PCE stock solution were added directly to the assay vials to achieve final aqueous PCE concentrations ranging from 5 – 150 µM. For *Dhc* strain BAV1 cell suspensions, 2 – 550 µL *c*DCE stock (from a 5.0 mM aqueous stock solution) or 12 – 630 µL VC stock (from a 2.0 mM aqueous stock solution) were added to achieve final aqueous *c*DCE and VC concentrations ranging from 1 – 500 µM and 3 – 150 µM, respectively. The total aqueous volume in all vials was 4.9 mL before introducing 0.1 mL of cell suspension. Replicate vials at each initial PCE and *c*DCE concentration received N_2O to achieve 0, 10, and 60 µM, and VC-amended vials received N_2O to achieve 0, 15, and 50 µM dissolved phase N_2O concentrations.

The added N_2O concentrations were quantified in all assay vials prior to and at the end of the incubation period and determined constant N_2O concentrations. Following equilibration, each assay vial received 0.1 mL of the respective cell suspension (corresponding to 56.3 $\pm$ 2.2 µg protein per vial for *Geo* strain SZ and 19.7 $\pm$ 1.4 µg protein per vial for *Dhc* strain BAV1) using plastic syringes to start dechlorination activity. Vials that received 0.1 mL sterile mineral salt medium instead of cell suspension, and vials that received 0.1 mL heat-killed cell suspension served as negative controls. During the 6-hour assay incubation, 1.0 mL liquid samples were collected from sacrificial assay vials every 60 minutes and transferred to 20-mL glass auto-sampler vials containing 0.1 mL of 25 mM H_2SO_4 to terminate dechlorination activity. The cell titers and substrate concentrations were chosen such that the dechlorination rates could be determined within the 6-hour incubation period and no more than 80% of the initial chlorinated ethene concentration had been consumed at the end of the incubation period.

2.3.5 Analytical procedures.

Chlorinated ethenes and ethene were analyzed with an Agilent G1888 headspace sampler connected to an Agilent 7890 gas chromatograph (GC) equipped with a flame ionization detector (method detection limit ~ 0.2 µM) and a DB-624 capillary column (60 m length $\times$ 0.32 mm diameter, 1.8 µm film thickness).[34] Fumarate and succinate were quantified using an Agilent 1200

series high-performance liquid chromatography system equipped with an Aminex HPX-87H column and a dual-wavelength absorbance detector set to 210 nm.[38] N_2O was analyzed by injecting 100 µL headspace samples into an Agilent 7890A GC equipped with an HP-PLOT Q column (30 m length x 0.320 mm diameter, 20 µm film thickness) and a micro-electron capture detector. The OD measurements were conducted with a PerkinElmer Lambda 35 UV-Vis spectrophotometer by transferring 1-mL cell suspension into a cuvette and recording readings at 600 nm.

2.3.6 Dechlorination kinetics and inhibition models.

The shortest doubling times reported for *Geo* strain SZ and *Dhc* strain BAV1 are 6 hours[3] and 2.2 days,[4,33] respectively. Therefore, additional cell growth was considered negligible over the assay period (< 6h) and confirmed by constant OD_{600} values. For this reason, the Michaelis-Menten model (**Table 2.2**), rather than the Monod model for systems involving cell growth, was used to analyze the cell suspension dechlorination data. Therefore, the half-velocity constant K_m, rather than the Monod half-saturation constant K_s, was applied in the analyses of cell suspension kinetic parameters. For each treatment at a different initial substrate concentration [S], an initial dechlorination rate v, normalized to the amount of protein per vial, in units of nmoles Cl^- released min^{-1} mg $protein^{-1}$, was calculated from the sum of all dechlorination products measured with the GC. In brief, the amended PCE, *c*DCE or VC concentrations

in the respective assay vials served as the initial substrate concentrations, and the corresponding dechlorination rates were determined from the slope of progression curves representing total Cl^- released. The linear regression analysis included five data points and at least three for the assays with a low initial chlorinated ethene concentration. Thus, each datum point in the Michaelis-Menten plots represents a dechlorination rate extracted from one initial substrate concentration (**Table 2.3 – 2.5**).

The maximum dechlorination rate V_{max} and the half-velocity constant K_m for each treatment were calculated using the Michaelis-Menten nonlinear regression method in the Enzyme Kinetics Module for SigmaPlot 13 (Systat Software Inc., Chicago, IL, USA). This software module evaluated competitive, noncompetitive, and uncompetitive inhibition models for best fit to the rate data based on the highest coefficient of determination (R^2), the lowest corrected Akaike's Information Criterion (AICc) values, and the lowest standard deviation of the residuals (Sy.x.). The best-fit model (i.e., noncompetitive inhibition) was used to determine the inhibitory constant, K_I, for N_2O on reductive dechlorination. For data visualization, Michaelis-Menten (V over [S]), Lineweaver-Burk (1/V over 1/[S]), and Dixon (1/V over [I]) plots were generated using the SigmaPlot Enzyme Kinetics Module for each inhibition model and the different electron acceptors (i.e., PCE, *c*DCE and VC).

2.4 Results

2.4.1 N_2O affects reductive dechlorination performance in *Geobacter lovleyi* strain SZ cultures.

In the absence of N_2O, *Geo* strain SZ cultures completely dechlorinated 38.1 ± 3.1 µmoles of PCE to stoichiometric amounts of *c*DCE over a 5-day incubation period, and an average PCE-to-*c*DCE dechlorination rate of 155.6 ± 27.2 µmoles Cl^- L^{-1} d^{-1} was measured (**Figure 2.1A**). Cultures amended with 9.5 µM or higher concentrations of N_2O exhibited decreased dechlorination rates and incomplete PCE-to-*c*DCE dechlorination. In the presence of 9.5 µM N_2O, *Geo* strain SZ cultures dechlorinated the initial amount of PCE (38.0 ± 3.9 µmoles) at a dechlorination rate of 90.0 ± 21.6 µmoles Cl^- L^{-1} d^{-1}, leading to an extended time period of at least 7 days to achieve complete consumption of PCE. Although PCE was completely consumed in cultures that received 9.5 µM N_2O, small amounts of TCE (7.6 ± 0.3 µmoles) remained, even after an extended incubation period of 180 days (data not shown). With the addition of 19.1 µM N_2O, the average PCE dechlorination rate in *Geo* strain SZ cultures decreased to 64.2 ± 4.6 µmoles Cl^- L^{-1} d^{-1}, and no more than 78 ± 3.4% of the initial amount of PCE (38.5 ± 1.1 µmoles) was dechlorinated. Following an extended incubation period of 180 days, PCE (9.9 ± 0.2 µmoles), TCE (6.6 ± 1.6 µmoles) and *c*DCE (25.0 ± 3.2 µmoles) were measured in strain SZ cultures that had received an initial dose of 38.5 ± 1.1 µmoles of PCE and 19.1 µM N_2O. A further decline in dechlorination

rate to 12.0 ± 2.1 µmoles Cl^- L^{-1} d^{-1} was observed in cultures that received 57.3 µM N_2O, and 63.4 ± 4.5% of the initial amount of PCE (38.3 ± 3.7 µmoles) remained in culture bottles at the termination of the experiments. In all culture bottles with observed inhibition of dechlorination activity, electron donor (i.e., 5 mM acetate) was not limiting electron acceptor reduction. Furthermore, consistent with the absence of N_2O reductase (*nos*) operons in the genome of *Geo* strain SZ,[32] the amended N_2O remained constant throughout the experiment.

In addition to catalyzing PCE-to-*c*DCE dechlorination, *Geo* strain SZ also derives energy from acetate oxidation coupled to fumarate to succinate reduction.[3] In contrast to organohalide respiration catalyzed by corrinoid-dependent reductive dehalogenases, fumarate respiration via fumarate reductase does not involve a corrinoid-dependent enzyme system.[39] Therefore, investigating the impact of N_2O on fumarate reduction by *Geo* strain SZ cultures served as a control experiment to illustrate the selective effect of N_2O on the PCE RDase in *Geo* strain SZ. As shown in **Figure 2.1B**, the presence of 191.4 µM and 10 mM N_2O did not impact fumarate to succinate reduction rates and extents in *Geo* strain SZ cultures. In the absence of N_2O, *Geo* strain SZ reduced PCE and fumarate concomitantly (**Figure 2.1C, top panel**); however, in cultures amended with 191.4 µM N_2O, only fumarate was reduced to succinate and no PCE reductive dechlorination occurred (**Figure 2.1C, bottom panel**).

2.4.2 N_2O affects *c*DCE and VC reductive dechlorination performance in *Dhc* strain BAV1 cultures.

Without N_2O, *Dhc* strain BAV1 dechlorinated *c*DCE (97.2 ± 3.1µmoles) to stoichiometric amounts of ethene (102.3 ± 6.1 µmoles) within a 14-day incubation period at an average *c*DCE-to-ethene dechlorination rate of 146.1 ± 21.6 µmoles Cl^- L^{-1} d^{-1} (**Figure 2.2A**). In contrast, cultures amended with 9.5 µM or higher N_2O concentrations all exhibited incomplete transformation of *c*DCE and VC, and required longer incubation periods (up to 28 days) before stable dechlorination product patterns were observed. Cultures that received 9.5 µM N_2O showed a significantly lower dechlorination rate of 66.8 ± 21.6 µmoles Cl^- L^{-1} d^{-1}, and the initial amount of *c*DCE (97.2 ±1.2 µmoles) was dechlorinated to a mixture of VC (74.1 ± 1.2 µmoles) and ethene (23.1 ± 0.7 µmoles). Cultures that received 29.0 µM N_2O dechlorinated only about half (50.7 ± 3.3%) of the initial amount of *c*DCE (96.3 ± 1.1 µmoles) to predominantly VC (48.8 ± 3.2 µmoles) at a rate of 24.4 ± 1.1 µmoles Cl^- L^{-1} d^{-1} and only small amounts of ethene (4.7 ± 0.2%) were produced. At a higher N_2O concentration of 57.3 µM, strain BAV1 dechlorinated *c*DCE to VC at a dechlorination rate of 18.9 ± 0.7 µmoles Cl^- L^{-1} d^{-1}, no ethene was formed, and about one third (26.3 ± 0.4 µmoles) of the initial amount of *c*DCE remained. Extended incubation periods of up to 6 months did not result in further dechlorination in all tested strain BAV1 culture vessels with N_2O. Notably, in all N_2O-amended *Dhc* strain BAV1 cultures, the VC-to-ethene dechlorination

step occurred at such low rates resulting in VC, rather than ethene formation as the major product.

To further investigate the impact of N_2O on the reductive dechlorination of VC, *Dhc* strain BAV1 cultures amended with VC as electron acceptor received N_2O at concentrations of 2.9, 5.7, and 19.1 µM. Cultures without N_2O completely dechlorinated the initial amount of 41.2 ± 0.4 µmoles of VC to ethene within 11 days at an average VC dechlorination rate of 37.2 ± 2.7 µmoles Cl^- L^{-1} d^{-1} (**Figure 2.2B**). N_2O had a profound impact on VC dechlorination in *Dhc* strain BAV1 cultures, and the VC dechlorination rates decreased to 18.3 ± 2.1 and 9.8 ± 0.4 µmoles Cl^- L^{-1} d^{-1} in the presence of 2.9 and 5.7 µM N_2O, respectively. Compared to the complete VC to ethene conversion in control incubations without N_2O, the amount of VC dechlorinated to ethene was diminished by 37.0 ± 1.3% and 76.2 ± 4.1%, respectively, in cultures amended with 2.9 and 5.7 µM N_2O. The most pronounced inhibition was observed in *Dhc* strain BAV1 cultures that received 19.1 µM of N_2O, and only negligible amounts (< 1.6 ± 0.6 µmoles) of ethene were formed even after extended incubation periods of 180 days, indicating that the VC to ethene step was particularly susceptible to N_2O inhibition.

2.4.3 Quantification of N_2O inhibition in whole cell suspension dechlorination assays.

To further investigate the inhibitory effects of N_2O on reductive dechlorination, whole cell suspension assays were performed. Plots of dechlorination rates versus initial substrate concentrations with increasing N_2O concentrations are presented in **Figures 2.3 and 2.4**. In all cases, the maximum dechlorination rates decreased with the addition of increasing N_2O concentrations. In *Geo* strain SZ cell suspensions without N_2O addition, a maximum PCE-to-*c*DCE dechlorination rate ($V_{max,PCE}$) of 76.3 ± 2.6 nmoles Cl^- released min^{-1} mg $protein^{-1}$ was calculated using non-linear regression in the Michaelis-Menten model (**Figure 2.3A and Table 2.1**). With the addition of 10 and 60 µM N_2O, $V_{max,PCE}$ in *Geo* strain SZ cell suspensions declined to 61.3 ± 4.1 and 30.9 ± 4.2 nmoles Cl^- released min^{-1} mg $protein^{-1}$, respectively. Even more pronounced inhibitory effects of N_2O were observed for *c*DCE and VC dechlorination in *Dhc* strain BAV1 assays. In the presence of 10 and 60 µM N_2O, the maximum *c*DCE-to-VC dechlorination rate decreased from a $V_{max,cDCE}$ of 119.4 ± 2.1 nmoles Cl^- released min^{-1} mg $protein^{-1}$ in assays without N_2O to 81.1 ± 5.1 and 31.2 ± 2.4 nmoles Cl^- released min^{-1} mg $protein^{-1}$, respectively (Figure 4A and Table 1). The strongest inhibitory effect of N_2O was observed in whole cell suspension assays of strain BAV1 with VC as electron acceptor. Compared to the maximum VC-to-ethene dechlorination rate $V_{max,VC}$ of 123.3 ± 2.2 nmoles Cl^- released min^{-1} mg $protein^{-1}$ without N_2O, the addition of 15 and 50 µM N_2O

reduced $V_{max,VC}$ to 78.9 ± 2.1 and 19.9 ± 1.3 nmoles Cl^- released min^{-1} mg $protein^{-1}$, respectively (**Figure 2.4C and Table 2.1**). No dechlorination was detected in control incubations (data not shown), confirming that suspended cells, rather than any abiotic reactions, were responsible for the observed dechlorination activity.

2.4.4 Kinetic parameters reveal pronounced N_2O inhibition.

The experimental data generated in *Geo* strain SZ cell suspension assays (**Table 2.3**) fit the Michaelis-Menten model and the corresponding Lineweaver-Burk plot ($R^2 > 0.95$) (**Figure 2.3**). A maximum PCE dechlorination rate $V_{max,PCE}$ of 76.3 ± 2.6 nmoles Cl^- released min^{-1} mg $protein^{-1}$ and a half-velocity constant $K_{m,PCE}$ of 25.1 ± 2.9 µM characterized PCE-to-*c*DCE dechlorination kinetics for strain SZ in the absence of N_2O (**Table 2.1, Figure 2.3B**). Without N_2O and in the presence of 10 and 60 µM N_2O, the PCE-to-*c*DCE dechlorination data fit the competitive, uncompetitive and noncompetitive inhibition models ($R^2 > 0.90$); however, with the noncompetitive inhibition model exhibited the highest R^2 and the lowest AICc and Sy.x. values (**Figure 2.3 and Table 2.6**). Using the noncompetitive inhibition model, an inhibitory constant, K_I, of N_2O for PCE dechlorination in *Geo* strain SZ whole cell suspensions of 40.8 ± 3.8 µM was determined (**inserted Dixon plot, Figure 2.3B; Table 2.1**).

The experimental data generated in *Dhc* strain BAV1 whole cell suspension assays (**Tables 2.4 and 2.5**) also fit the Michaelis-Menten model

simulations and the corresponding Lineweaver-Burk plots ($R^2 > 0.90$) (**Figure 2.4**). In the presence of increasing N_2O concentrations, both *c*DCE-to-VC and VC-to-ethene reductive dechlorination assays showed the best fit to the noncompetitive inhibition model based on the highest R^2 and the lowest AICc and Sy.x. values (**Figure 2.4 and Table 2.6**). While *Dhc* strain BAV1 assays produced comparable $V_{max,cDCE}$ and $V_{max,VC}$ values of 119.4 ± 2.1 and 123.3 ± 2.2 nmoles Cl^- released min^{-1} mg $protein^{-1}$, respectively, the K_I of N_2O for *c*DCE dechlorination (21.2 ± 3.5 µM) was approximately 2-fold greater than for VC dechlorination (9.6 ± 0.4 µM) (**inserted Dixon plots, Figures 2.4B and 2.4D; Table 2.1**), consistent with the greater inhibitory effect of N_2O observed for the VC dechlorination step. To investigate if the differences in susceptibility of the *c*DCE and VC dechlorination steps to N_2O resulted from different affinities of the BvcA RDase for *c*DCE and VC, the K_m values for these two electron acceptors were compared. Based on the *Dhc* strain BAV1 assays, similar $K_{m,cDCE}$ (19.9 ± 2.5 µM) and $K_{m,VC}$ (18.9 ± 1.3 µM) values were determined (**Figure 4B and 4D; Table 1**), indicating that the substrate affinity of the BvcA RDase does not explain the more potent inhibition of the VC-to-ethene dechlorination step by N_2O.

2.5 Discussion

2.5.1 Effects of N_2O on corrinoid-dependent processes.

Toxic effects of N_2O were first observed in the mid 1950s after two patients died following prolonged N_2O inhalation.[40] This incident triggered studies to elucidate the mechanism underlying N_2O toxicity, and detailed investigations revealed that N_2O reacts with cobalt-containing corrinoids (e.g., cobalamin) when the coordinated cobalt atom is in the reduced Co(I) state.[25,26] Due to the vital roles of enzyme systems with corrinoid prosthetic groups,[30,41] the N_2O-mediated oxidation of the Co(I) supernucleophile interferes with key metabolic functions in all domains of life.[42,43] For example, N_2O inhibits the corrinoid-dependent methionine synthase (MetH) required for the biosynthesis of the essential amino acid methionine.[44] When used as inhalation anesthetic for human patients, N_2O can lead to a malfunction of MetH, resulting in elevated levels of homocysteine in plasma (i.e., hyperhomocysteinemia).[45] Patients generally recover from N_2O exposure after 3 – 4 days,[44] presumably through *de novo* MetH synthesis or replenishment of Co(I) corrinoid.[46]

The lowest reported N_2O concentration that affected MetH activity in animals and humans was around 4.1 mM (~1,000 ppm);[46] however, much lower N_2O concentrations inhibited members of the Bacteria and Archaea, presumably due to the more diverse roles of corrinoid-dependent enzyme systems in their metabolisms.[41] For example, in the denitrifying bacterium *Paracoccus*

denitrificans strain PD1222, 0.1 mM N_2O not only repressed MetH but also modulated the expression of anabolic genes under the control of vitamin B_{12} riboswitches.[47] To compensate for the loss of MetH function, organisms such as *P. denitrificans* and *Escherichia coli* activate a corrinoid-independent methionine synthase, MetE.[41,47] *Geo* strain SZ possesses both the *metE* and *metH* genes,[32] what may explain the observation that up to 10 mM N_2O did not inhibit the bacterium's growth with fumarate in defined minimal medium. In contrast, N_2O at micromolar concentrations inhibited the growth of *Geo* strain SZ cultures when PCE served as the sole electron acceptor. These observations corroborate that the inhibitory effect of N_2O to organisms varies markedly based on whether corrinoid-dependent enzyme systems are essential for key metabolic steps, including respiratory energy conservation.

2.5.2 OHRB as a model to study the effects of N_2O inhibition.

A key feature of OHRB is the involvement of corrinoid-dependent RDases in electron transfer to the chlorinated organohalogen electron acceptor.[1,28,29,48] Functional and structural analyses demonstrated that RDases represent a distinct subfamily of corrinoid-dependent enzymes and a Co(I) supernucleophile is crucial for RDases to initiate the cleavage of carbon-chlorine bonds.[28,29,49] Since corrinoid-dependent RDases are essential in the energy metabolism of OHRB, N_2O inhibition on Co(I) corrinoid-dependent RDases can be readily observed by quantitative measurement of dechlorination activity and growth

when alternate electron acceptors are absent, or the energy metabolism of the OHRB is restricted to chlorinated electron acceptors, as is the case for *Dhc*.[4] This effect was convincingly demonstrated in both *Geo* strain SZ and *Dhc* strain BAV1 cultures amended with chlorinated electron acceptors and N_2O. Thus, OHRB are excellent model organisms to assess the inhibitory effects of N_2O on enzymes involving the Co(I) supernucleophile in catalysis. Consistent with this assumption, experimental results showed that N_2O at micromolar concentrations exhibited strong inhibitory effects on reductive dechlorination performance in both *Geo* strain SZ and *Dhc* strain BAV1 cultures. Theoretically, a shortage of methionine caused by N_2O inhibition on MetH could also have affected dechlorination activity; however, growth of *Geo* strain SZ with fumarate was not impaired at much higher N_2O concentrations of up to 10 mM, indicating that N_2O inhibition of RDases diminished dechlorination performance.

The PCE-to-*c*DCE dechlorinating *Geo* strain SZ tolerated at least 3-fold higher N_2O concentrations than *Dhc* strain BAV1 before cessation of dechlorination activity was observed, which possibly relates to strain SZ's ability for *de novo* cobamide biosynthesis.[32] Active cobamide biosynthesis may allow strain SZ to maintain some level of catalytically active PCE RDase. In contrast, the characterized obligate organohalide-respiring *Dhc* strains[4,50] and *Dehalogenimonas* spp., including the VC-respiring *Candidatus* Dehalogenimonas etheniformans,[5] cannot *de novo* synthesize corrinoid, although exceptions may exist.[51] All characterized *c*DCE and VC dechlorinators strictly require exogenous

corrinoid, which renders these bacteria more susceptible to N_2O inhibition, and low micromolar concentrations of N_2O (i.e., 3 – 10 µM) repressed the growth of the corrinoid-auxotroph *Dhc* strain BAV1. Unlike corrinoid-auxotrophic Dehalococcoidia, the majority of PCE-to-TCE and TCE-to-*c*DCE-dechlorinating OHRB are corrinoid prototrophs,[52] a feature that may enable these organisms to tolerate higher N_2O concentrations. The difference in the ability for *de novo* corrinoid biosynthesis is one possible explanation why PCE and TCE dechlorination to *c*DCE is generally achieved at sites with nitrate,[16,53] but ethene is not produced.[7-10]

Corrinoid-dependent enzyme systems fulfill essential metabolic functions for organisms in all branches of life, but only a subset of the bacteria and archaea have the machinery for *de novo* corrinoid biosynthesis.[41,54,55] Therefore, N_2O effects on microbial processes that hinge on the activity of corrinoid-dependent enzyme systems may expand beyond organohalide respiration.

2.5.3 Elevated groundwater N_2O and kinetic parameters.

Based the current day atmospheric N_2O concentration of 330 ppb, the theoretical equilibrium concentration of N_2O in groundwater should be around 7 nM, assuming no mass transfer limitations; however, much higher groundwater N_2O concentrations were reported indicating other sources exist.[31,56] For example, the increased usage of synthetic nitrogen fertilizer for agricultural production causes substantial nitrate run-off and elevated N_2O concentrations in

groundwater.[19,31] Indeed, correlations between fertilizer application and associated nitrate run-off with elevated groundwater N_2O concentrations have been established.[19,56] Nitrate is not conservative and processes including denitrification,[18,19] respiratory ammonification (i.e., dissimilatory nitrate reduction to ammonium, DNRA)[57] and ensuing nitrification,[21] as well as chemodenitrification[38] contribute to the formation of N_2O. Such biogeochemical processes are likely responsible for elevated N_2O concentrations and up to 140 µM N_2O were observed in watersheds impacted by agricultural activities.[31] Thus, the N_2O concentrations measured in many groundwater aquifers exceed the theoretical equilibrium with atmospheric N_2O by up to 5 orders in magnitude, and intensified agriculture will exacerbate this issue.

A K_I value indicates the inhibitor (i.e., N_2O) concentration, at which the maximum reaction rate V_{max} (i.e., the reductive dechlorination rates of chlorinated ethenes) is reduced by 50%. The determined K_I values for N_2O on reductive dechlorination of PCE, *c*DCE and VC are in the range of 40, 20 and 10 µM, respectively, well below reported N_2O concentrations encountered in many groundwater aquifers, particularly at sites impacted by agricultural run-off.[31] Consequently, N_2O inhibition could be a major cause for incomplete reductive dechlorination and *c*DCE and VC stalls observed at field sites.[7-10,53] Of note, a 50% $V_{max,cDCE}$ and $V_{max,VC}$ inhibition occurred in strain BAV1 at 2- and 4-fold lower N_2O concentrations, respectively, compared to the same level of inhibition of $V_{max,PCE}$ in strain SZ. The higher K_I values for N_2O determined for *Geo* strain

SZ compared to strain BAV1 may be related to the ability of strain SZ for *de novo* corrinoid biosynthesis (see above), or to mechanistic differences in the dechlorination steps catalyzed by the PceA versus the BvcA RDases. Similar K_m values for *c*DCE and VC were determined in strain BAV1 indicating the organism exhibits similar affinities for *c*DCE and VC; however, the 2-fold higher K_I value for the *c*DCE versus the VC dechlorination step cannot be easily explained considering the same BvcA RDase is involved in both dechlorination steps,[52,58] and detailed mechanistic studies are warranted.

Predicting the fate of chlorinated ethenes at bioremediation sites relies on accurate estimates of the intrinsic kinetic parameters of OHRB;[59] however, kinetic constants determinations using various dechlorinating cultures at different cell densities reported highly variable V_{max} and K_m values (or K_S values when Monod kinetics were applied).[12,60,61] Likely explanations for these discrepancies are that different, potentially competing types of dechlorinators with distinct RDases and present in varied abundances contributed to *c*DCE reductive dechlorination.[12,62,63] The current study accomplished kinetic measurements in axenic cultures under defined conditions and over short incubation periods (< 6h, no growth occurred), which facilitates the determination of intrinsic kinetic parameters.[59] The Michaelis-Menten model simulations predicted the behaviors of *Geo* strain SZ and *Dhc* strain BAV1 (R^2 >0.90) and both organisms fit the noncompetitive inhibition model (R^2 >0.96) with micromolar levels of N_2O as the inhibitor. These findings imply N_2O as a noncompetitive inhibitor that oxidizes the

Co(I) corrinoid cofactor of RDases, thereby decreasing reductive dechlorination rates.

2.5.4 Implications for *in situ* bioremediation.

Electron donor (i.e., hydrogen) limitations,[6] nutrient availability (e.g., fixed nitrogen),[15] unfavorable redox potential,[7,11] low pH conditions,[14] or toxic and/or inhibitory effects of co-contaminants (e.g., sulfide, chloroform, 1,1,1-trichloroethane),[12,62] can impact the microbial reductive dechlorination process. The findings of the current study indicate that decreased reductive dechlorination performance can be the result of N_2O inhibition. A common strategy to improve *in situ* degradation of chlorinated ethenes involves the injection of nutrients (i.e., biostimulation), typically fermentable substrates aimed at increasing the flux of hydrogen.[2,64] The formulations can include fertilizer (nitrate, ammonium, urea, phosphorus) to proactively address possible nutrient limitations.[2,13,15,65] Biogeochemical transformations of fixed nitrogen will generate N_2O,[21,38,57] and exert inhibitory effects on microbial reductive dechlorination, which can result in undesirable *c*DCE or VC stalls. Thus, practitioners should carefully evaluate the need for fixed nitrogen additions to avoid possible N_2O inhibition.

The inhibitory constants, K_I, for N_2O inhibition of PCE, *c*DCE and VC dechlorination were within the N_2O concentration ranges observed in groundwater aquifers (i.e., up to 143 µM),[31] suggesting that N_2O should be of concern at contaminated sites where practitioners seek to rely on microbial

reductive dechlorination as a remedial strategy. Considering the relevance of the microbial reductive dechlorination process for achieving cleanup goals and the commonality of elevated N_2O concentrations in aquifers, groundwater monitoring regimes should include nitrate/nitrite and N_2O measurements, so that potential inhibition and *c*DCE and VC stalls can be explained and predicted.

2.6 Acknowledgments

This work was supported by the Strategic Environmental Research and Development Program (SERDP project ER-2312) and, in part, by awards from National Institute of Environmental Health Sciences (R01ES024294) and the National Science Foundation (Dimensions DEB1831599). Y. Y participates in the China-University of Tennessee One-Hundred Scholars Program, and the authors acknowledge the support by the China Scholarship Council and the University of Tennessee.

2.7 References

(1) Adrian, L.; Löffler, F. E., *Organohalide-respiring bacteria*. Springer: Berlin Heidelberg: 2016.

(2) Löffler, F. E.; Edwards, E. A., Harnessing microbial activities for environmental cleanup. *Curr Opin Biotechnol* **2006,** *17* (3), 274-284.

(3) Sung, Y.; Fletcher, K. E.; Ritalahti, K. M.; Apkarian, R. P.; Ramos-Hernández, N.; Sanford, R. A.; Mesbah, N. M.; Löffler, F. E., *Geobacter lovleyi* sp. nov. strain SZ, a novel metal-reducing and tetrachloroethene-dechlorinating bacterium. *Appl Environ Microbiol* **2006,** *72* (4), 2775-2782.

(4) Löffler, F. E.; Yan, J.; Ritalahti, K. M.; Adrian, L.; Edwards, E. A.; Konstantinidis, K. T.; Müller, J. A.; Fullerton, H.; Zinder, S. H.; Spormann, A. M., *Dehalococcoides mccartyi gen. nov., sp. nov.*, obligately organohalide-respiring anaerobic bacteria relevant to halogen cycling and bioremediation, belong to a novel bacterial class, *Dehalococcoidia classis nov.*, order *Dehalococcoidales ord. nov.* and family *Dehalococcoidaceae fam. nov*., within the phylum *Chloroflexi*. *Int J Syst Evol Microbiol* **2013,** *63* (2), 625-635.

(5) Yang, Y.; Higgins, S. A.; Yan, J.; Simsir, B.; Chourey, K.; Iyer, R.; Hettich, R. L.; Baldwin, B.; Ogles, D. M.; Löffler, F. E., Grape pomace compost harbors organohalide-respiring Dehalogenimonas species with novel reductive dehalogenase genes. *ISME J* **2017,** *11* (12), 2767-2780.

(6) Fennell, D. E.; Gossett, J. M.; Zinder, S. H., Comparison of butyric acid, ethanol, lactic acid, and propionic acid as hydrogen donors for the reductive dechlorination of tetrachloroethene. *Environ Sci Technol* **1997,** *31* (3), 918-926.

(7) Schmidt, K. R.; Tiehm, A., Natural attenuation of chloroethenes: identification of sequential reductive/oxidative biodegradation by microcosm studies. *Water Sci Technol* **2008,** *58* (5), 1137-1145.

(8) Amaral, H. I.; Aeppli, C.; Kipfer, R.; Berg, M., Assessing the transformation of chlorinated ethenes in aquifers with limited potential for natural attenuation: added values of compound-specific carbon isotope analysis and groundwater dating. *Chemosphere* **2011,** *85* (5), 774-781.

(9) Dugat-Bony, E.; Biderre-Petit, C.; Jaziri, F.; David, M. M.; Denonfoux, J.; Lyon, D. Y.; Richard, J. Y.; Curvers, C.; Boucher, D.; Vogel, T. M.; Peyretaillade, E.; Peyret, P., *In situ* TCE degradation mediated by complex dehalorespiring communities during biostimulation processes. *Microb Biotechnol* **2012,** *5* (5), 642-653.

(10) Tillotson, J. M.; Borden, R. C., Rate and extent of chlorinated ethene removal at 37 ERD sites. *J Environ Eng* **2017,** *143* (8), 04017028.

(11) Nelson, D. K.; Hozalski, R. M.; Clapp, L. W.; Semmens, M. J.; Novak, P. J., Effect of nitrate and sulfate on dechlorination by a mixed hydrogen-fed culture. *Bioremed J* **2002,** *6* (3), 225-236.

(12) Berggren, D. R.; Marshall, I. P.; Azizian, M. F.; Spormann, A. M.; Semprini, L., Effects of sulfate reduction on the bacterial community and kinetic parameters of a dechlorinating culture under chemostat growth conditions. *Environ Sci Technol* **2013,** *47* (4), 1879-1886.

(13) Steffan, R. J.; Schaefer, C. E., Current and future bioremediation applications: bioremediation from a practical and regulatory perspective. In *Organohalide-respiring bacteria*, Adrian, L.; Löffler, F. E., Eds. Springer Berlin Heidelberg: Berlin, Heidelberg, 2016; pp 517-540.

(14) Yang, Y.; Capiro, N. L.; Marcet, T. F.; Yan, J.; Pennell, K. D.; Löffler, F. E., Organohalide respiration with chlorinated ethenes under low pH conditions. *Environ Sci Technol* **2017,** *51* (15), 8579-8588.

(15) Lendvay, J. M.; Löffler, F. E.; Dollhopf, M.; Aiello, M. R.; Daniels, G.; Fathepure, B. Z.; Gebhard, M.; Heine, R.; Helton, R.; Shi, J., Bioreactive barriers: a comparison of bioaugmentation and biostimulation for chlorinated solvent remediation. *Environ Sci Technol* **2003,** *37* (7), 1422-1431.

(16) Lee, J.; Im, J.; Kim, U.; Löffler, F. E., A data mining approach to predict In situ detoxification potential of chlorinated ethenes. *Environ Sci Technol* **2016,** *50* (10), 5181-5188.

(17) He, J.; Sung, Y.; Krajmalnik-Brown, R.; Ritalahti, K. M.; Löffler, F. E., Isolation and characterization of *Dehalococcoides sp*. strain FL2, a trichloroethene (TCE)-and 1,2-dichloroethene-respiring anaerobe. *Environ Microbiol* **2005,** *7* (9), 1442-1450.

(18) Zumft, W. G., Cell biology and molecular basis of denitrification. *Microbiol Mol Biol Rev* **1997,** *61* (4), 533-616.

(19) Thomson, A. J.; Giannopoulos, G.; Pretty, J.; Baggs, E. M.; Richardson, D. J., Biological sources and sinks of nitrous oxide and strategies to mitigate emissions. *Philos Trans R Soc Lond B Biol Sci* **2012,** *367* (1593), 1157-1168.

(20) Zhu, X.; Burger, M.; Doane, T. A.; Horwath, W. R., Ammonia oxidation pathways and nitrifier denitrification are significant sources of N_2O and NO under low oxygen availability. *Proc Natl Acad Sci USA* **2013,** *110* (16), 6328-6333.

(21) Daims, H.; Lücker, S.; Wagner, M., A new perspective on microbes formerly known as nitrite-oxidizing bacteria. *Trends Microbiol* **2016,** *24* (9), 699-712.

(22) Balderston, W. L.; Payne, W. J., Inhibition of methanogenesis in salt marsh sediments and whole-cell suspensions of methanogenic bacteria by nitrogen oxides. *Appl Environ Microbiol* **1976,** *32* (2), 264-269.

(23) Klüber, H. D.; Conrad, R., Inhibitory effects of nitrate, nitrite, NO and N_2O on methanogenesis by *methanosarcina barkeri* and *Methanobacterium bryantii*. *FEMS Microbiol Ecol* **1998,** *25*, 331-339.

(24) Tugtas, A. E.; Pavlostathis, S. G., Inhibitory effects of nitrogen oxides on a mixed methanogenic culture. *Biotechnol Bioeng* **2007,** *96* (3), 444-455.

(25) Banks, R. G. S.; Henderson, R. J.; Pratt, J. M., Reactions of gases in solution. Part III. Some reactions of nitrous oxide with transition-metal complexes. *J Chem Soc Sec A* **1968,** (0), 2886-2889.

(26) Blackburn, R.; Kyaw, M.; Swallow, A. J., Reaction of cob(I)alamin with nitrous oxide and cob(III)alamin. *J Chem Soc, Faraday Trans I* **1977,** *73* (0), 250-255.

(27) Fischer, R.; Thauer, R. K., Methanogenesis from acetate in cell extracts of *Methanosarcina barkeri*: isotope exchange between CO_2 and the carbonyl group of acetyl-CoA, and the role of H_2. *Arch Microbiol* **1990,** *153* (2), 156-162.

(28) Bommer, M.; Kunze, C.; Fesseler, J.; Schubert, T.; Diekert, G.; Dobbek, H., Structural basis for organohalide respiration. *Science* **2014,** *346* (6208), 455-458.

(29) Payne, K. A.; Quezada, C. P.; Fisher, K.; Dunstan, M. S.; Collins, F. A.; Sjuts, H.; Levy, C.; Hay, S.; Rigby, S. E.; Leys, D., Reductive dehalogenase structure suggests a mechanism for B_{12}-dependent dehalogenation. *Nature* **2015,** *517* (7535), 513-516.

(30) Yan, J.; Bi, M.; Bourdon, A. K.; Farmer, A. T.; Wang, P. H.; Molenda, O.; Quaile, A. T.; Jiang, N.; Yang, Y.; Yin, Y.; Şimşir, B.; Campagna, S. R.; Edwards, E. A.; Löffler, F. E., Purinyl-cobamide is a native prosthetic group of reductive dehalogenases. *Nat Chem Biol* **2018,** *14* (1), 8-14.

(31) Jurado, A.; Borges, A. V.; Brouyere, S., Dynamics and emissions of N_2O in groundwater: A review. *Sci Total Environ* **2017,** *584*, 207-218.

(32) Wagner, D. D.; Hug, L. A.; Hatt, J. K.; Spitzmiller, M. R.; Padilla-Crespo, E.; Ritalahti, K. M.; Edwards, E. A.; Konstantinidis, K. T.; Löffler, F. E., Genomic determinants of organohalide-respiration in *Geobacter lovleyi*, an unusual member of the *Geobacteraceae*. *BMC Genomics* **2012,** *13* (1), 200.

(33) He, J.; Ritalahti, K. M.; Yang, K. L.; Koenigsberg, S. S.; Löffler, F. E., Detoxification of vinyl chloride to ethene coupled to growth of an anaerobic bacterium. *Nature* **2003,** *424* (6944), 62-65.

(34) Yan, J.; Şimşir, B.; Farmer, A. T.; Bi, M.; Yang, Y.; Campagna, S. R.; Löffler, F. E., The corrinoid cofactor of reductive dehalogenases affects dechlorination rates and extents in organohalide-respiring *Dehalococcoides mccartyi*. *ISME J* **2016,** *10* (5), 1092-1101.

(35) Wolin, E. A.; Wolin, M. J.; Wolfe, R. S., Formation of methane by bacterial extracts. *J Biol Chem* **1963,** *238* (8), 2882-2886.

(36) Sander, R., Compilation of Henry's law constants (version 4.0) for water as solvent. *Atmos Chem Physics* **2015,** *15* (8), 4399-4981.

(37) Bradford, M. M., A rapid and sensitive method for the quantitation of microgram quantities of protein utilizing the principle of protein-dye binding. *Anal Biochem* **1976,** *72* (1), 248-254.

(38) Onley, J. R.; Ahsan, S.; Sanford, R. A.; Löffler, F. E., Denitrification by *Anaeromyxobacter dehalogenans*, a common soil bacterium lacking the nitrite reductase genes *nirS* and *nirK*. *Appl Environ Microbiol* **2018,** *84* (4), e01985-17.

(39) Iverson, T. M.; Luna-Chavez, C.; Cecchini, G.; Rees, D. C., Structure of the *Escherichia coli* fumarate reductase respiratory complex. *Science* **1999,** *284* (5422), 1961-1966.

(40) Lassen, H. C. A.; Henriksen, E.; Neukirch, F.; Kristensen, H., Treatment of tetanus. Severe bone-marrow depression after prolonged nitrous-oxide anaesthesia. *Lancet* **1956**, 527-530.

(41) Matthews, R. G., Cobalamin- and corrinoid-dependent enzymes. *Met Ions Life Sci* **2009,** *6*, 53-114.

(42) Drummond, J. T.; Matthews, R. G., Nitrous oxide degradation by cobalamin-dependent methionine synthase: characterization of the reactants and products in the inactivation reaction. *Biochemistry* **1994,** *33*, 3732-3741.

(43) Drummond, J. T.; Matthews, R. G., Nitrous oxide inactivation of cobalamin-dependent methionine synthase from *Escherichia coli*: characterization of the damage to the enzyme and prosthetic group. *Biochemistry* **1994,** *33* (12), 3742-3750.

(44) Royston, B. D.; Nunn, J. F.; Weinbren, H. K.; Royston, D.; Cormack, R. S., Rate of inactivation of human and rodent hepatic methionine synthase by nitrous oxide. *Anesthesiology* **1988,** *68* (2), 213-216.

(45) Singer, M. A.; Lazaridis, C.; Nations, S. P.; Wolfe, G. I., Reversible nitrous oxide-induced myeloneuropathy with pernicious anemia: case report and literature review. *Muscle Nerve* **2008,** *37* (1), 125-129.

(46) Weimann, J., Toxicity of nitrous oxide. *Best Prac Res Clin Anaesthesiol* **2003,** *17* (1), 47-61.

(47) Sullivan, M. J.; Gates, A. J.; Appia-Ayme, C.; Rowley, G.; Richardson, D. J., Copper control of bacterial nitrous oxide emission and its impact on vitamin B_{12}-dependent metabolism. *Proc Natl Acad Sci USA* **2013,** *110* (49), 19926-19931.

(48) Wang, S.; Qiu, L.; Liu, X.; Xu, G.; Siegert, M.; Lu, Q.; Juneau, P.; Yu, L.; Liang, D.; He, Z.; Qiu, R., Electron transport chains in organohalide-respiring bacteria and bioremediation implications. *Biotechnol Adv* **2018,** *36* (4), 1194-1206.

(49) Fincker, M.; Spormann, A. M., Biochemistry of catabolic reductive dehalogenation. *Annu Rev Biochem* **2017,** *86*, 357-386.

(50) Seshadri, R.; Adrian, L.; Fouts, D. E.; Eisen, J. A.; Phillippy, A. M.; Methe, B. A.; Ward, N. L.; Nelson, W. C.; Deboy, R. T.; Khouri, H. M.; Kolonay, J. F.; Dodson, R. J.; Daugherty, S. C.; Brinkac, L. M.; Sullivan, S. A.; Madupu, R.; Nelson, K. E.; Kang, K. H.; Impraim, M.; Tran, K.; Robinson, J. M.; Forberger, H. A.; Fraser, C. M.; Zinder, S. H.; Heidelberg, J. F., Genome sequence of the PCE-dechlorinating bacterium *Dehalococcoides ethenogenes*. *Science* **2005,** *307* (5706), 105-108.

(51) Brisson, V. L.; West, K. A.; Lee, P. K. H.; Tringe, S. G.; Brodie, E. L.; Alvarez-Cohen, L., Metagenomic analysis of a stable trichloroethene-degrading microbial community. *ISME J* **2012,** *6* (9), 1702-1714.

(52) Schubert, T.; Adrian, L.; Sawers, R. G.; Diekert, G., Organohalide respiratory chains: composition, topology and key enzymes. *FEMS Microbiol Ecol* **2018,** *94* (4), fiy035.

(53) Verce, M. F.; Madrid, V. M.; Gregory, S. D.; Demir, Z.; Singleton, M. J.; Salazar, E. P.; Jackson, P. J.; Halden, R. U.; Verce, A., A long-term field study of *in situ* bioremediation in a fractured conglomerate trichloroethene source zone. *Bioremed J* **2015,** *19* (1), 18-31.

(54) Shelton, A. N.; Seth, E. C.; Mok, K. C.; Han, A. W.; Jackson, S. N.; Haft, D. R.; Taga, M. E., Uneven distribution of cobamide biosynthesis and dependence in bacteria predicted by comparative genomics. *ISME J* **2018,** *DOI.org/10.1038/s41396-018-0304-9*.

(55) Zhang, Y.; Rodionov, D. A.; Gelfand, M. S.; Gladyshev, V. N., Comparative genomic analyses of nickel, cobalt and vitamin B_{12} utilization. *BMC Genomics* **2009,** *10* (1), 78.

(56) Reay, D. S.; Davidson, E. A.; Smith, K. A.; Smith, P.; Melillo, J. M.; Dentener, F.; Crutzen, P. J., Global agriculture and nitrous oxide emissions. *Nat Clim Change* **2012,** *2* (6), 410-416.

(57) Yoon, S.; Cruz-García, C.; Sanford, R.; Ritalahti, K. M.; Löffler, F. E., Denitrification versus respiratory ammonification: environmental controls of two competing dissimilatory NO_3^-/NO_2^- reduction pathways in *Shewanella loihica* strain PV-4. *ISME J* **2015,** *9* (5), 1093-1104.

(58) Tang, S.; Chan, W. W. M.; Fletcher, K. E.; Seifert, J.; Liang, X.; Löffler, F. E.; Edwards, E. A.; Adrian, L., Functional characterization of reductive dehalogenases by using blue native polyacrylamide gel electrophoresis. *Appl Environ Microbiol* **2013,** *79* (3), 974-981.

(59) Huang, D.; Becker, J. G., Determination of intrinsic monod kinetic parameters for two heterotrophic tetrachloroethene (PCE)-respiring strains and insight into their application. *Biotechnol Bioeng* **2009,** *104* (2), 301-311.

(60) Baelum, J.; Scheutz, C.; Chambon, J. C.; Jensen, C. M.; Brochmann, R. P.; Dennis, P.; Laier, T.; Broholm, M. M.; Bjerg, P. L.; Binning, P. J.; Jacobsen, C. S., The impact of bioaugmentation on dechlorination kinetics and on microbial dechlorinating communities in subsurface clay till. *Environ Pollut* **2014,** *186*, 149-157.

(61) Mayer-Blackwell, K.; Fincker, M.; Molenda, O.; Callahan, B.; Sewell, H.; Holmes, S.; Edwards, E. A.; Spormann, A. M., 1,2-dichloroethane exposure alters the population structure, metabolism, and kinetics of a trichloroethene-dechlorinating *Dehalococcoides mccartyi* consortium. *Environ Sci Technol* **2016,** *50* (22), 12187-12196.

(62) Chan, W. W.; Grostern, A.; Löffler, F. E.; Edwards, E. A., Quantifying the effects of 1,1,1-trichloroethane and 1,1-dichloroethane on chlorinated ethene reductive dehalogenases. *Environ Sci Technol* **2011,** *45* (22), 9693-9702.

(63) Buttet, G. F.; Murray, A. M.; Goris, T.; Burion, M.; Jin, B.; Rolle, M.; Holliger, C.; Maillard, J., Coexistence of two distinct Sulfurospirillum populations respiring tetrachloroethene—genomic and kinetic considerations. *FEMS Microbiol Ecol* **2018,** *94* (5), fiy018.

(64) McCarty, P. L., Groundwater contamination by chlorinated solvents: History, remediation technologies and strategies. In *In Situ remediation of chlorinated*

solvent plumes, Stroo, H. F.; Ward, C. H., Eds. Springer New York: New York, NY, 2010; pp 1-28.

(65) Schaefer, C. E.; Lippincott, D. R.; Steffan, R. J., Field-scale evaluation of bioaugmentation dosage for treating chlorinated ethenes. *Groundwater Monit Remediat* **2010,** *30* (3), 113-124

2.8 Appendix

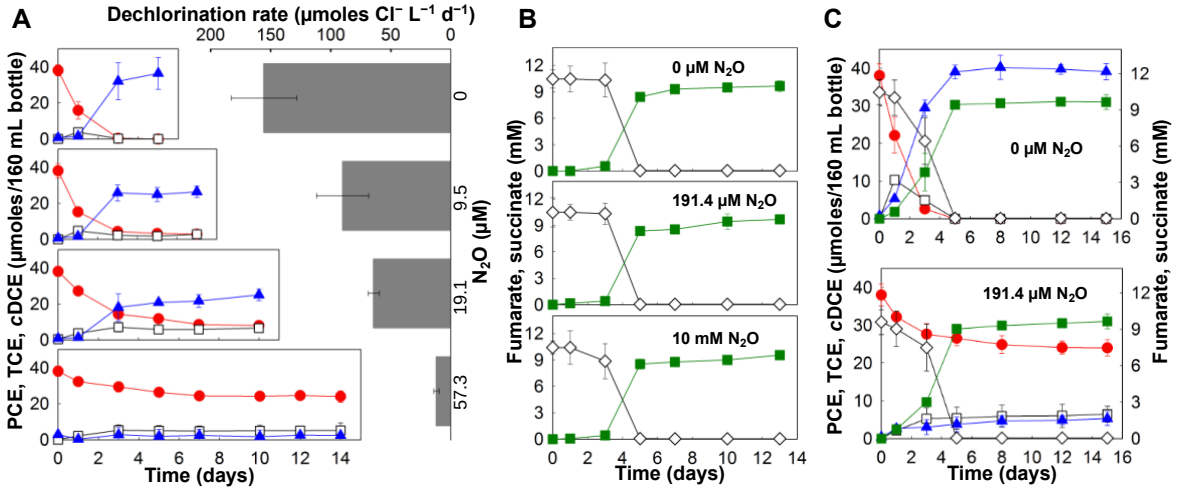


Figure 2.1. Effect of N_2O on the consumption of PCE (A), fumarate (B), or both PCE and fumarate (C) as electron acceptors in cultures of *Geo* strain SZ. (A) PCE-to-*c*DCE reductive dechlorination rates and extents in *Geo* strain SZ cultures without N_2O and in the presence of 9.5, 19.1 and 57.3 μM N_2O. **(B)** Fumarate-to-succinate reduction in *Geo* strain SZ cultures without N_2O and in the presence of 191.4 μM and 10 mM N_2O. **(C)** PCE-to-*c*DCE reductive dechlorination and fumarate-to-succinate reduction in *Geo* strain SZ cultures in the absence of N_2O and in the presence of 191.4 μM N_2O (bottom panel). Solid red circles, PCE; open squares, TCE; solid blue triangles, *c*DCE; open diamonds, fumarate; and solid green squares, succinate. Error bars represent the s.d. of triplicate cultures.

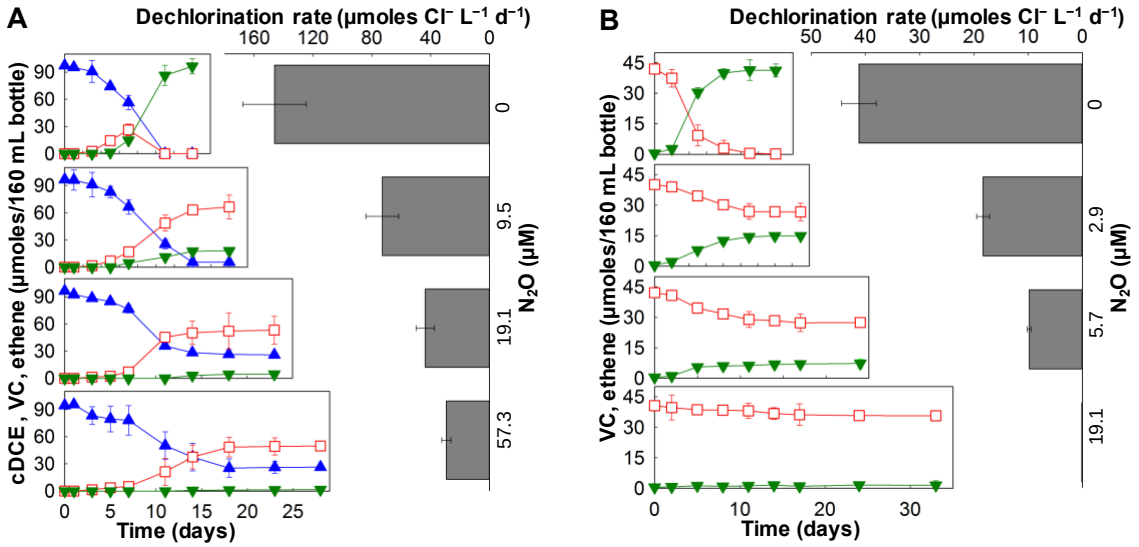


Figure 2.2. Effect of N_2O on reductive dechlorination of *c*DCE (A) and VC (B) in corrinoid auxotrophic *Dhc* strain BAV1. (A) *c*DCE reductive dechlorination rates and extents in *Dhc* strain BAV1 without N_2O (top panel) and in the presence of 9.5, 29.0 and 57.3 µM N_2O. **(B)** VC reductive dechlorination rates and extents in *Dhc* strain BAV1 without N_2O (top panel) and in the presence of 2.9, 5.7 and 19.1 µM N_2O. Solid blue triangles, *c*DCE; open red squares, VC; inverted, solid green triangles, ethene. Error bars represent the s.d. of triplicate cultures.

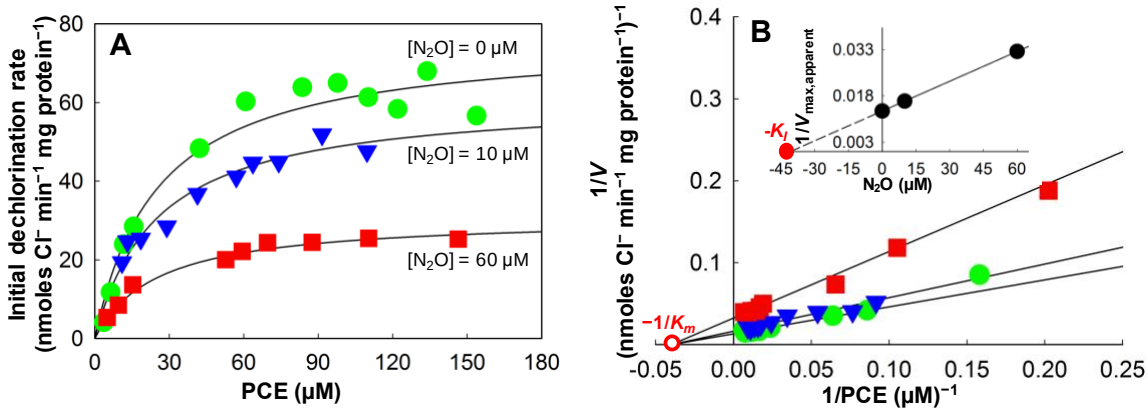


Figure 2.3. Kinetics of *c*DCE-to-VC and VC-to-ethene reductive dechlorination in cell suspensions of *Dhc* strain BAV1 in the presence of increasing concentrations of N_2O. (A) Michaelis-Menten plot of initial *c*DCE-to-VC dechlorination in cell suspension of *Dhc* strain BAV1 without and in the presence of 10 and 60 μM N_2O. **(B)** Lineweaver-Burk plot with inserted Dixon plot illustrating N_2O inhibition of *c*DCE-to-VC reductive dechlorination. **(C)** Michaelis-Menten plot of initial VC-to-ethene dechlorination in cell suspension of *Dhc* strain BAV1 without and in the presence of 15 and 50 μM N_2O. **(D)** Lineweaver-Burk plot with inserted Dixon plot illustrating N_2O inhibition of VC-to-ethene reductive dechlorination. Solid lines represent the best fit to each data set based on nonlinear regression using the noncompetitive inhibition model. Solid green circles represent rate data measured in the absence of N_2O; solid blue triangles and solid red squares show dechlorination rate data measured in the presence of N_2O (panels A and B, *c*DCE; panels C and D, VC). The solid and open red circles shown in panels B and D depict the graphical determination of $-K_I$ and $-1/K_m$, respectively.

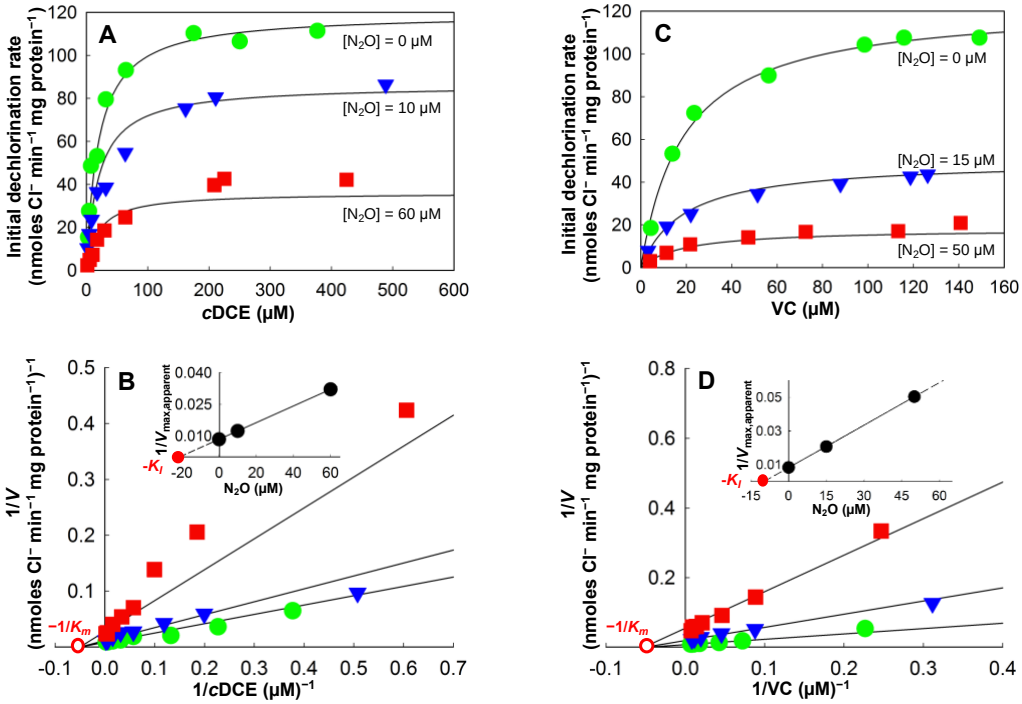


Figure 2.4. Kinetics of *c*DCE-to-VC and VC-to-ethene reductive dechlorination in cell suspensions of *Dhc* strain BAV1 in the presence of increasing concentrations of N_2O. (A) Michaelis-Menten plot of initial *c*DCE-to-VC dechlorination in cell suspension of *Dhc* strain BAV1 without and in the presence of 10 and 60 μM N_2O. **(B)** Lineweaver-Burk plot with inserted Dixon plot illustrating N_2O inhibition of *c*DCE-to-VC reductive dechlorination. **(C)** Michaelis-Menten plot of initial VC-to-ethene dechlorination in cell suspension of *Dhc* strain BAV1 without and in the presence of 15 and 50 μM N_2O. **(D)** Lineweaver-Burk plot with inserted Dixon plot illustrating N_2O inhibition of VC-to-ethene reductive dechlorination. Solid lines represent the best fit to each data set based on nonlinear regression using the noncompetitive inhibition model. Solid green circles represent rate data measured in the absence of N_2O; solid blue triangles and solid red squares show dechlorination rate data measured in the presence of N_2O (panels A and B, *c*DCE; panels C and D, VC). The solid and open red circles shown in panels B and D depict the graphical determination of $-K_I$ and $-1/K_m$, respectively.

Table 2.1. Kinetic (V_{max}, K_m) and inhibition (K_I) parameters for PCE, cDCE and VC reductive dechlorination in cell suspension of Geo strain SZ and Dhc strain BAV1 in response to increasing N_2O concentrations.[a]

Electron Acceptor	Culture	N_2O (μM)	V_{max} (nmol Cl^- min^{-1} mg $protein^{-1}$)	K_m (μM)	K_I (μM)
PCE	Strain SZ	0	76.3 (±2.6)		
		10	61.3 (±4.1)	25.1 (±2.9)	40.8 (±3.8)
		60	30.9 (±4.2)		
*c*DCE	Strain BAV1	0	119.4 (±4.1)		
		10	81.1 (±5.1)	19.9 (±2.5)	21.2 (±3.5)
		60	31.2 (±2.4)		
VC	Strain BAV1	0	123.3 (±3.2)		
		15	78.9 (±2.1)	18.9 (±1.3)	9.6 (±0.4)
		50	19.9 (±1.3)		

[a]The best fit data were achieved with the Michaelis-Menten noncompetitive inhibition model. Error values represent 95% confidence intervals.

Table 2.2 Inhibition models used in whole cell suspension assays.

Michaelis-Menten Equation: $v_0 = \frac{V_{max}[S]}{K_m+[S]}$ (1)	Noncompetitive inhibition: $v_0 = \frac{V_{max}[S]}{\alpha(K_m+[S])}$ (3)
Competitive inhibition: $v_0 = \frac{V_{max}[S]}{(\alpha K_m+[S])}$ (2)	Uncompetitive inhibition: $v_0 = \frac{V_{max}[S]}{(K_m+\alpha[S])}$ (4)
For simplification, the inhibitor concentrations and inhibition constants in equations (2), (3) and (4) are expressed as α, whereby $\alpha = 1 + \frac{[I]}{K_i}$	

Table 2.3 Initial PCE-to-*c*DCE dechlorination rates versus PCE concentrations in *Geo* strain SZ cell suspension assays in the presence of 0, 10 and 60 μM N_2O.

PCE (μM)	*V* [a]	PCE (μM)	*V* [a]	PCE (μM)	*V* [a]
No N_2O		10 μM N_2O		60 μM N_2O	
3.6	4.1	10.9	19.3	4.9	5.3
6.3	11.7	13.1	24.7	9.5	8.5
11.7	24.0	18.5	25.3	15.3	13.6
15.7	28.5	29.0	28.5	52.7	20.0
42.2	48.4	41.3	36.8	59.4	22.1
60.8	60.3	57.0	41.2	69.5	24.3
83.6	63.9	63.6	44.7	87.5	24.5
97.8	65.0	74.1	45.0	110.4	25.5
110.2	61.3	91.6	51.9	124.3	25.4
122.0	58.4	109.7	47.6	146.5	25.2
133.9	68.0				
153.9	56.7				

[a] Initial dechlorination rate (nmol Cl^- released min^{-1} mg $protein^{-1}$).

Table 2.4 Initial *c*DCE-to-VC dechlorination rate versus *c*DCE concentrations in *Dhc* strain BAV1 cell suspension assays in the presence of 0, 10 and 60 μM N_2O.

***c*DCE (μM)**	***V*** [a]	***c*DCE (μM)**	***V*** [a]	***c*DCE (μM)**	***V*** [a]
No N_2O		10 μM N_2O		60 μM N_2O	
2.7	15.4	1.9	10.3	1.7	2.4
4.4	27.6	5.0	16.9	5.4	4.9
7.5	48.6	8.4	23.6	10.1	7.2
17.5	53.2	17.5	36.4	17.5	14.2
31.7	79.5	31.7	38.5	29.5	18.5
64.5	93.1	63.4	54.6	63.4	24.7
174.9	110.3	161.8	75.4	208.8	39.6
250.3	106.5	211.0	80.5	225.2	42.6
377.1	111.4	488.6	86.4	424.6	42.1

[a] Initial dechlorination rate (nmol Cl^- released min^{-1} mg $protein^{-1}$).

Table 2.5 Initial VC-to-ethene dechlorination rate versus VC concentrations in Dhc strain BAV1 cell suspension assays in the presence of 0, 15 and 50 μM N_2O.

VC (μM)	***V*** [a]	**VC (μM)**	***V*** [a]	**VC (μM)**	***V*** [a]
No N_2O		15 μM N_2O		50 μM N_2O	
4.4	18.5	3.2	7.9	4.1	3.0
13.9	53.3	11.4	19.2	11.3	7.0
23.5	72.4	22.0	25.2	21.7	10.9
56.3	89.9	51.4	34.4	47.3	14.2
98.5	104.3	87.9	39.2	72.6	16.7
116.0	107.6	118.0	42.6	113.3	17.1
149.0	107.6	126.0	43.5	140.8	20.9

[a] Initial dechlorination rate (nmol Cl^- released min^{-1} mg $protein^{-1}$).

Table 2.6 Statistical parameters (R^2, AICc and Sy.x values) used for determining the best-fit inhibition model and inhibition constants in cell suspension amended with N_2O as inhibitor.

Culture	Substrate	Tested models	Statistical Parameters			K_I (μM)
			R^2	AICc	Sy.x	
		Noncompetitive	**0.971**	**81.338**	**3.350**	**40.8 ± 3.8**
Geo strain SZ	PCE	Uncompetitive	0.966	86.477	3.639	29.1 ± 3.1
		Competitive	0.944	102.041	4.678	9.2 ± 1.9
		Noncompetitive	**0.968**	**107.060**	**6.422**	**21.2 ± 3.5**
Dhc strain BAV1	*c*DCE	Competitive	0.952	117.928	7.853	2.3 ± 0.5
		Uncompetitive	0.938	124.696	8.902	25.9 ± 2.9
		Noncompetitive	**0.996**	**43.791**	**2.386**	**9.6 ± 0.4**
Dhc strain BAV1	VC	Uncompetitive	0.986	69.426	4.393	7.0 ± 0.6
		Competitive	0.974	82.243	5.961	1.6 ± 0.3

R^2, the Coefficient of Determination, gives information about the fit of the measured data to the different models tested, and the model with highest R^2 value provides the best data fit.

The AICc (i.e., corrected Akaike's Information Criterion) offers an estimate of the relative quality of tested models, and the model with the lowest AICc value represents the relative best fit among the tested models.

The Sy.x represents the Standard Deviation of the Residuals, and the model with the lowest Sy.x value provides best prediction of the data.

In all cell suspensions assays, the noncompetitive model (highlighted in bold) gave the highest R^2 and the lowest AIC and Sy.x values.

CHAPTER THREE:
THE OVERLOOKED NEGATIVE FEEDBACK OF NITROUS OXIDE ON METHANOGENESIS

3.1 Abstract

Human activities accelerate the emission of greenhouse gases including methane (CH_4) and nitrous oxide (N_2O). While the major microbial sources and sinks of these gases have been identified, knowledge of feedback loops and how environmental changes alter the fluxes of these two greenhouse gases are largely lacking. My research shows that micromolar concentrations (10 – 130 µM) of N_2O negatively impact CH_4 production and growth yields of axenic and mixed methanogenic cultures grown with different methanogenic substrates (i.e., acetate, H_2/CO_2, or MeOH), revealing a heretofore overlooked negative feedback loop. N_2O interferes with the Cobalt(I) (Co(I)) corrinoid, a critical enzyme cofactor that methanogens rely on for shuttling methyl group(s) that leads toCH_4 production and is directly linked to energy conservation. Kinetic evaluation of the inhibitory effect of N_2O on methanogenesis using axenic and mixed methanogen cultures showed that CH_4 production from different methanogenic substrates exhibited distinct sensitivities to N_2O inhibition. The determined inhibitory constants (K_I) of N_2O for *Methanosarcina barkeri* strain Fusaro grown with acetate, H_2/CO_2, or MeOH were 24.8(±2.6), 90.6(±10.8) and 130.9(±4.7) µM, respectively, indicating that N_2O in these concentration ranges reduced the respective maximum CH_4 production rate (V_{max}) by 50%. More pronounced N_2O inhibition was observed for methanogenic enrichment cultures enriched with acetate, H_2/CO_2, or MeOH, respectively. Accordingly, the determined K_I values for N_2O inhibition in these microcosms were 17.7(±1.8), 62.1(±6.4) and

109.9(±6.8) μM, respectively. In all cases, CH_4 production from acetate, the major methanogenic substrate in nature, was most sensitive to N_2O inhibition, followed by methanogenesis from H_2/CO_2 and MeOH. Large uncertainty exists in current and future greenhouse gases emissions from critical ecosystems, and recognizing relevant feedback loops between N_2O and CH_4 production is essential to augment existing Earth System Models and improve their predictive capabilities.

3.2 Introduction

While CO_2 receives most attention, methane (CH_4) and nitrous oxide (N_2O) are other relevant greenhouse gases [1]. Without controlling their emissions, the central objective of the Paris Agreement, which is to hold global the average temperature increase to "well below 2°C above preindustrial levels" [2], cannot be met. Global climate feedbacks of both CH_4 and N_2O are ultimately controlled by microbial processes [3-5]; however, human intrusion into the C and N cycles massively disturbed the natural balance of microbial production and consumption of these greenhouse gases [6,7]. As a result, in excess of 17 Tg CH_4 [8] and 6.8 Tg N_2O [9] are being released into the environment annually, and are predicted to increase in the following decades [10-12]. The increasing trends of CH_4 and N_2O releases necessitates comprehensive knowledge of microbial processes and mechanisms controlling their dynamics in the environment. To date, little emphasis has been placed on understanding the interactions and feedbacks between microbially mediated N_2O and CH_4 formation, particularly in critical ecosystems that are large reservoirs of both C and N, such as wetlands, marine/freshwater sediments and permafrost soils.

Phylogenetically diverse methanogenic archaea are the main driver of biogenic CH_4, accounting for around 50% of global CH_4 production [13-17]. Under anoxic conditions, methanogens strictly rely on acetate, H_2/CO_2, or methylated compounds such as MeOH or methylamines for CH_4 production and energy metabolism [18,19]. Although only members of the *Methanosarcinales* are capable

of catalyzing acetoclastic methanogenesis (i.e., produce CH_4 from acetate), approximately two-third of the CH_4 produced in nature is generated from acetate, with the remaining one third mainly arising from H_2/CO_2 (hydrogenotrophic pathway) and methylated compounds (methylotrophic pathways) [20-24]. Activation of methanogenesis in all known methanogenic pathways requires the Co(I) corrinoid supernucleophile as it is an essential cofactor that methanogens rely on for transferring methyl group(s) to initiate CH_4 production and energy conservation [21,23,25-27].

Multiple mechanistically distinct types of Co(I) corrinoid-containing enzyme complexes have been found in the different methanogenic pathways (**Figure 3.1**). Owing to the low redox potential of the Co(I) corrinoid supernucleophile, methanogens can be very sensitive elevated redox conditions and N_2O, which is known to oxidize Co(I) and interfere with Co(I) corrinoid-dependent enzyme systems [28,29]. Detailed studies with corrinoid-dependent enzymes have demonstrated selective N_2O inhibition for Co(I) corrinoid-dependent enzymatic processes, including methionine biosynthesis and reductive dechlorination [14,30-32]; however, the inhibitory effects of N_2O on methanogenesis have led to inconsistent or even contradictory results [33-36]. Experiments with axenic methanogen cultures exposed to N_2O concentrations ranging from 19 - 950 µM have exhibited no, partial, or complete inhibition of methane formation. These prior studies suggested electron donor competition, redox potential changes, and/or toxicity to corrinoid-dependent enzymes are liekely explanation for the

observed inhibition [33,35,37]. Based on the available information, the most likely explanation is a direct inhibitory interaction of N_2O with the Co(I) supernucleophile causing the inhibition of the corrinoid-dependent enzyme complexes [33]. This information suggested that N_2O can negatively impact some methanogen cultures; however, no general conclusion regarding the sensitivity of methanogens to N_2O could be drawn. Systematic investigations of the effects of N_2O on major methanogenic pathways are necessary to elucidate unrecognized, but possibly relevant feedback loops between N_2O and CH_4.

Considering the critical role of microbial processes for controlling fluxes of both CH_4 and N_2O in the environment, a better understanding of the negative feedback of N_2O on CH_4 formation can substantially improve global prediction of greenhouse gas emissions. This study investigates the impact of N_2O on CH_4 formation from major methanogenic substrates (i.e., acetate, H_2/CO_2 and MeOH), characterizes the impact of N_2O on methanogenic community profiles, and determines the inhibitory constants (K_I) of N_2O for CH_4 production from major methanogenic substrates using axenic and enriched methanogenic cultures.

3.3 Materials and Methods

3.3.1 Methanogenic isolates, consortia, and growth conditions.

The negative feedback of N_2O on methanogenesis was investigated with *Methanosarcina barkeri* strain Fusaro (*Ms barkeri*) and three methanogenic consortia enriched with H_2/CO_2, acetate, or MeOH, respectively. *Ms barkeri* is

capable of utilizing all of the methanogenic substrates mentioned above for CH_4 production. The three methanogenic consortia were enriched with the different substrates from Kuwahee Wastewater Treatment Plant anaerobic digester at Knoxville and continuously enriched with the same substrates for 6 - 8 transfers. All cultures were grown in 60-mL serum bottles with 30 mL N_2/CO_2 (80/20, vol/vol) headspace and 30 mL 0.5 mM sulfide-reduced, 50 mM bicarbonate-buffered mineral salt medium (PH 7.2) at 37°C as described [38,39]. *Ms barkeri* cultures and different methanogenic consortia received 20 mM acetate, 30 mM MeOH, or replace headspace with 30 mL H_2 as substrate. For inoculation, culture vessels received 3% (vol/vol) inocula from actively growing cultures maintained under the respective incubation conditions. All experiments used triplicate culture bottles, and culture vessels without N_2O and without inoculum served as positive and negative controls, respectively. Culture vessels were incubated without agitation at 37°C in the dark with the stoppers facing up.

3.3.2 Inhibition experiments.

For *Ms barkeri* cultures, undiluted or 10-fold diluted (with N_2) N_2O gas was directly added to incubation vessels to achieve final aqueous N_2O concentrations of 50 and 100 µM in H_2/CO_2 cultures, of 20 and 50 µM in acetate grown cultures, and of 100 and of 200 µM in MeOH grown cultures. For acetate-, H_2/CO_2- or MeOH-grown methanogenic consortia, 10-fold diluted N_2O gas was introduced to achieve final aqueous phase N_2O concentrations of 10 and 30 µM in the culture

vessels. The dissolved N_2O concentrations in culture bottles were calculated from the headspace concentrations using a Henry's constant of 1.94 for N_2O at 30°C as described [32,40]. CH_4 and N_2O at various time points were analyzed by injecting 100 µL headspace samples into an Agilent 3000A micro gas chromatograph (Micro GC, Palo Alto, CA) equipped with a thermal conductivity detector (TCD). The Micro GC system installed with a molecular sieve column and a PLOT Q column for CH_4 and N_2O measurements, respectively.

3.3.3 Whole cell suspension assays.

Biomass of *Ms barkeri* and methanogenic consortia grown on acetate, MeOH or H_2/CO_2, respectively, as substrates were anaerobically harvested from 1.6 L cultures in the late log phase. After centrifugation at 10,000 x *g* at room temperature for 30 minutes, the cell pellets were washed with reduced mineral salts medium and ultimately suspended in the same medium in 2 mL vials at a final volume of 1.6 mL, resulting in 1000-fold increase in cell density. Total cell protein in whole cell assays was measured by using the Bradford assay [41] after an aliquot of 0.2 mL of concentrated cell suspension was lysed by boiling with 0.2 M MeOH for 3 minutes. All cell suspensions were freshly prepared following identical procedures to ensure consistency between replicate experiments.

Cell suspension assays were performed in 20-mL glass vials sealed with butyl rubber stopper. In brief, prior to the start of the assays, assay vials received a total of 0.9 mL reduced mineral salts medium and increasing concentrations of

substrates (i.e., acetate, MeOH, or H_2/CO_2, respectively) and N_2O as indicated in **Table 3.1**. Following equilibration, experiments were started by introducing 0.1 mL cell suspension into the assay vials. The total reaction mixture volume in each vial was 1 mL. During a 3-hour assay incubation period, 100 µL headspace samples were withdrawn from assay vials every 30 minutes and to analyze CH_4 and N_2O using a gas chromatograph (Agilent 7890 GC series) equipped with a flame ionization detector (FID) or a micro-electron capture detector (µECD), respectively, as described [32,38]. The columns used for CH_4 and N_2O measurements were a DB-624 capillary column (60 m length × 0.32 mm diameter, 1.8 µm film thickness) and a HP-PLOT Q column (30 m length x 0.320 mm diameter, 20 µm film thickness), respectively.

Vials that received 0.1 mL of sterile mineral salt medium, and vials that received 0.1 mL of heat-killed cell suspension served as negative controls. The N_2O concentrations were quantified prior to and at the end of the incubation periods to verify that constant N_2O concentrations were maintained throughout the experiment. The cell titers and substrate concentrations were chosen such that CH_4 production rates could be determined within the 3-hour incubation period and no more than 50% of the initial substrates had been consumed at the end of the incubation period.

3.3.4 Kinetics of methane generation and inhibition models.

Cell growth was considered negligible during a 3-hour assay period and confirmed by constant OD_{600} values. Therefore, the Michaelis-Menten model, rather than Monod model for systems involving cell growth, was used to analyze the cell suspension assay data. For each treatment at a different initial substrate concentration [S], an initial CH_4 production rate *v*, normalized to the amount of protein per vial, in units of nmoles CH_4 min^{-1} mg $protein^{-1}$, was calculated. In brief, the amended acetate, MeOH, or H_2 in the respective assay vials served as the initial substrate concentrations, and the corresponding CH_4 production rates were determined from the slope of progression curves representing total CH_4 produced (linear regression analysis including at least four data points). Thus, each datum point in the Michaelis-Menten plots represents a CH_4 production rate from one initial substrate concentration.

The maximum CH_4 production rate V_{max} and the half-velocity constant K_m for each treatment were calculated using the nonlinear regression models built in *R* software environment. Data sets from assays amended with increasing N_2O concentrations were fit to the competitive, noncompetitive, uncompetitive and mixed inhibition models to determine the inhibitory constant, K_I, of N_2O on CH_4 production from different substrates. The best fit inhibition model presented was chosen based on the highest coefficient of determination (R^2) and the lowest standard deviation of the residuals (Sy.x.). From the best fit inhibition models, the Michaelis-Menten plots were generated for each major methanogenic substrate

(i.e., acetate, MeOH, or H_2/CO_2) for data visualization and the determination of K_I.

3.3.5 DNA isolation and 16S rRNA gene amplicon sequencing

Genomic DNA of *Ms barkeri* and methanogenic enrichment cultures were isolated using Qiagen DNeasy PowerLyzer PowerSoil DNA kit by following the manufacturer's instructions. DNA concentrations were determined with a NanoDrop-2000 spectrophotometer (Thermo Fischer Scientific, Wilmington, DE, USA) and Qubit 3.0 fluorometer (Life Technologies). A Qubit double stranded DNA (dsDNA) BR Assay Kit was used with fluorometer according to manufacturer's instructions. DNA samples extracted from methanogenic enrichment cultures were sent to Center for Environmental Biotechnology (University of Tennessee Knoxville, Knoxville, TN, USA) for PCR assays and amplicon sequencing. The resulting purified DNA samples were PCR-amplified using barcoded-primers F515/R806 targeting the V4 region of the 16S rRNA gene. The amplicon sequencing approach followed established procedures[42]. Raw sequences were analyzed using Qiime2 software package and *R* following MiSeq standard operating procedures.

3.3.6 Quantitative real-time PCR (qPCR)

The previously reported specific primers and TaqMan probes targeting total bacterial and methanogenic archaea 16S rRNA genes [50] were used to enumerate and monitor targeted-16S rRNA genes in *Ms barkeri* and

methanogenic consortia (**Table 2**). The TaqMan reaction mixture included 5 µL of TaqMan Universal PCR Master Mix No AmpErase UNG (Applied Biosystems, Foster City, CA), 0.3 µM of each primer, 0.3 µM of probe, 2.0 µL of diluted-template DNA (1:10) and nuclease-free water for final volume of 10 µL. The qPCR assays were run under following conditions: initial step of 10 min at 95°C, then followed by 40 cycles of denaturation at 95°C for 15 sec and 1 min at 60°C for annealing/extension. The qPCR runs were performed as triplicate for samples and standards in 384 well-plates on QuantStudio 12K Flex Real-Time PCR System (Life Technologies, Grand Island, NY) and the results were analyzed using the QuantStudio 12K Flex System Software v.1.2.2 (Life Technologies, Grand Island, NY).

Standard curves for each qPCR assay were generated with 10-fold serial dilutions (~10^8 to 10^1 gene copies/µL template) of 500 bp-linear DNA fragment (GeneArt, Thermo Scientific) of each target 16S rRNA gene (500 bp-linear gene fragment of *Dehalococcoides mccartyi* strain GT 16S rRNA gene for total bacterial 16S assay and 500 bp-linear gene fragment of *Merhanosarcina barkeri* for methanogenic archaea 16S rRNA gene). The target assays had amplification efficiencies between 1.8 to 1.9, a standard curve slope between -3.6 to -3.9 and a standard curve with $R^2 > 0.998$. Limit of detection (LOD) and limit of quantification (LOQ) were determined as 12 and 120 copies per reaction, respectively.

3.3.7 Growth yield calculations

The average growth yields were calculated from the change in 16S rRNA gene copy numbers measured by qPCR divided by total amount of CH_4 produced over the same time period. Decay of biomass was assumed negligible as no apparent changes were detected in the average 16S rRNA gene copy numbers during the experiment. The growth yields are reported in 16S rRNA gene copies per µmol of CH_4 formed. In addition, the percentages of the total archaea and bacteria in methanogenic enrichment cultures were determined through qPCR measurement of 16S rRNA gene abundances.

3.4 Results

3.4.1 N_2O inhibits CH_4 production and growth yields of *Ms barkeri*

CH_4 production in *Ms barkeri* cultures grown with acetate, H_2/CO_2, or MeOH in the presence of increasing N_2O concentrations were monitored over a 42-day incubation period (**Figure 3.2**). Notably, N_2O exhibited distinct inhibitory patterns for *Ms barkeri* cultures grown with the different methanogenic substrates. The most pronounced N_2O inhibition was observed in acetate-grown *Ms barkeri* cultures, followed by H_2/CO_2 and MeOH-grown cultures.

For MeOH-grown *Ms barkeri*, cultures without N_2O converted 895 $\pm$ 10 µmol MeOH to stoichiometric amounts of 635 $\pm$ 34 µmol CH_4 (i.e., $4CH_3OH \rightarrow 3CH_4 + CO_2 + 2H_2O$) over a 6-day incubation period with an average growth yield

of $(1.6 \pm 0.1) \times 10^7$ 16S rRNA gene copies per µmol CH_4 formed (**Figure 3.2A and 3.2B**). In contrast, cultures that received 100 or 200 µM N_2O produced negligible amounts of CH_4 from MeOH within the same incubation period of 6 days. Following an extended 38-day incubation period, cultures with 100 µM N_2O produced 626 ± 20 µmol CH_4 after a prolonged 11-day lag phase. In addition, the average growth yield from *Ms barkeri* cultures treated with 100 µM N_2O decreased 63.6 ± 7.8% compared with cultures without N_2O, with an average growth yield of $(5.8 \pm 1.2) \times 10^6$ 16S rRNA gene copies per µmol CH_4. More pronounced inhibition was observed in cultures that received 200 µM N_2O. The total amount of CH_4 produced in cultures with 200 µM N_2O reduced to an average of 55 ± 11 µmol, resulting in approximately 10-fold decrease compared with cultures without N_2O. While the growth yields in cultures with 200 µM N_2O reduced to $(2.7 \pm 1.3) \times 10^6$ 16S rRNA gene copies per µmol CH_4, resulting in approximately 6-fold decrease.

Increasing N_2O concentrations caused more potent inhibition for H_2/CO_2 grown *Ms barkeri* (**Figure 3.2C and 3.2D**). In the absence of N_2O, *Ms barkeri* produced 318 ± 21 µmol CH_4 and an average of $(2.4 \pm 0.6) \times 10^6$ 16S rRNA gene copies per µmol CH_4 within 11 days. In the presence of 50 and 100 µM N_2O, H_2/CO_2 grown *Ms barkeri* cultures exhibited prolonged lag phases of 13 and 17 days, respectively, before CH_4 production started. H_2/CO_2 grown *Ms barkeri* cultures with 50 µM N_2O produced stoichiometric amounts (i.e., $4H_2 + CO_2 \rightarrow CH_4 + 2H_2O$) of 311 ± 7 µmol CH_4 after an extended 38-day incubation period.

Cultures received 100 μM N_2O only generated 17± 3.2 μmol CH_4 even after the extended 38-day incubation period, resulting in 63.2 ± 11.3% decrease in total CH_4 production. Furthermore, the average growth yields in cultures that received 50 μM N_2O declined to $(3.7 \pm 0.9) \times 10^5$ 16S rRNA gene copies per μmol CH_4 produced, resulting in approximately 6.5-fold decrease in growth yields compared to cultures without N_2O. Although some CH_4 production (17.4 ± 2.2 μmol) was observed in *Ms barkeri* cultures treated with 100 μM N_2O, the amount of CH_4 was too low to result in reliable growth yield calculation.

The most pronounced N_2O inhibition was observed in *Ms barkeri* cultures grown with acetate as substrate, and 20, 50 μM N_2O completely inhibited its methanogenic activity (**Figure 3.2E**). In the absence of N_2O, *Ms barkeri* produced 588 ± 24 μmol CH_4 from 605 ± 17 μmol acetate (i.e., $CH_3COOH \rightarrow CH_4 + CO_2$) over a 40-day incubation period. In the presence of 20 and 50 μM N_2O, *Ms barkeri* cultures only produced 21.3 ± 4.1 and 20.4 ± 3.8 μmol CH_4 at the termination of the experiments, respectively, leading to over 96% decrease in total CH_4 production. Growth yields of acetate-grown *Ms barkeri* cultures were also affected by increasing N_2O concentrations (**Figure 3.2F**). Compared to the average yield of $(6.4 \pm 2.0) \times 10^6$ 16S rRNA gene copies per μmol CH_4 in acetate-grown cultures without N_2O, *Ms barkeri* cultures that received 20 and 50 μM N_2O produced (4.5 ± 0.7) and $(3.1 \pm 0.9) \times 10^6$ 16S rRNA gene copies per μmol CH_4, resulting in 30.4 ± 3.3% and 52.5 ± 12.6% decreases in growth yields, respectively. In all culture bottles with observed inhibition of methanogenic

activity, amended N_2O concentrations remained constant throughout the experiment, consistent with the absence of N_2O reductase (*nos*) operons in the genome of *Ms barkeri*.

3.4.2 N_2O affects CH_4 production and community composition of methanogenic enrichment cultures

To examine whether major methanogen groups also exhibit distinct sensitivities to N_2O, mixed methanogenic cultures continuously enriched with acetate, H_2/CO_2, or MeOH were used as simplified model systems and treated with increasing concentrations of N_2O. Microbial community compositions of tested enrichment cultures were analyzed with 16S amplicon sequencing. As expected, cultures maintained with acetate, H_2/CO_2, or MeOH dominated by distinct methanogen genus. For example, 16S rRNA sequences representing the genus *Methanobacterium* dominated in cultures that received H_2 as electron donor. In contrast, sequences belonging to *Methanosarcina* genus dominated in cultures fed with acetate, and methylotrophic *Methanomethylovorans* dominated in cultures that received MeOH. All enrichment cultures without N_2O addition actively produced CH_4 from the different substrates; however, the presence of 10 and 30 µM N_2O exhibited a potent inhibitory effect for all methanogenic enrichment cultures, with acetate grown methanogenic enrichment cultures most sensitive to N_2O, followed by H_2/CO_2 and MeOH grown enrichment cultures (**Figure 3.3**). In the absence of N_2O, the total CH_4 production from acetate-,

H_2/CO_2-, or MeOH-grown methanogenic enrichment cultures were 589.2 ± 33.7, 316.5 ± 25.4 and 542.6 ± 23.3 µmol CH_4, respectively (**Figure 3.3A, 3.3D and 3.3G**). In the presence of 10 µM N_2O, the total CH_4 production in acetate-, H_2/CO_2-, or MeOH-grown enrichment cultures declined approximately 50%, 80% and 60%, respectively, compared to the incubations without N_2O. Even more pronounced inhibitory effects of N_2O were observed for enrichment cultures that received 30 µM N_2O. Only negligible amounts of CH_4 were produced in incubation with the different substrates even after an extended incubation period of 42 days.

Consistent with observations in *Ms barkeri* cultures, the growth yields of enrichment cultures also decreased with the increased N_2O concentrations. In the absence of N_2O, the average archaea growth yields of enrichment cultures maintained with acetate, H_2/CO_2, or MeOH were $(2.4 \pm 0.2) \times 10^6$, $(1.6 \pm 0.8) \times 10^5$ and $(1.6 \pm 0.2) \times 10^7$ 16S rRNA gene copies per µmol of CH_4. In the presence of 10 µM N_2O, the average archaea growth yields declined approximately 50%, 60% and 90% in cultures amended with acetate-, H_2/CO_2, and MeOH, respectively (**Figure 3.3C, 3.3F and 3.3I**). Although minimal archaeal growth yields were measured in 30 µM N_2O treated cultures, the amount of CH_4 produced was too low for average growth yield calculations.

Due to the decreased growth yields of methanogens in N_2O-treated enrichment cultures, the percentage of methanogens in enrichment cultures decreased with increasing N_2O concentrations. For acetate-enriched

methanogenic cultures, the percentages of archaeal 16S rRNA genes decreased from 81.2 ± 5.0% in cultures without N_2O to 63.1 ± 16.2% and 54.4 ± 2.8% in cultures amended with 10 and 30 µM N_2O, respectively (**Figure 3.3H**). Similar trends were also observed in H_2/CO_2- and MeOH-grown enrichment cultures (**Figure 3.3B and 3.3E**). The ratio of archaeal 16S rRNA genes in H_2/CO_2- or MeOH-grown enrichment cultures without N_2O were 36.8 ± 16.4 % and 92.8 ± 6.7%, respectively. In the presence of 10 and 30 µM N_2O, the ratio of archaeal 16S rRNA genes in H_2/CO_2-grown enrichment cultures decreased to 12.8 ± 9.8% and 11.0 ± 2.4%; while in MeOH-grown enrichment cultures, the ratio of archaeal 16S rRNA genes decreased to 78.0 ± 0.7% and 52.6 ± 8.4%, respectively. No significant N_2O decreases were observed in N_2O-treated acetate and H_2/CO_2 grown methanogenic enrichment cultures, while MeOH-grown enrichment still possessed the capacity for N_2O reduction and periodic additions of N_2O were necessary to maintain inhibitory N_2O concentrations in the culture vessels.

3.4.3 Kinetic characterization of N_2O inhibition on methanogenesis

To provide comparable results for assessing the inhibitory effects of N_2O on CH_4 production from the three different methanogenic substrates, whole cell suspension assays were performed (**Table 3.1**). Michaelis-Menten plots of CH_4 production rates versus initial substrate concentrations with increasing N_2O concentrations are presented in **Figures 3.4**. In all cases, the maximum CH_4 production rates (V_{max}) decreased with increasing N_2O concentrations. Notably,

for both *Ms barkeri* and enrichment cultures, the V_{max} values of acetate-fed cultures were most strongly affected by increasing N_2O concentrations, followed by the H_2 and MeOH-fed cultures.

The initial CH_4 production rate assays with *Ms barkeri* cell suspensions were performed in batch assay vials with acetate, H_2, or MeOH as methanogenic substrate, respectively. Rate data generated in cell suspension assays fit the Michaelis-Menten single-substrate single-inhibitor model ($R^2 > 0.95$). For comparison, CH_4 production rate data versus increasing methanogenic substrate concentrations and the best-fit model simulations are presented (**Figure 3.4**). In the absence of N_2O, the maximum substrate-to-CH_4 rate values (i.e., V_{max}) from acetate-, H_2/CO_2-, or MeOH-treated *Ms barkeri* assays were determined to be 40.8 ± 4.7, 138.1 ± 6.9 and 440.4 ± 10.2 nmol CH_4 min^{-1} mg $protein^{-1}$, respectively (**Figure 3.4A, Table 3.2**). In the presence of 100 and 200 µM N_2O, the V_{max} values of MeOH-fed *Ms barkeri* assays declined to 244.1 ± 38.4 and 188.8 ± 32.5 nmol CH_4 min^{-1} mg $protein^{-1}$, respectively. From the best fit uncompetitive inhibition model, an inhibitory constant, K_I, of N_2O for CH_4 production in MeOH-treated *Ms barkeri* assays was determined as 130.9 ± 4.7 µM. More pronounced N_2O inhibition was observed in H_2/CO_2-treated *Ms barkeri* cell suspensions (**Figure 3.4B**). The addition of 50 and 100 µM N_2O decreased the V_{max} value in H_2/CO_2-treated *Ms barkeri* cell suspension assays to 82.8 ± 29.5 and 59.9 ± 5.9 nmol of CH_4 min^{-1} mg $protein^{-1}$, respectively. Accordingly, a smaller K_I value of N_2O was determined as 90.6 ± 10.8 µM for H_2/CO_2-fed *Ms*

barkeri assays, but with a best fit to the noncompetitive inhibition model. *Ms barkeri* assays with acetate as substrate were most strongly affected by N_2O (**Figure 3.4C**). In vessels amended with 20 and 40 µM N_2O, the V_{max} values decreased to 32.1 ± 4.2 and 22.8 ± 2.5 nmol of CH_4 min^{-1} mg $protein^{-1}$, respectively. In acetate-fed *Ms barkeri* cell suspension assays, the best-fit noncompetitive inhibition model determined a K_I value for N_2O inhibition of 24.8 ± 2.6 µM.

Similar kinetic responses were observed for cell suspension assays conducted with methanogenic enrichment cultures maintained with acetate, H_2/CO_2, or MeOH as substrate(s), respectively. Results of batch kinetic tests with cells harvested from the enrichment cultures are presented (**Figure 3.4**). The Michaelis-Menten model simulations captured the trends of CH_4 production rate data versus increasing substrate concentrations from cell suspension assays of enrichment cultures (**Figure 3.4D, 3.4E and 3.4F**). From the best fit inhibition models, the maximum CH_4 production rate values were determined to be 29.4 ± 2.4, 105.8 ± 3.7 and 209.0 ± 4.4 nmol CH_4 min^{-1} mg $protein^{-1}$ for acetate, H_2/CO_2, or MeOH-treated cell suspensions, respectively. For MeOH-treated cell suspension assays, the presence of 50 and 100 µM N_2O decreased the V_{max} values by 37.4 ± 10.8 and 75.4 ± 21.4%, respectively, compared to assays without N_2O. The best fit noncompetitive inhibition model determined a K_I value of 109.9 ± 6.8 µM for CH_4 production in MeOH-treated cell suspension assays (**Figure 3.4D**). For H_2/CO_2-treated assays, the presence of 30 and 60 µM N_2O

decreased the V_{max} values by 32.3 ± 9.8 and 65.4 ± 12.9%, respectively, compared to assays without N_2O (**Figure 3.4E**). The best-fit noncompetitive inhibition model determined a K_I value of 62.1 ± 6.4 µM for CH_4 production in H_2/CO_2-fed assays. Similar to the N_2O inhibition patterns in *Ms barkeri* cell suspension assays, the most pronounced N_2O inhibition was observed in acetate-feed cell suspension assays (**Figure 3.4F**). In the presence of 10 and 30 µM N_2O, the V_{max} values for acetate-fed cell suspension assays decreased by 38 ± 7.8 and 74.9 ± 16.0%, respectively, compared to assays without N_2O. Accordingly, a much smaller K_I value of 17.7 ± 1.8 µM was determined for N_2O inhibition of CH_4 production in acetate-fed cell suspension assays with the best-fit non-competitive inhibition model. All reported initial CH_4 production rate data represent values that were corrected for the trace amount of CH_4 formed in corresponding control vials. Constant N_2O concentrations were maintained throughout the assays.

3.5 Discussion

Soil microbes are the main driver of global C and N cycling and ultimately control CH_4 and N_2O emission to the atmosphere[10-12]. Knowledge of the responses of relevant functional microbial groups to changing environmental conditions therefore is vital to harness microbial processes involved in CH_4 and N_2O turnover for managing greenhouse gas fluxes and emissions [8]. Although the microbial processes contributing to the turnover of CH_4 and N_2O have been

extensively explored, possible linkages and feedback loops between CH_4 and N_2O dynamics in the environment are largely lacking.

Methanogenic archaea are a phylogenetically diverse, physiologically distinct group of Euryarchaeota that are widely distributed across many ecosystems [18]. Methanogen isolates grown with different substrates exhibited distinct sensitivities to N_2O inhibition [33-36]. To address these research questions, systematic evaluation of the impact of N_2O on CH_4 production from major methanogen groups and methanogenic substrates (i.e., acetate, H_2/CO_2 and MeOH) using simplified systems [33-37] are necessary to elucidate the potency of N_2O inhibition for major methanogen groups. Therefore, *Ms barkeri* [36] grown with different methanogenic substrates (i.e., acetate, H_2/CO_2, or MeOH), and mixed methanogenic cultures enriched with acetate, H_2/CO_2, or MeOH, respectively, were used as simplified systems for investigating the impact of N_2O on CH_4 production of major methanogen groups. The differently maintained enrichment cultures mainly comprised *Methanosarcina*, *Methanobacterium* or *Methanomethylovorans*, representing simplified acetoclastic, hydrogenotrophic or methylotrophic methanogen groups, respectively.

N_2O at micromolar concentrations exhibited pronounced and distinct inhibitory effects for *Ms barkeri* and methanogenic enrichment cultures, indicating that potent N_2O inhibition on CH_4 production is not an uncommon phenomenon. CH_4 production from acetate was most strongly inhibited by N_2O, followed by CH_4 production from H_2/CO_2 and MeOH. One of the reasons for the observed

inhibition pattern could be that distinct methanogenic pathways employ different types and/or amounts of Co(I)corrinoid-dependent methyl-transfer systems for catalyzing CH_4 production and energy conservation [27]. For example, in addition to the membrane-anchored, energy-conserving CoM-MTase complex (Mtr), the acetoclastic methanogenesis pathway requires at least one additional Co(I)-corrinoid iron-sulfur protein (CP) in Eastern branch of the WL pathway for producing methyl-CoM [43] (**Figure 1**). In comparison, the methyl reduction methanogenesis pathway directly generates methyl-CoM from one-carbon compounds (e.g., MeOH) via the substrate-specific non-energy conserving Co(I)-CP [44]. The involvement of multiple Co(I) corrinoid-dependent enzymes may render acetoclastic methanogens more sensitive to N_2O inhibition. Accordingly, the results showed that CH_4 production from acetate-grown *Ms barkeri* was completely inhibited N_2O concentrations exceeding 20 µM, while MeOH-grown *Ms barkeri* tolerated 10-fold higher N_2O concentrations and still maintained some methanogenesis ability, indicating that more pronounced N_2O inhibition is to be expected on methanogens that rely on acetate for growth and CH_4 production.

Thermodynamic consideration can explain the more pronounced N_2O inhibition on acetate-grown *Ms barkeri* than both MeOH-and H_2/CO_2-grown *Ms barkeri*. The Gibbs free energy change associated with acetoclastic acetate fermentation (35 kJ mol $^{-1}$) is much lower than the free energy changes associated with CH_4 formation from MeOH (105 kJ mol $^{-1}$) and H_2/CO_2 (131 kJ mol $^{-1}$) [18]. In addition to the lowest energy yield from acetate, N_2O inhibition

would render acetate-grown *Ms barkeri* spend more energy for maintaining multiple catalytically active Co(I)-corrinoids in its acetoclastic pathway. As a result, cultures would have less energy to maintain cellular metabolism and eventually, higher sensitivity to N_2O inhibition. In addition, both acetoclastic and hydrogenotrophic methanogens rely on a methyl transfer step catalyzed by the corrinoid-dependent Mtr complex for energy conservation [45]. N_2O inhibition of Mtr therefore potentially affects energy conservation in methanogens that depend on these two methanogenic pathways. In support of this hypothesis, acetate- and H_2/CO_2-grown *Ms barkeri* cultures exhibit 2- and 5-fold higher sensitivity to N_2O, respectively, than MeOH-grown *Ms barkeri* cultures. Considering that acetate and H_2/CO_2 are the two major methanogenic substrates in nature [20-24], accounting for almost all of the biological CH_4 on global scale, the observed potent N_2O inhibition on CH_4 production from these two substrates indicates that the N_2O in many anoxic ecosystems may impact CH_4 production.

Results from growth yields measurements showed that N_2O strongly affected not only the total CH_4 production, but also the amount of energy captured for cellular growth, revealing a progressive negative feedback of N_2O for CH_4 production in methanogenic communities. The reduced growth yields of all N_2O-treated methanogenic cultures also support the assumption that N_2O inhibition would cause decreased growth efficiency and slower overall growth rates, lower growth yields, and hence higher substrate concentrations required for positive growth. For example, to combat the undesired oxidation by oxygen or

increased redox potential, acetogenic bacteria such as *Acetobacterium woodii* employ an ATP-dependent activating enzyme to maintain catalytically active Co(I)-corrinoids [46,47]. Similarly, methanogens utilize electrons from reduced iron-sulfur cluster(s) in corrinoid enzyme complexes to maintain Co(I)-corrinoids [45]. Maintaining iron-sulfur cluster(s) eventually requires reducing power and a fraction of the electrons from the substrate is diverted to corrinoid at the expense of energy [48]. Together, the observed low growth yields in the presence of N_2O corroborated that N_2O inhibition affects the growth and energy metabolism of methanogenic pathways, with acetoclastic pathway being most affected, followed by hydrogenotrophic and methylotrophic pathways.

Pronounced N_2O inhibition was also observed in mixed methanogenic cultures enriched with acetate, MeOH, and H_2/CO_2. Interestingly, in all cases, 30 µM N_2O completely inhibited CH_4 production and growth of methanogens, indicating the potency of N_2O to affect methanogenic communities. For example, H_2/CO_2-grown enrichment cultures were completely inhibited by 30 µM N_2O while H_2/CO_2-grown *Ms barkeri* still maintained low activity at a much higher concentration of 100 µM N_2O. One possible explanation could be that methanogens with single methanogenic pathway are more vulnerable to N_2O inhibition compared to metabolically versatile *Ms barkeri* that possesses more than three major methanogenic pathways. In support of these findings, previous studies showed that hydrogenotrophic *Methanobacterium bryantii* strain Bab1 completely lost its methanogenesis ability in presence of 95 µM N_2O while *Ms*

barkeri strain MS was still able to maintain methanogenesis activity with 950 µM N_2O under the same growth conditions [33]. The dominant methanogen genus in H_2/CO_2-grown enrichment cultures derived from anaerobic digester sludge and used in this study was a *Methanobacterium* sp., which typically contain single methanogenic pathway [19], a result may explain why enrichment cultures were more sensitive to N_2O. Considering that the majority of methanogens only have one methanogenic pathway and only several strains in family of *Methanosarcinaceae* have been found contain multiple pathways [21], the findings suggest that N_2O may exhibit an overlooked potent inhibitory effect for major methanogen groups.

In accordance with the growth experiments, kinetic evaluation of N_2O inhibition for CH_4 production from the major methanogenic substrates in both *Ms barkeri* and enrichment cultures showed distinct patterns, with the maximum CH_4 production rate V_{max} from acetate-treated cultures being most strongly affected by N_2O. The lowest K_I values ranging from 17.7 – 24.8 µM were observed for acetate-fed cultures, indicating that N_2O concentration at the 20 µM level reduced the V_{max} of acetate-fed methanogenic cultures by 50%. The determined K_I values for H_2/CO_2- and MeOH-fed cultures were between 60 – 90 µM and 100 – 130 µM, respectively. The determined K_I values for tested cultures fall in the detected N_2O range (0 - 140 µM) at sites affected by agricultural activities [49], suggesting that N_2O inhibition on CH_4 is expected at sites with high N_2O concentrations. While these measured K_I values may not necessarily be

applicable for all ecosystems and functional methanogenic groups, the results here demonstrate that the inhibitory effect of N_2O for microbial CH_4 production should not be ignored, particularly under conditions where both bio-accessible C and N exist.

As our knowledge of the microbial response to changing environmental conditions remains limited, many factors involved in the global CH_4 and N_2O budgets, including the feedback loop identified in this study, have not been included in climate models. To improve the understanding of climate change and feedback responses by terrestrial microorganisms, expanded monitoring of the identified feedback loop is important to reconcile the source-sink imbalance, particularly as managing greenhouse gas fluxes require careful multidisciplinary efforts.

3.6 Acknowledgement

I thank Fadime Murdoch for assistance with molecular analysis and Robert Murdoch for help with the analyses of 16S amplicon sequencing data. I also thank Gao Chen for suggestions and contributions on experiments and manuscript preparation.

3.7 References

(1) Change, I. C., Mitigation of climate change. *Contribution of Working Group III to the Fifth Assessment Report of the Intergovernmental Panel on Climate Change* **2014,** *1454*.

(2) UNFCCC, V., Adoption of the Paris agreement. *United Nations Office at Geneva, Geneva* **2015**.

(3) Lashof, D. A.; Ahuja, D. R., Relative contributions of greenhouse gas emissions to global warming. *Nature* **1990,** *344* (6266), 529-531.

(4) Skinner, C.; Gattinger, A.; Krauss, M.; Krause, H. M.; Mayer, J.; van der Heijden, M. G. A.; Mader, P., The impact of long-term organic farming on soil-derived greenhouse gas emissions. *Sci Rep* **2019,** *9* (1), 1702.

(5) Luan, J.; Wu, J.; Liu, S.; Roulet, N.; Wang, M., Soil nitrogen determines greenhouse gas emissions from northern peatlands under concurrent warming and vegetation shifting. *Commun Biol* **2019,** *2*(1), 132.

(6) Parn, J.; Verhoeven, J. T. A.; Butterbach-Bahl, K.; Dise, N. B.; Ullah, S.; Aasa, A.; Egorov, S.; Espenberg, M.; Jarveoja, J.; Jauhiainen, J.; Kasak, K.; Klemedtsson, L.; Kull, A.; Laggoun-Defarge, F.; Lapshina, E. D.; Lohila, A.; Lohmus, K.; Maddison, M.; Mitsch, W. J.; Muller, C.; Niinemets, U.; Osborne, B.; Pae, T.; Salm, J. O.; Sgouridis, F.; Sohar, K.; Soosaar, K.; Storey, K.; Teemusk, A.; Tenywa, M. M.; Tournebize, J.; Truu, J.; Veber, G.; Villa, J. A.; Zaw, S. S.; Mander, U., Nitrogen-rich organic soils under warm well-drained conditions are global nitrous oxide emission hotspots. *Nat Commun* **2018,** *9* (1), 1135.

(7) Dijkstra, F. A.; Morgan, J. A.; Follett, R. F.; Lecain, D. R., Climate change reduces the net sink of CH4 and N_2O in a semiarid grassland. *Glob Chang Biol* **2013,** *19* (6), 1816-1826.

(8) Reay, D. S.; Smith, P.; Christensen, T. R.; James, R. H.; Clark, H., Methane and global environmental change. *Annu Rev Environ Resour* **2018,** *43* (1), 165-192.

(9) Hu, H. W.; Chen, D.; He, J. Z., Microbial regulation of terrestrial nitrous oxide formation: understanding the biological pathways for prediction of emission rates. *FEMS Microbiol Rev* **2015,** *39* (5), 729-749.

(10) Mosier, A.; Schimel, D.; Valentine, D.; Bronson, K.; Parton, W., Methane and nitrous oxide fluxes in native, fertilized and cultivated grasslands. *Nature* **1991,** *350* (6316), 330.

(11) Schulze, E. D.; Luyssaert, S.; Ciais, P.; Freibauer, A.; Janssens, I. A.; Soussana, J. F.; Smith, P.; Grace, J.; Levin, I.; Thiruchittampalam, B.; Heimann, M.; Dolman, A. J.; Valentini, R.; Bousquet, P.; Peylin, P.; Peters, W.; Rödenbeck, C.; Etiope, G.; Vuichard, N.; Wattenbach, M.; Nabuurs, G. J.; Poussi, Z.; Nieschulze, J.; Gash, J. H., Importance of methane and nitrous oxide for Europe's terrestrial greenhouse-gas balance. *Nat Geosci* **2009,** *2* (12), 842-850.

(12) Singh, B. K.; Bardgett, R. D.; Smith, P.; Reay, D. S., Microorganisms and climate change: terrestrial feedbacks and mitigation options. *Nat Rev Microbiol* **2010,** *8* (11), 779-790.

(13) Emilson, E. J. S.; Carson, M. A.; Yakimovich, K. M.; Osterholz, H.; Dittmar, T.; Gunn, J. M.; Mykytczuk, N. C. S.; Basiliko, N.; Tanentzap, A. J., Climate-driven shifts in sediment chemistry enhance methane production in northern lakes. *Nat Commun* **2018,** *9* (1), 1801.

(14) Banger, K.; Tian, H.; Lu, C., Do nitrogen fertilizers stimulate or inhibit methane emissions from rice fields? *Glob Chang Biol* **2012,** *18* (10), 3259-3267.

(15) Walter Anthony, K.; Daanen, R.; Anthony, P.; Schneider von Deimling, T.; Ping, C. L.; Chanton, J. P.; Grosse, G., Methane emissions proportional to permafrost carbon thawed in Arctic lakes since the 1950s. *Nat Geosci* **2016,** *9* (9), 679-682.

(16) Kirschke, S.; Bousquet, P.; Ciais, P.; Saunois, M.; Canadell, J. G.; Dlugokencky, E. J.; Bergamaschi, P.; Bergmann, D.; Blake, D. R.; Bruhwiler, L.; Cameron-Smith, P.; Castaldi, S.; Chevallier, F.; Feng, L.; Fraser, A.; Heimann, M.; Hodson, E. L.; Houweling, S.; Josse, B.; Fraser, P. J.; Krummel, P. B.; Lamarque, J.-F.; Langenfelds, R. L.; Le Quéré, C.; Naik, V.; O'Doherty, S.; Palmer, P. I.; Pison, I.; Plummer, D.; Poulter, B.; Prinn, R. G.; Rigby, M.; Ringeval, B.; Santini, M.; Schmidt, M.; Shindell, D. T.; Simpson, I. J.; Spahni, R.; Steele, L. P.; Strode, S. A.; Sudo, K.; Szopa, S.; van der Werf, G. R.; Voulgarakis, A.; van Weele, M.; Weiss, R. F.; Williams, J. E.; Zeng, G., Three decades of global methane sources and sinks. *Nat Geosci* **2013,** *6* (10), 813-823.

(17) Jungkunst, H. F., Soil science: Arctic thaw. *Nat Geosci* **2010,** *3* (5), 306.

(18) Thauer, R. K.; Kaster, A. K.; Seedorf, H.; Buckel, W.; Hedderich, R., Methanogenic archaea: ecologically relevant differences in energy conservation. *Nat Rev Microbiol* **2008,** *6* (8), 579-591.

(19) Enzmann, F.; Mayer, F.; Rother, M.; Holtmann, D., Methanogens: biochemical background and biotechnological applications. *AMB Express* **2018,** *8* (1), 1.

(20) Ferry, J. G. In *Acetate-based methane production*, Bioenergy, 2008; American Society of Microbiology: 2008; pp 155-170.

(21) Ferry, J. G., Fundamentals of methanogenic pathways that are key to the biomethanation of complex biomass. *Curr Opin Struct Biol* **2011,** *22* (3), 351-357.

(22) Lessner, D. J., Methanogenesis biochemistry. *eLS* **2009**.

(23) Lyu, Z.; Shao, N.; Akinyemi, T.; Whitman, W. B., Methanogenesis. *Curr Biol* **2018,** *28* (13), 727-732.

(24) Carr, S. A.; Schubotz, F.; Dunbar, R. B.; Mills, C. T.; Dias, R.; Summons, R. E.; Mandernack, K. W., Acetoclastic *Methanosaeta* are dominant methanogens in organic-rich Antarctic marine sediments. *ISME J* **2018,** *12* (2), 330-342.

(25) Sperfeld, M.; Diekert, G.; Studenik, S., Kinetic regulation of a corrinoid-reducing metallo-ATPase by its substrates. *Mol Microbiol* **2014,** *92* (3), 598-608.

(26) Goetzl, S.; Jeoung, J. H.; Hennig, S. E.; Dobbek, H., Structural basis for electron and methyl-group transfer in a methyltransferase system operating in the reductive acetyl-CoA pathway. *J Mol Biol* **2011,** *411* (1), 96-109.

(27) Fu, H.; Goettge, M. N.; Metcalf, W. W., Biochemical characterization of the methylmercaptopropionate:cob(I)alamin methyltransferase from Methanosarcina acetivorans. *J Bacteriol* **2019,** *201* (12), e00130-19.

(28) Banks, R. G. S.; Henderson, R. J.; Pratt, J. M., Reactions of gases in solution. Part III. Some reactions of nitrous oxide with transition-metal complexes. *J Chem Soc Sec A* **1968,** (0), 2886-2889.

(29) Blackburn, R.; Kyaw, M.; Swallow, A. J., Reaction of cob(I)alamin with nitrous oxide and cob(III)alamin. *J Chem Soc, Faraday Trans I* **1977,** *73* (0), 250-255.

(30) Drummond, J. T.; Matthews, R. G., Nitrous oxide inactivation of cobalamin-dependent methionine synthase from *Escherichia coli*: characterization of the damage to the enzyme and prosthetic group. *Biochemistry* **1994,** *33* (12), 3742-3750.

(31) Drummond, J. T.; Matthews, R. G., Nitrous oxide degradation by cobalamin-dependent methionine synthase: characterization of the reactants and products in the inactivation reaction. *Biochemistry* **1994,** *33*, 3732-3741.

(32) Yin, Y.; Yan, J.; Chen, G.; Murdoch, F. K.; Pfisterer, N.; Löffler, F. E., Nitrous oxide is a potent inhibitor of bacterial reductive dechlorination. *Environ Sci Technol* **2018,** *53* (2), 692-701.

(33) Klüber, H. D.; Conrad, R., Inhibitory effects of nitrate, nitrite, NO and N_2O on methanogenesis by *methanosarcina barkeri* and *Methanobacterium bryantii*. *FEMS Microbiol Ecol* **1998,** *25*, 331-339.

(34) Tugtas, A. E.; Pavlostathis, S. G., Inhibitory effects of nitrogen oxides on a mixed methanogenic culture. *Biotechnol Bioeng* **2007,** *96* (3), 444-455.

(35) Balderston, W. L.; Payne, W. J., Inhibition of methanogenesis in salt marsh sediments and whole-cell suspensions of methanogenic bacteria by nitrogen oxides. *Appl Environ Microbiol* **1976,** *32* (2), 264-269.

(36) Fischer, R.; Thauer, R. K., Methanogenesis from acetate in cell extracts of *Methanosarcina barkeri*: isotope exchange between CO_2 and the carbonyl group of acetyl-CoA, and the role of H_2. *Arch Microbiol* **1990,** *153* (2), 156-162.

(37) Clarens, M.; Bernet, N.; Delgenès, J.-P.; Moletta, R., Effects of nitrogen oxides and denitrification by Pseudomonas stutzeri on acetotrophic methanogenesis by Methanosarcina mazei. *FEMS Microbiol Ecol* **1998,** *25* (3), 271-276.

(38) Yan, J.; Şimşir, B.; Farmer, A. T.; Bi, M.; Yang, Y.; Campagna, S. R.; Löffler, F. E., The corrinoid cofactor of reductive dehalogenases affects dechlorination rates and extents in organohalide-respiring *Dehalococcoides mccartyi*. *ISME J* **2016,** *10* (5), 1092-1101.

(39) Yan, J.; Bi, M.; Bourdon, A. K.; Farmer, A. T.; Wang, P. H.; Molenda, O.; Quaile, A. T.; Jiang, N.; Yang, Y.; Yin, Y.; Şimşir, B.; Campagna, S. R.; Edwards, E. A.; Löffler, F. E., Purinyl-cobamide is a native prosthetic group of reductive dehalogenases. *Nat Chem Biol* **2018,** *14* (1), 8-14.

(40) Sander, R., Compilation of Henry's law constants (version 4.0) for water as solvent. *Atmos Chem Physics* **2015,** *15* (8), 4399-4981.

(41) Bradford, M. M., A rapid and sensitive method for the quantitation of microgram quantities of protein utilizing the principle of protein-dye binding. *Anal Biochem* **1976,** *72* (1), 248-254.

(42) Caporaso, J. G.; Lauber, C. L.; Walters, W. A.; Berg-Lyons, D.; Lozupone, C. A.; Turnbaugh, P. J.; Fierer, N.; Knight, R., Global patterns of 16S rRNA diversity at a depth of millions of sequences per sample. *Proc Natl Acad Sci USA* **2011,** *108* (Supplement 1), 4516-4522.

(43) Ferry, J. G., Methane from acetate. *J Bacteriol* **1992,** *174* (17), 5489-5495.

(44) Welander, P. V.; Metcalf, W. W., Loss of the *mtr* operon in *Methanosarcin*a blocks growth on methanol, but not methanogenesis, and reveals an unknown methanogenic pathway. *Proc Natl Acad Sci USA* **2005,** *102* (30), 10664-10669.

(45) Matthews, R. G., Cobalamin- and corrinoid-dependent enzymes. *Met Ions Life Sci* **2009,** *6*, 53-114.

(46) Xia, A.; Cheng, J.; Ding, L.; Lin, R.; Huang, R.; Zhou, J.; Cen, K., Improvement of the energy conversion efficiency of *Chlorella pyrenoidosa* biomass by a three-stage process comprising dark fermentation, photofermentation, and methanogenesis. *Bioresour Technol* **2013,** *146*, 436-443.

(47) Farnberger, J. E.; Richter, N.; Hiebler, K.; Bierbaumer, S.; Pickl, M.; Skibar, W.; Zepeck, F.; Kroutil, W., Biocatalytic methylation and demethylation via a shuttle catalysis concept involving corrinoid proteins. *Commun Chem* **2018,** *1* (1), 82.

(48) Matthews, R. G.; Koutmos, M.; Datta, S., Cobalamin-dependent and cobamide-dependent methyltransferases. *Curr Opin Struct Biol* **2008,** *18* (6), 658-666.

(49) Jurado, A.; Borges, A. V.; Brouyere, S., Dynamics and emissions of N_2O in groundwater: A review. *Sci Total Environ* **2017,** *584*, 207-218.

(50) Kleindienst, S., Chourey, K., Chen, G., Murdoch, R. W., Higgins, S. A., Iyer, R. L. & Löffler, F. E. (2019). Proteogenomics reveals novel reductive dehalogenases and methyltransferases expressed during anaerobic dichloromethane metabolism. Appl. Environ. Microbiol., *85*(6), e02768-18.

3.7 Appendix

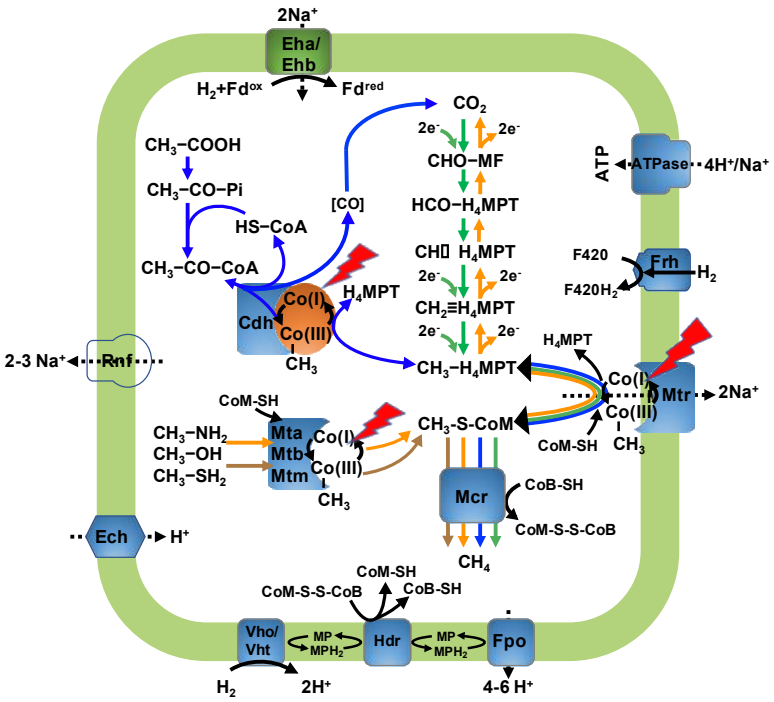


Figure 3.1. The major methanogenic pathways examined in this study. Acetoclastic pathway, hydrogenotrophic pathway, methylotrophic pathway and methyl-reduction pathway. The steps catalyzed by corrinoid-dependent enzyme complexes are indicated. CHO-MF, formyl-methanofuran; CHO-H_4SPT, formyl-tetrahydrosarcinapterin; CH=H_4SPT, methenyl-tetrahydrosarcinapterin; CH_2≡H_4SPT, methylenetetrahydrosarcinapterin; CH_3-H_4SPT, methyl-tetrahydrosarcinapterin; CH_3-CoM, methyl-coenzyme M; CoM, coenzyme M; CoB, coenzyme B; CoM-CoB, mixed disulfide of CoM and CoB; MP and MPH_2, oxidized and reduced methanophenazine; F420/$F420H_2$, oxidized and reduced Factor 420; Fd^{ox}/Fd^{red}, oxidized and reduced ferredoxin; CH_3-COOH, acetate; CH_3-CO-Pi, acetyl-phosphate; CH_3-CO-CoA, acetyl-CoA; Ech, ferredoxin-dependent hydrogenase; Frh, F420-dependent hydrogenase; Vho, methanophenazine-dependent hydrogenase; Fpo, F420 dehydrogenase.

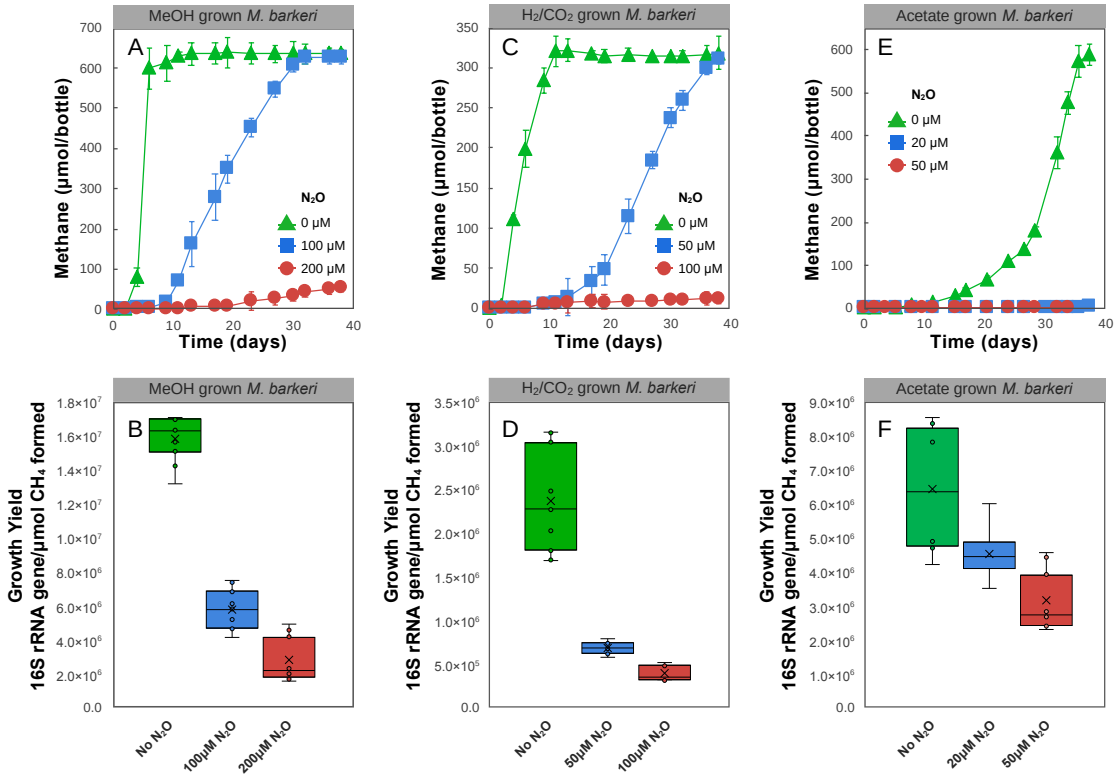


Figure 3.2. Effect of N_2O on CH_4 production and growth yields of *Ms barkeri*. (A), (C) and **(E)** CH_4 production from MeOH, H_2/CO_2 and acetate, respectively. **(B)**, **(D)** and **(F)** Calculated growth yields of *Ms barkeri* grown with MeOH, H_2/CO_2 and acetate, respectively.

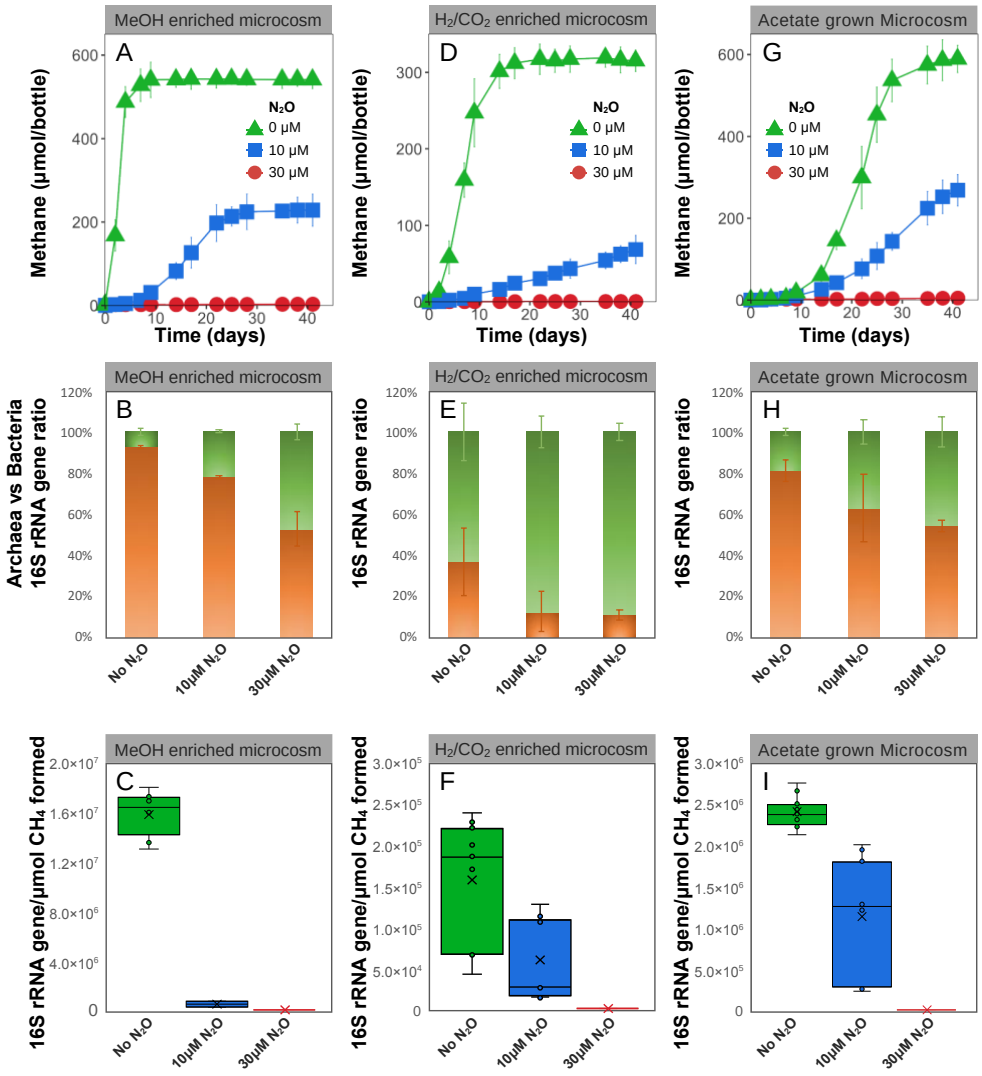


Figure 3.3. Effect of N_2O on CH_4 production and growth yields of methanogenic enrichments maintained with MeOH, H_2/CO_2 and acetate, respectively. (A), **(D)** and **(G)** CH_4 production from MeOH, H_2/CO_2 and acetate, respectively. **(B)**, **(E)** and **(H)** Total Archaea and Bacteria 16S rRNA gene ratio under different N_2O concentrations for each enrichment culture.

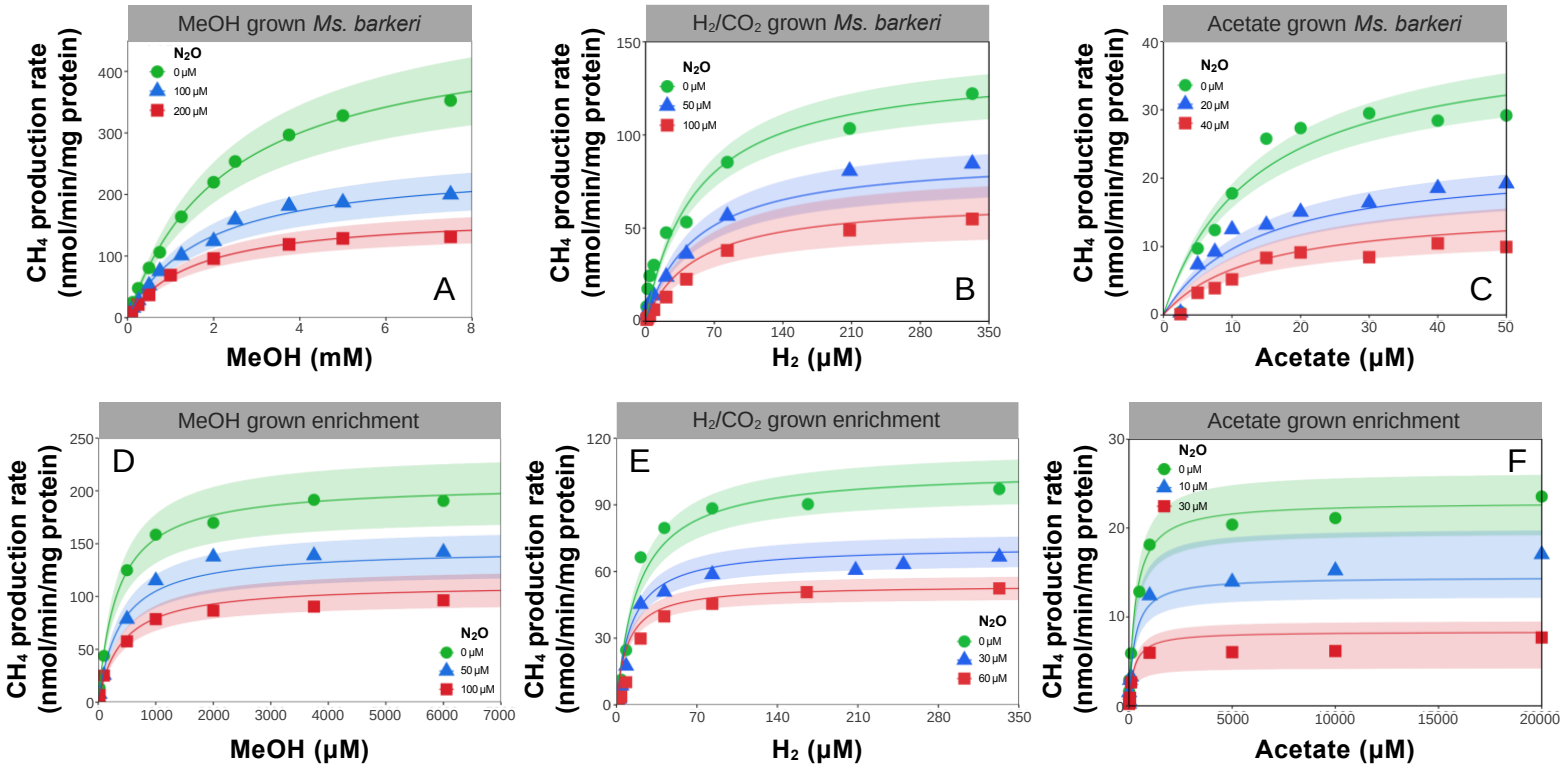


Figure 3.5. Kinetics of CH_4 production from MeOH, H_2/CO_2 and acetate, respectively, in cell suspensions of *Ms barkeri* and enrichment cultures in the presence of increasing concentrations of N_2O. **(A)**, **(B)** and **(C)** Michaelis-Menten plots of CH_4 production rates versus respective substrate(s) concentrations in cell suspension of *Ms barkeri* without and in the presence of increasing N_2O concentrations. **(D)**, **(E)** and **(F)** Michaelis-Menten plot of CH_4 production rates versus respective substrate(s) concentrations in cell suspension of methanogenic enrichments without and in the presence of increasing N_2O concentrations.

Table 3.1 Cell suspension assay arrangements

Substrate	*Ms barkeri*			Enrichments		
	Ace-Fed	H_2/CO_2-Fed	MeOH-Fed	Ace-Fed	H_2/CO_2-Fed	MeOH-Fed
Ace (μM)	2.5-50×10^3	-	-	2.5-20×10^3	-	-
H_2/CO_2 (μM)	-	1.0-333	-	-	0.2-333	-
MeOH (mM)	-	-	0.2 – 7.5	-	-	0.1-10

Ms barkeri assay grown with acetate, H_2/CO_2, or MeOH received final N_2O concentrations of 0, 20 and 40 μM, of 0, 50 and 100 μM, and of 0, 100 and 200 μM, respectively; while enrichment cultures assay grown with acetate, H_2/CO_2, or MeOH received final N_2O concentrations of 0, 10 and 30 μM, of 0, 30 and 60 μM, and of 0, 50 and 100 μM, respectively.

Table 3.1 Kinetic (V_{max}, K_m) and inhibition (K_I) parameters for CH_4 production from acetate, H_2/CO_2 and MeOH in cell suspensions of *Ms barkeri* and methanogenic enrichment cultures in response to increasing N_2O concentrations [a].

Culture	Substrate	Inhibitor	V_{max} (nmol CH_4 min^{-1} mg $protein^{-1}$)	K_m (μM)	K_I (μM)	Inhibition Model [b]
Ms barkeri	Acetate	N_2O	40.8(±4.7)	13.4(±2.1) × 10^3	24.8(±2.6)	Non
Ms barkeri	H_2/CO_2	N_2O	138.1(±6.9)	51.1(±7.2)	90.6(±10.8)	Non
Ms barkeri	MeOH	N_2O	440.4(±10.2)	2.1(±0.1) × 10^3	130.9(±4.7)	Un
Enrichment	Acetate	N_2O	29.4(±2.4)	302.2(±46.2)	17.7(±1.8)	Mix
Enrichment	H_2/CO_2	N_2O	105.8(±3.7)	19.0(±2.3)	62.1(±6.4)	Non
Enrichment	MeOH	N_2O	209.0(±4.4)	359.3(±30.8)	109.9(±6.8)	Non

[a] Data listed show results from the best fit Michaelis-Menten inhibition model. Error values represent 95% confidence intervals.

[b] The resulted best fit model. Non, non-competitive; Un, un-competitive; Mix, mix-inhibition.

Table 3.2 Primers and Probes used in this study

Target DNA	Primer and Probe sets	Sequence (5' – 3')
Total Bacteria 16S rRNA gene	Bac1055YF	ATGGYTGTCGTCAGCT
	Bac1392R	ACGGGCGGTGTGTAC
	Bac1115-probe	FAM-CAACGAGCGCAACCC-MGB
Total Archaea16S rRNA gene	Mtgen835F	GGGRAGTACGKYCGCAAG
	Mtgen918R	GAVTCCAATTRARCCGCA
	Mtgen831-probe	FAM-CCAATTCCTTTAAGTTTCA-MGB

CHAPTER FOUR:
ORGANOHALIDE RESPIRATION OF CHLORINATED ETHENES UNDER NITROUS OXIDE INHIBITION: METABOLIC RESPONSES AND POTENTIAL MITIGATITION STRATEGIES

4.1 Abstract

Organohalide-respiring bacteria (OHRB) are keystone organisms for reductive dechlorination of toxic and carcinogenic chlorinated contaminants. Nitrous oxide (N_2O), a common observed metabolite of microbial nitrification and denitrification at groundwater sites, inhibits dechlorination capability of OHRB via affecting the corrinoid-dependent reductive dehalogenases. Results of growth experiments and metabolomic analyses with dechlorinating consortium SDC-9 show that N_2O modulates reductive dechlorination activity, and affects the metabolic profile, as well as corrinoids yield in microbial dechlorinating community. Amendment of 100 µM N_2O diminished vinyl chloride (VC) dechlorination ability and significantly changed the metabolic profile of SDC-9. In the presence of N_2O, metabolites associated with reactions catalyzed by corrinoid-dependent enzymes, such as methionine sulfoxide and succinate/methylmalonate, were significantly up- and down-regulated, respectively. Yields of total corrinoids as well as the abundance of specific corrinoids (i.e., DMB-Cba) known to support the functionality of *Dehalococcoides mccartyi* (*Dhc*) decreased by 10% and 20%, respectively, revealing an impact of N_2O on corrinoids pools. Transcriptional analysis of *metH* and *metE* in *Geobacter lovleyi* strain SZ revealed that N_2O amendment triggers the switch from corrinoid-dependent to corrinoid-independent metabolism. Introducing N_2O reducers harboring functional clade I (i.e., *Pseudomonas stutzeri* strain DCP-Ps1) or clade II nitrous oxide reductase (NosZ) (i.e., *Anaeromyxobacter dehalogenans* strain

2CP-C) restored the dechlorination activity of *Geo* strain SZ cultures that were inhibited by N_2O, indicated an unrecognized detoxification role of N_2O reducers for OHRB. These findings emphasize that N_2O negatively impacts corrinoids dynamics in microbial communities with consequences for corrinoid-dependent microbial processes, including reductive dechlorination. Considering the vital role of RDase enzyme systems with corrinoid cofactor for detoxification of chlorinated solvents, effective N_2O mitigating strategies must be exploited to achieve successful bioremediation.

4.2 Introduction

Chlorinated solvents, including tetrachloroethene (PCE) and trichloroethene (TCE), are widespread and toxic groundwater pollutants [1]. Incomplete transformation of PCE and TCE in the environment leads to the accumulation of more toxic *cis*-1,2-dichloroethene (*c*DCE) and vinyl chloride (VC) [2-5]. Organohalide-respiring bacteria (OHRB) are capable of coupling the detoxification of chlorinated solvents to growth, and thus are effective bioremediation solutions for treating contamination with chlorinated compounds [1,6]. Several phylogenetically distinct OHRB are capable of dechlorinating PCE and TCE to *c*DCE, while only strains of *Dehalococcoides mccartyi* (*Dhc*) [7], and the recently identified *Candidatus* Dehalogenimonas etheniformans [8], are known as the key players for the complete detoxification of carcinogenic *c*DCE and VC to environmentally benign ethene. In organohalide respiration, OHRB such as *Geo* strain SZ [9] and *Dhc* strain BAV1, are capable of catalyzing carbon-chlorine bond cleavage with reductive dehalogenases (RDases) and conserving energy for growth [10].

Corrinoid (in complete form, cobamide) is an essential enzymatic cofactor for RDases and has to be maintained in the super-reduced form (i.e., Co(I)-corrinoid) to support dechlorination activities of OHRB [11-14]. Genomic analysis revealed that *Dhc* strains lack the *de novo* corrinoid biosynthesis pathway, but possess the machinery for corrinoid scavenging and remodeling [12,15,16]. Nonfunctional or different types of corrinoids can be incorporated into *Dhc* cells

and used for producing functional cobalamin with the available of favorable lower ligand 5,6-dimethylbenzimidazole (DMB) [12,17,18]. Therefore, growth of *Dhc* in microbial communities strictly rely on corrinoids produced by community members or addition of exogenous cobalamin (DMB-cobamide, DMB-Cba) [19]. *Dhc* strains have different preferences for different types of corrinoids [18]. Robust *Dhc* growth requires sufficient DMB-Cba, while unfavorable corrinoid types can either compromise (e.g., 5-methoxybenzimidazole, 5-OMeBza-Cba; and benzimidazole, Bza-Cba) or completely abolish (e.g., 5-hydroxybenzimidazole, 5-OHBza-Cba) *Dhc* reductive dechlorination activity [20]. In essence, corrinoid limitations, both quantitative and qualitative, could hinder *Dhc* dechlorination activities.

A recent study demonstrated that micromolar concentrations of N_2O inhibit bacterial reductive dechlorination via affecting corrinoid-dependent RDase systems of *Geobacter* and *Dhc* [21]. The N_2O inhibition observed for corrinoid-dependent RDase systems is of interest for two reasons: first, N_2O is a commonly observed metabolite of microbial nitrogen metabolism including denitrification and nitrification [22-25] and its concentration in the environment has steadily increased over the past decades [26-28]; second, corrinoids are essential enzymatic cofactors in the majority of organisms in microbial communities, such as homoacetogens [29], methanogens [30] and OHRB [31], and involved in a wide range of biochemical reactions, such as methionine production and folate cycling [21,32-36]. Therefore, elevated N_2O concentrations has the potential to negatively

affect many organisms in addition to OHRB in microbial communities; however, knowledge of the impacts of N_2O on corrinoid-dependent metabolisms in microbial communities is lacking. In addition, phylogenetically diverse denitrifying and non-denitrifying N_2O reducers possessing clade I and clade II NosZ have been found widely distributed in various environments [37,38], including dechlorinating communities. Whether these N_2O reducers have a detoxification role for alleviating N_2O inhibition for other community members are also unclear. Therefore, understanding the metabolic responses of dechlorinating communities to N_2O inhibition and how they manage to address this inhibition is vital for achieving better bioremediation of chlorinated compounds contaminations.

In view of the commonality of high concentrations of N_2O observed at many groundwater sites, particularly at sites affected by nitrate contamination [39], physiological as well as metabolic changes in microbial communities induced by N_2O are to be expected. I hypothesize that the presence of N_2O affects metabolic and corrinoid profiles of microbial communities with consequences for dechlorination activities. This chapter investigates the impact of N_2O on the metabolic and corrinoid profiles of microbial communities using a well characterized dechlorinating consortium, Shaw Dechlorinating Culture 9 (SDC-9). Also explored were the recovery potentials of N_2O affected *Geo* strain SZ and *Dhc* strain BAV1 via introducing N_2O reducers that harbor functional clade I (i.e., *Pseudomonas stutzeri* strain DCP-Ps1) or clade II NosZ (i.e., *Anaeromyxobacter dehalogenans* strain 2CP-C).

4.3 Materials and Methods

4.3.1 Chemicals

PCE, *c*DCE (both ≥99.5%), VC (≥99.5%), ethene (≥99.9%), vitamin B_{12} (≥98%), sodium fumarate (≥98%) and N_2O (≥99%) were purchased from Sigma-Aldrich (St Louis, MO, USA). All other chemicals used in this study were reagent grade or higher.

4.3.2 Cultures and growth condition

Geo strain SZ, *Dhc* strain BAV1, *P* strain DCP-Ps1 and *Adehal* strain 2CP-C used for recovery experiments were routinely maintained in the laboratory. Consortium SDC-9 containing *Dhc* was a gift from Dr. Paul Hatzinger at APTIM (NJ, USA). All cultures were grown in 160-mL serum bottles containing a CO_2/N_2 (20/80, vol/vol) headspace and 100 mL of synthetic, bicarbonate-buffered (30 mM, pH 7.3) mineral salt medium as described [20,21,40]. Strain SZ cultures received 5 mM acetate as electron donor and 38 µmoles/bottle PCE as electron acceptor, and a vitamin B_{12}-free Wolin vitamin mix [41]. *Dhc* strain BAV1 culture vessels received 10 mL of hydrogen, 0.8 mM (90 µmoles/bottle) *c*DCE, and 5 mM acetate as electron donor, electron acceptor, and carbon source, respectively. SDC-9 culture vessels received 10 mM lactate, 0.25 mM (40 µmoles/bottle) VC as electron donor and electron acceptor, respectively. For

inoculation, culture vessels received 3% (vol/vol) inocula from actively dechlorinating cultures maintained under the same conditions.

4.3.3 N_2O inhibition and recovery experiments

Sterilized N_2O gas was directly injected to culture vessels using plastic syringes (BD, Franklin Lakes, NJ, USA) to achieve final aqueous N_2O concentrations of 30 and 100 µM for both *Geo* strain SZ and *Dhc* strain BAV1 cultures, and of 100 µM for SDC-9 cultures in all N_2O-amended vessels. The aqueous phase concentrations (in µM) of N_2O in all medium bottles were calculated from the headspace concentrations using a dimensionless Henry's constant of 1.94 for N_2O at 30°C [42] according to $C_{aq} = \frac{C_g}{H_{cc}}$, where C_{aq}, C_g, and H_{cc} are the aqueous concentration (in µM), the headspace concentration (in µmoles L^{-1}) and the dimensionless Henry's constant, respectively.

Recovery experiments using *Geo* strain SZ, *Dhc* strain BAV1, *P.* strain DCP-Ps1 and *Anaeromyxobacter* strain 2CP-C cultures used triplicate culture bottles. SDC-9 cultures for inhibitory exeriments and metabolomic assays used six replicate culture bottles. Culture bottles without N_2O and without inoculum served as positive and negative controls, respectively. Culture vessels were incubated without agitation at 30°C in the dark with the stoppers facing up. At various time points, 100 µL headspace samples were withdrawn from culture bottles and CH_4 and N_2O were analyzed using gas chromatographs (Agilent 7890 GC series) equipped with a flame ionization detector (FID) or a micro-

electron capture detector (μECD), respectively, as described [21,40]. The columns used for GC-FID and GC-μECD were a DB-624 capillary column (60 m length × 0.32 mm diameter, 1.8 μm film thickness) and a HP-PLOT Q column (30 m length x 0.320 mm diameter, 20 μm film thickness), respectively.

4.3.4 Corrinoid extraction and analysis

Cellular corrinoids were extracted in the cyano form and purified using potassium cyanide (KCN) following an established protocol with modifications [12,43]. Briefly, triplicate 300 mL SDC-9 culture biomass were harvested immediately at the end of inhibitory experiments by centrifugation in 500-mL plastic bottles at 10,000 × *g* for 20 min at room temperature. Following removal of supernatants, the cell pellets were suspended in 5 mL of deionized water in sterile 50 mL falcon tubes, the pH was adjusted to 5−6 with 3% (v/v) glacial acid, and KCN was added to a final concentration of 10 mM. The suspensions were vigorously mixed and incubated in a boiling water bath for 20 min. Following centrifugation at 10,000 × *g* for 15 min, the supernatants were collected for corrinoid extraction. To increase corrinoid extraction efficiency, the cell pellets were extracted a second time by repeating the steps above and the extracts were combined with those from the first extraction. The combined supernatants were loaded onto pre-equilibrated (via loading 2 mL pure methanol followed by 40 mL deionized water) Sep-Pak C18 cartridges (Waters Corp, Milford, MA, USA). Following sample loading, the cartridges were washed with 10 mL

deionized water and 7.5 mL 10% methanol. Retained corrinoids on cartridges were eluted with 3 mL 100 % methanol to clean vials. The slightly pink-colored solutions were vacuum dried, dissolved in 0.5 mL deionized water and transferred to sterile 1.5 mL plastic tubes.

Corrinoid samples extracted from SDC-9 cultures were analyzed with an Agilent 1200 high-performance liquid chromatography (HPLC) system (Santa Clara, CA, USA) equipped with an Eclipse XDB-C18 column (5 µm, 4.6 × 234 150 mm) operated with a flow rate of 1mL min L^{-1} at 30°C. The eluent consisted of 0.1% (v/v) formic acid (≥ 88%, w/v) in water (eluent A) and 0.1% formic acid in methanol (eluent B), and a linear change to 25%/75% (A/B) over a 3-min time period followed by a 5 min hold was applied before the column was equilibrated to initial conditions.

4.3.5 Metabolite extraction

Immediately after inhibitory experiments, triplicate 50 mL sacrificial SDC-9 cultures were removed from culture vessels and metabolites were extracted following a revised protocol [44]. The culture suspensions were first vacuum filtered onto polycarbonate filters (47 mm diameter, 0.2 µM pore size). The filters were then place upside down in a petri dish (47 mm) containing 1.3 mL of pre-chilled (-20 °C) extraction solvent (40:40:20 acetonitrile:methanol:water with 0.1 M formic acid). After 15-20 min of extraction at -20 °C, the filters were flipped right side up and washed with the same extraction solvent. The extraction solvents were

transferred to 2-mL microcentrifuge tubes, while the filters were washed again with another 300 µL pre-chilled (-20 °C) extraction solvent and added to the microcentrifuge tubes. The combined extracts were centrifuged at 13.2 rpm at 4 °C for 5 min. After centrifugation, the supernatants were collected in 2-mL microcentrifuge tubes, and the pellets were transferred to clean vials and extracted a second time with 200 µL chilled extraction solvent for 15 minutes at -20 °C. Following extraction, the metabolite-containing solvents were centrifuged again at 13.2 rpm at 4 °C for 5 min. The supernatants containing metabolites were collected and combined with the previously collected supernatant, and the extraction processes was repeated. The combined supernatants were then dried under a stream of nitrogen gas and the dry residues were stored at -80 °C until downstream analysis.

4.3.6 Ultra-performance liquid chromatography high-resolution mass spectrometry

Metabolite analysis followed established procedures [45]. Prior to analysis, samples were reconstituted in 300 µL of sterile MilliQ water and transferred to 1.5-mL glass autosampler vials. Samples were then placed in an autosampler tray kept at 4 °C. Ten µL from each sample was injected through a Synergi 2.5 micron Hydro-RP 100, 100 x 2.00 mm LC column (Phenomex. Torrance, CA) kept at 25°C and eluted using the following solvents: (A) 97:3 water:methanol, 10 mM tributylamine, and 15 mM acetic acid, (B) methanol; and gradient: t = 0 min;

0% B; t = 2.5 min, 0% B; t = 5 min, 20% B; t = 7.5 min, 20% B; t = 13 min, 55% B, t = 15.5 min, 95% B; t = 18.5 min, 95% B; t = 19 min, 0% B; t = 25 min, 0% B; using a flow rate of 200 µL min L^{-1}. The eluent sample was then introduced into the mass spectrometer (MS) via electrospray ionization (ESI) attached to a Thermo Scientific Exactive Plus Orbitrap MS (Waltham, MA). Data were collected in full scan mode, with negative ionization mode, using an adapted method [46]. Samples were run with a spray voltage of 3kV. The nitrogen sheath gas was set to a flow rate of 10 psi, with a capillary temperature of 320 °C. AGC target was set to 3×10^6. Samples were analyzed with a resolution of 140,000. A scan window of 85 to 800 m/z (mass-to-charge) was used from 0 to 9 minutes, and a window of 110 to 1000 m/z from 9 to 25 minutes.

4.3.7 DNA and RNA isolation and cDNA synthesis

Genomic DNA was isolated using Qiagen DNeasy PowerLyzer PowerSoil DNA kit from 2 mL of culture samples. DNA extraction followed the manufacturer's instructions and used a bead-beating method (OMNI Bead Rupter Homogenizer, high speed for 3 min) for cell lysis. DNA was eluted into nuclease-free water and DNA concentration and quality were determined with a NanoDrop spectrophotometer (NanoDrop Technologies, Wilmington, DE, USA) and a Qubit fluorometer (Invitrogen) using the double stranded DNA (dsDNA) BR assay kit.

For total RNA extraction, 6 mL of culture suspension was filtered through a Durapore hydrophilic polyvinylidene fluoride membrane (0.22 µm, Millipore,

Billerica, MA) to collect biomass. The filters were immediately placed into 50-mL conical tubes and stored at -80^{o}C. Total RNA extraction from frozen filters was carried out using Qiagen RNeasy Mini Kit (Qiagen, Valencia, CA). RNA extraction, DNase treatment and purification steps were performed as described [47]. Prior to cell lysis by bead-beating, 2 µL of 10^{10} transcripts per µL luciferase control mRNA (1 mg mL^{-1}, Promega, Madison, WI, USA) was added as an internal standard for determination of RNA loss during the extraction process [47,48]. To remove any remaining DNA, DNase I treatment was performed twice using Qiagen RNase-free DNase set kit. Then RNA was purified using RNeasy MinElute Clean-up Kit (Qiagen, Valencia, CA). Finally, RNA was eluted in RNase-free water, total RNA concentration was determined using Qubit RNA HS Assay Kit (Invitrogen) and aliquots were stored at -80 ^{o}C for further use. cDNA synthesis was performed with Superscript III Reverse Transcriptase (Invitrogen, Carlsbad, CA, USA) as described [47-49]. The obtained cDNA was purified using QIAquick PCR purification Kit (Qiagen, Valencia, CA) and stored at -20^{o}C for downstream applications.

4.3.8 Primer design and qPCR

Specific primer and TaqMan probe sequences targeting total bacteria, total archaea, *Geobacter*, *Dhc* 16S rRNA genes, *metE* and *metH* genes (specific to *Geo* strain SZ) were designed using Geneious R11.0.2 (http://www.geneious.com, [50]) and primers were synthesized by IDT (Integrated

DNA Technologies). In order to ensure specific hybridization at a uniform temperature, TaqMan probes with Minor Groove Binder (MGB) modification were synthesized by Thermo Fisher Scientific. The specificity of the primers and probes was also verified using primer-BLAST analysis [51].

To validate each assay, primers were used first with SYBR Green chemistry using QuantStudio 12K Flex Real-Time PCR System (Life Technologies, Grand Island, NY). The 10 µL qPCR mixture was composed of 5 µL of Power SYBR Green PCR Master Mix (Applied Biosystems, Foster City, CA), 0.3 µM of each primer, 2.0 µL of template DNA and the remaining volume sterile nuclease-free water. The PCR cycle parameters applied were as follows: 2 min at 50°C and 10 min at 95°C, followed by 40 cycles of 15 s at 95°C and 1 min at 60°C. After amplification, a melt curve analysis was carried out to confirm that the signal obtained in SYBR Green qPCR originated from amplicons of the target gene, not from primer dimers or non-specific amplicons.

For standard curve preparation, 500 bp-linear double stranded DNA fragments including target region for each target gene were used as standards in qPCR runs. Standard curves with a linear range of 10^0 to 10^8 gene copies/mL were prepared by a 10-fold serial dilution of linear DNA fragments and standards were run in triplicate for each dilution. In order to confirm specificity of assays, genomic DNA obtained from *Geobacter lovleyi* pure culture was also used as a template in SYBR Green qPCR and melt curve analysis was performed to check for any nonspecific amplification.

Following validation and optimization of each assay with SYBR Green qPCR, the primers and probe for each target assay were used for TaqMan qPCR. Each 10 µL mixture contained 5 µL of TaqMan Universal PCR Master Mix No AmpErase UNG (Applied Biosystems, Foster City, CA), 0.3 µM of each primer, 0.3 µM of probe and 2.0 µL of template DNA. TaqMan qPCR assays were run using QuantStudio 12K Flex Real-Time PCR System under the same PCR cycle conditions as described for SYBR Green qPCR. The target assays had amplification efficiencies between 90-100%, a standard curve slope between -3.31 to -3.6 and a standard curve with $R^2 > 0.9985$. These values met the parameters suggested in the literature [47,48,52]. The default instrument settings were used and LOD and LOQ values were determined as 10^1 and 10^2 copies per mL for each assay, respectively.

The DNA samples were analyzed in triplicate at two dilutions (i.e. 1:10 and 1:100) to determine if any contaminants were present that would interfere with TaqMan qPCR analysis. The qPCR assay results were analyzed using the QuantStudio 12K Flex System Software (provided by Life Technologies). For transcriptional analysis, all qPCR data were corrected for luciferase mRNA recovery and the standard curve for luciferase gene was prepared as described above. A standard curve with 10-fold of serial dilutions of luciferase DNA was prepared (10^0 to 10^8 copies per mL) and recovery calculations were performed [49].

4.4 Results

4.4.1 N_2O affects dechlorination performance and corrinoid profile of consortium SDC-9

SDC-9 cultures without N_2O completely dechlorinated the initial amount of 54.1 ± 0.2 µmol VC to 52.9 ± 5.1 µmol ethene within a 15-day incubation period (**Figure 4.1A**). SDC-9 cultures amended with 100 µM N_2O only produced 8.3 ± 3.5 µmol of ethene from the initial 54.5 ± 0.3 µmol of VC even after an extended 28-day incubation period, resulting in less than 20% biotransformation of the initial amount of VC (**Figure 4.1B**). SDC-9 cultures were capable of reducing N_2O to N_2, and N_2O was re-spiked periodically in order to maintain inhibitory N_2O concentrations (i.e., > 50 µM) in N_2O-treated culture bottles. In contrary to the stalled VC-to-ethene dechlorination observed in cultures that received repeated additions of N_2O to maintain and N_2O level of 100 µM, SDC-9 cultures that received a one-time amendment of 100 µM N_2O restored dechlorination ability after complete depletion of N_2O (data not shown). Consistent with the previous findings [21], N_2O exhibited a strong inhibitory effect on VC dechlorination.

Enumeration of total bacteria, archaea and *Dhc* 16S rRNA genes at the end of the incubation period (i.e., day 28) showed that SDC-9 cultures with or without N_2O had distinct growth yields of bacteria, archaea and *Dhc* (**Figure 4.1D, 4.1E and 4.1F**). Compared to initial SDC-9 cultures not receiving any substrates, the complete dechlorination of 54.1 ± 0.2 µmol of VC in cultures

without N_2O addition led to an average increase of $(5.4 \pm 0.6) \times 10^6$ *Dhc* 16S rRNA genes mL^{-1}, while no apparent change was detected in total bacterial 16S rRNA yields. In comparison, VC-grown SDC-9 cultures that received 100 µM N_2O only produced $(2.1 \pm 0.2) \times 10^6$ *Dhc* 16S rRNA genes mL^{-1}, resulting in over 63% fewer *Dhc* cell. Due to the repeated N_2O additions, the bacterial 16S rRNA genes mL^{-1} in all SDC-9 cultures that received 100 µM N_2O increased from $(1.0 \pm 0.0) \times 10^9$ to a final $(1.5 \pm 0.2) \times 10^9$, regardless of VC provided as electron acceptor. Interestingly, the total archaeal 16S rRNA gene copies in cultures that received N_2O did not increase but rather decreased from $(7.0 \pm 0.1) \times 10^6$ in cultures without substrates to approximately (1.2 ± 0.1) to $(2.1 \pm 0.3) \times 10^6$. These findings suggest that N_2O exhibits inhibitory effect for archaeal cell growth.

VC stall and lower *Dhc* growth yields in SDC-9 cultures treated with 100 µM N_2O suggested that corrinoid-dependent VC RDase (i.e., VcrA) were not functional in SDC-9 cultures, and VC was not used as an electron acceptor. Insufficient corrinoid supply, either qualitative or quantitative, negatively affects dechlorination activity and growth yields of organohalide-respiring *Dhc* [17,40]. Therefore, to investigate whether N_2O modulates corrinoid yields and profiles in SDC-9 cultures exposed to N_2O, the cultures described above were used for downstream corrinoid analysis after the growth experiments had been completed. The total corrinoid yield in the initial SDC-9 cultures was determined as 11.4 nM, with the major corrinoids identified as Bza-[Cba] (4.7 nM), DMB-[Cba] (3.5 nM), 5-OHBza-[Cba] (2.3 nM), while smaller amounts of Pur-[Cba] (0.6

nM) and 5-MeBza-[Cba] (0.3 nM) were also present (**Figure 4.1C**). For cultures that completed VC degradation, the total corrinoid yield decreased to 8.9 nM but with no apparent decrease in the major corrinoids (i.e., Bza-[Cba], 3.9 nM). Interestingly, an apparent decrease in 5-OHBza-[Cba] and a slight increase in DMB-[Cba] were observed in all VC-grown cultures, which is consistent with previous findings that *Dhc* strains have strict requirement for DMB-Cba for function and are capable of remodeling unfavorable corrinoids to functional DMB-Cba [17].

The corrinoid profiles determined in VC-grown SDC-9 cultures amended with 100 µM N_2O differed from the initial cultures not receiving any substrates. Compared to initial or VC dechlorinating SDC-9 cultures, the total corrinoid yield (8.3 nM) in N_2O-treated VC-grown cultures decreased by approximately 25% or 10%. Although the most remarkable changes were seen in Bza-Cba (4.9 nM), 5-OHBza-[Cba] (0.2 nM) and Pur-[Cba] (0.2 nM), the presence of 100 µM N_2O reduced the DMB-Cba yield in VC-grown SDC-9 cultures by around 20% compared with VC grown SDC-9 cultures without N_2O. The decreased total corrinoid amount and the DMB-Cba yields in N_2O-treated SDC-9 cultures are in accordance with the decreased *Dhc* cell abundances (**Figure 4.2**).

4.4.2 N_2O modulates the metabolome profile of the SDC-9 culture

To investigate the impact of N_2O on the metabolome of dechlorinating consortium SDC-9, Metabolomic analysis was performed with SDC-9 cultures

that were grown in the presence of 100 µM N_2O and without N_2O. From the over 3,000 metabolites detected, a total 130 identified metabolites were observed in SDC-9 cultures with and without N_2O. The identified metabolites were further normalized to total bacterial and archaeal 16S rRNA genes for downstream analysis. Principle component analysis (PCA) of the identified metabolites with the first two axes explaining 56.1% and 17.9 % of the variation between SDC-9 cultures with and without N_2O, respectively (**Figure 4.2A**). Average PCA scores of the metabolomes identified significant separation in SDC-9 exposed to N_2O or VC or both from the control (i.e., initial SDC-9 cultures not receiving any substrates) (**Figure 4.3A**). For VC-grown cultures that received 100 µM N_2O, metabolites that rely on corrinoid-dependent enzymes substantially contributed the separation between treatments (**Figure 4.3B**). Particularly, under the stress of N_2O, unique changes were detected with metabolites that require corrinoid-dependent enzymes, such as methionine sulfoxide, homocysteic acid, succinate/sethylmalonate and S-Ribosyl-L-homocysteine, etc. (**Figure 4.3B**). Interestingly, significant separations were identified between cultures amended and not amended with N_2O, regardless of whether VC was present. These observations demonstrated the substantial influence of N_2O on the metabolome profile of dechlorinating SDC-9 community.

Compared with cultures that completely dechlorinated VC, metabolome profile of the SDC-9 cultures with 100 µM N_2O exhibited distinct changes (**Figure 4.2C**). Apart from metabolites associated with corrinoid-dependent enzymes,

significant differences were observed for the majority of the identified metabolites in both treatments. Over 38 out of 130 identified metabolites increased more than 2-fold in N_2O-inhibited cultures, while 25 other metabolites decreased more than 2-fold (**Figure 4.2B**). For example, some metabolites of TCA cycle, such as fumarate, increased over 10,000 fold compared to SDC-9 cultures without N_2O; however, some other TCA cycle metabolites, such as succinate and methylmalonate decreased around 3 fold. The metabolic profile changes between SDC-9 cultures that actively dechlorinated VC and control cultures without any substrates were mainly caused by increased lactate and hydroxyisocaproate concentrations in the VC-dechlorinating cultures. These metabolites were either the provided substrate (lactate) or a precursor of amino acid leucine (hydroxyisocaproiate), with the latter suggesting active microbial metabolism.

4.4.3 N_2O affects the expression of genes involved in corrinoid metabolism

Because of the changes observed in metabolites that link to corrinoid-dependent enzymes, the effects of N_2O on the expression of representative genes controlled by the corrinoids were investigated in the organohalide-respiring *Geo* strain SZ. Methionine synthesis can be accomplished by two different types of enzymes, a corrinoid-dependent methionine synthase (MetH) and a corrinoid-independent methionine synthase (MetE). The expression levels of *metH* and *metE* in *Geo* strain SZ in the presence of N_2O were verified by RT-qPCR (**Figure**

4.2D and **4.2E**). In cultures growing with PCE as electron acceptor, both *metH* and *metE* were expressed in *Geo* strain SZ, with *metE* transcripts present in approximately 10-fold higher numbers than *metH* transcripts (**Figure 4.2D**). In contrast, the presence of 100 µM N_2O had a major effect on the expression of the *metH* gene, and no transcripts of *metH* were measured in N_2O-inhibited cultures. Significant changes were also observed in *metE* expression, which decreased approximately 20-fold in the presence of N_2O (**Figure 4.2E**). When the *metH* transcript abundances were normalized to 16S rRNA gene copy numbers, an up-regulation of *metE* expression by about 2-fold was apparent in the N_2O-inhibited cultures (**Figure 4.2F**). This observation is consistent with previous findings that MetE is capable of compensating the functional loss of MetH [53]. These results suggest that both *metE* and *metH* genes are subject to regulation by N_2O.

4.4.4 Recovery of dechlorination activity in N_2O-inhibited organohalide-respiring cultures

The removal of N_2O from N_2O-inhibited *Geo* strain SZ and *Dhc* strain BAV1 cultures restored reductive dechlorination activity. For *Geo* strain SZ cultures, the presence of 30 and 100 µM N_2O resulted in partial and complete inhibition of PCE dechlorination during the 15-day incubation period (**Figure 4.3A, 4.3B and 4.3C**). After flushing the culture headspace with sterile N_2/CO_2 (80/20), N_2O-inhibited *Geo* strain SZ cultures gradually recovered dechlorination

activities and completely dechlorinated the amended 57.4 ± 0.9 µmol TCE to stoichiometric amounts *c*DCE. Similar recovery trends were observed in N_2O-inhibited *Dhc* strain BAV1 cultures (**Figure 4.3D, 4.3E and 4.3F**). Flushing the culture headspace with N_2/CO_2 (80/20) removed N_2O from culture vessels, and *Dhc* strain BAV1 cultures recovered *c*DCE-to-ethene dechlorination activity, albeit extended incubation periods were required. For example, after removing N_2O from culture bottles, *Dhc* strain BAV1 inhibited by 30 µM N_2O required an extended 40-day incubation to completely dechlorinate 84.3 ± 1.4 µmol *c*DCE to 80.3 ± 9.4 µmol ethene. These findings demonstrate the reversibility of N_2O inhibition in cultures of *Geobacter lovleyi* strain SZ and *Dhc* strain BAV1, and it is likely that other organohalide-respiring bacteria show similar behavior.

To explore if N_2O-consuming bacteria can rescue bacterial reductive dechlorination from N_2O inhibition, actively growing N_2O reducers were introduced to N_2O-inhibited *Geo* strain SZ and *Dhc* strain BAV1 cultures. In *Geo* strain SZ cultures, the introduction of both clade I (*P* strain DCP-Ps1) and clade II (*Adehal* strain 2CP-C) N_2O reducers triggerred to the consumption of N_2O and led to complete recovery of dechlorination activities (**Figure 4.4**). *P* strain DCP-Ps1 augmented to N_2O-inhibited *Geo* strain SZ cultures was capable of removing 30 and 100 µM N_2O within 3 and 5 days, respectively, (**Figure 4.4A, 4.4B and 4.4C**). *Geo* strain SZ started dechlorinating after N_2O concentrations decreased below approximately 10 µM. After a prolonged 40-day incubation period, *Geo* strain SZ cultures initially inhibited by N_2O completely dechlorinated 51 ± 2.4

μmol TCE to 50 ± 5.4 μmol *c*DCE. Similarly, the introduction of *Adehal* strain 2CP-C to N_2O-inhibited *Geo* strain SZ cultures achieved N_2O removal within 2 days and stimulated TCE dechlorination activity in *Geo* strain SZ cultures before N_2O was completely removed (**Figure 44.D, 4.4E and 4.4F**). After an extended 37-day incubation period, all *Geo* strain SZ cultures dechlorinated the initial 51 ± 2.4 μmol of TCE to stoichiometric amounts of 51.4 ± 7.1 μmol *c*DCE.

N_2O-inhibited *Dhc* strain BAV1 cultures that received *P* strain DCP-Ps1 did not fully recover dechlorination activity (**Figure 4.5A, 4.5C and 4.5E**). For both 30 and 100 μM N_2O-inhibited *Dhc* strain BAV1 cultures, robust *c*DCE dechlorination was observed after the removal of N_2O by *P* strain DCP-Ps1 and 90.3 ± 0.6 μmol *c*DCE was completely dechlorinated; however, VC dechlorination to ethene was incomplete, resulting in a mixture of VC and ethene in all N_2O-treated culture bottles after an extended 80-day incubation period.

qPCR analysis confirmed that *Dhc* strain BAV1 did not grow in the presence of N_2O, but growth occurred after the removal of N_2O (**Figure 4.5B, 4.5D and 4.4F**). After the introduction of *P* strain DCP-Ps1 cultures, the *Dhc* 16S rRNA genes in *Dhc* strain BAV1 cultures inhibited with 30 μM N_2O increased from $(2.8 \pm 0.2) \times 10^7$ copies mL^{-1} to $(5.0 \pm 1.0) \times 10^7$ copies mL^{-1}, or a 78.5% increase in *Dhc* cell abundance. Similarly, *Dhc* strain BAV1 cultures inhibited with 100 μM N_2O produced a final $(4.6 \pm 1.0) \times 10^7$ 16S rRNA gene copies mL^{-1}, or a 65% increase in *Dhc* cell numbers compared to $(2.8 \pm 1.3) \times 10^7$ 16S rRNA gene copies mL^{-1} before the introduction of *P* strain DCP-Ps1. Although all cultures

bottles received similar amounts of *c*DCE (i.e., 90 µmol) as electron acceptor, the final *Dhc* cell abundance in cultures that received initial N_2O concentrations of 30 and 100 µM decreased approximately 15% and 20%, respectively, compared to the final Dhc cell abundance of $(5.8 \pm 1.0) \times 10^7$ 16S rRNA gene copies mL^{-1} measured in cultures without N_2O addition.

4.5 Discussion

4.5.1 N_2O toxicity and corrinoid metabolism in SDC-9

N_2O is known to react with cobalt(I)-containing corrinoids [32,33], an organometallic enzyme cofactor used in biology to catalyze essential biochemical reactions such as carbon skeleton rearrangement, methyl group transfer and reductive dehalogenation [20,54]. The potent inhibitory effects of N_2O have been observed in corrinoid-dependent enzymatic processes, including methionine synthesis [34,35], methanogenesis [55,56] and reductive dechlorination [21]. N_2O inhibition on OHRB, particularly *Dhc*, is of particular concern as incomplete detoxification of PCE and TCE leads to the formation of carcinogenic *c*DCE and VC in the environment [57]. The results showed that the corrinoid-auxotrophic *Dhc* strain BAV1 was more sensitive to N_2O toxicity than *Geo* strain SZ, which possibly relates to the inability of *Dhc* strains for *de novo* cobamide biosynthesis [21]. *Dhc* growth is much more robust in mixed cultures when other microorganisms such as methanogens, homoacetogens, syntrophs, and fermenters provide essential growth nutrients, including corrinoids [6]. However,

the source/availability of the corrinoid cofactor or the preferred DMB lower base to sustain *Dhc* reductive dechlorination activity, as well as how these supportive organisms shape the corrinoid pools for *Dhc* are largely unclear. Interestingly, many well-characterized corrinoid producers, such as methanogens and homoacetogens, that are known to support the growth of *Dhc* in mixed cultures strictly rely on corrinoid-dependent enzymes for key enzymatic steps [54] and are subject to N_2O inhibition [58]. For example, around 50 µM N_2O completely inhibited methanogenesis as well as the growth of *Methanosarcina barkeri* strain Fusaro with acetate as substrate (Chapter four, unpublished data). The effects of N_2O on hydrogenotrophic CO_2 reduction by homoacetogens have not been investigated but preliminary experiments suggested inhibition. Thus, N_2O will likely reduce corrinoid production and alter the corrinoid pool in mixed microbial cultures, which will negatively impact the growth and activity of corrinoid-auxotrophic organisms, including *Dhc*. Taken together, these findings suggest that N_2O exhibits a more complex impact on the corrinoid yields and profiles in microbial dechlorinating community, and thus corrinoid-auxotrophic organisms.

More than 17 naturally occurring corrinoids featured with one of the three major classes of lower ligands (i.e., benzimidazole, purine, and phenol derivitives) have been identified [19,54]. Corrinoids with different lower ligands are not functionally equivalent as cofactors [54]. For example, organisms such as *Escherichia coli* (ATCC 11105) and *Lactobacillus leichmannii* (ATCC 4797) can utilize up to 11 of the total 17 naturally occurring cobamides for growth [40]. On the

contrary, corrinoid-auxotrophic *Dhc* can only use DMB-Cba, or also MeBza-Cba in the case of *Dhc* strain BAV1, for synthesizing functional BvcA or VcrA RDases [40]. In agreement with these findings, unfavorable corrinoids (such as 5-OMeBza-Cba and 5-OHBza-Cba) have been shown not support or even inhibited growth and dechlorination activity of axenic *Dhc* strains [40]. These findings suggest that either reduced corrinoid supply or changed corrinoid profiles as a result of changes in biogeochemical conditions or microbial community compositions will affect the capability of *Dhc* for initiating robust dechlorination activities [17]. Accordingly, I found that the presence of N_2O substantially altered the corrinoid production profile of *Dhc*-containing SDC-9 consortium. Results showed that DMB-Cba and MeBza-Cba are among the major corrinoids in actively VC-dechlorinating SDC-9 cultures. On the contrary, the presence of 100 µM N_2O significantly changed the corrinoid profile of SDC-9 consortium. Compared to VC-dechlorinating SDC-9 cultures, the production of total corrinoid and DMB-Cba in N_2O-treated cultures decreased by 10 and 20%, respectively. One possible explanation is that N_2O-inhibited *Dhc* lost corrinoid scavenging ability and was not able to assemble functional DMB-Cba for growth, which was supported by the limited *Dhc* 16S rRNA gene production observed in these experiments. Other possible explanations are that organisms responsible for DMB-Cba production in SDC-9 cultures were also affected by N_2O. In fact, some homoacetogenic bacteria such as *Acetobacterium woodii* are capable of synthesizing DMB-Cba to support the cofactor demands for their methyltransferases in the Wood–

Ljungdahl pathway [29]. Since all known homoacetogens also have strict requirements for Co(I)-corrinoid, N_2O might have hindered their growth and decreased DMB-Cba production. In either scenario, N_2O repressed the production of preferred DMB-Cba for *Dhc*, which further contributed to the negative impact of N_2O on dechlorination activity.

Another interesting finding was that the production of 5-OHBza-Cba in all N_2O-treated cultures substantially decreased. These decreases in 5-OHBza-Cba correlate with decreased numbers of archaeal 16S rRNA gene copies suggesting that N_2O affects archaea growth. Methanogens such as *M. barkeri* are known to produce 5-OHBza-Cba [12] and are subject to N_2O inhibition. Based on previous findings ([55] and Chapter 3), N_2O in the concentration range of 10 – 130 µM can partially or completely inhibit methanogenesis and methanogen growth. Repressed growth of methanogens in SDC-9 cultures would reduce the amount of 5-OHBza-Cba synthesized. Although the exact mechanisms of how N_2O affects corrinoid metabolisms in microbial communities still remain to be explored, N_2O induced changes in yields and profiles of corrinoids in dechlorinating consortium SDC-9 revealed an unrecognized impact of N_2O on the corrinoids pool produced by the microbial community. Considering the commonality of elevated N_2O concentrations in groundwater and the vital roles of corrinoid-dependent enzyme systems for organisms that live in these environments, such as methanogens, homoacetogens and OHRB, the impacts of N_2O on corrinoid pools may have significant impact on various microbial

activities, including organohalide respiration. Therefore, more detailed studies elucidating the effects of N_2O on corrinoid-dependent metabolisms and nutrients dynamics in microbial communities are warranted.

4.5.2 N_2O toxicity and metabolic responses of the SDC-9 consortium

Alterations of metabolic pathways are associated with changes in metabolite production and metabolome profiles [59,60]. As such, exposing organisms to different environmental conditions will alter their biochemistries (metabolic pathways) [61]. Therefore, the use of metabolomics is becoming increasingly popular in environmental studies to characterize microbial processes of interest. In agreement with the assumption that N_2O has the potential to negatively affect a wide variety of metabolic processes in a microbial community, the metabolome profile of the SDC-9 consortium shifted significantly in response to the presence of N_2O. Interestingly, apart from some changes caused by the initial substrate (i.e., lactate), no divergent shifts were observed between VC-dechlorinating SDC-9 and control cultures without substrate supply, suggesting a stable metabolic profile of SDC-9 consortium in the absence of N_2O. While similar responses were observed in all N_2O-treated cultures (regardless whether provided with VC or not), cultures with VC and cultures with both VC and N_2O revealed distinct metabolomes, indicating that the metabolic profile of SDC-9 was significantly altered by N_2O.

With the observed decreases in dechlorination activity and significant changes in many metabolites, I speculate that the metabolome profile shifts observed for the SDC-9 culture exposed to N_2O may be attributed to altered metabolic pathways that involved corrinoid enzymes. Indeed, in the presence of 100 µM N_2O, metabolites such as methionine sulfoxide and succinate/methylmalonate, both of which are associated with corrinoid-dependent enzymes, showed around a 2-fold increase and a 3-fold decrease, respectively. These changed metabolites abundances together with shifts in the overall metabolic profile corroborate the significant impact of N_2O for corrinoid-related metabolisms. Although the metabolic pathways affected by N_2O cannot be identified, the unique metabolic profile changes when dechlorinating SDC-9 consortium was exposed to N_2O provided some insights for interpreting the potential effect of N_2O.

4.5.3 Mitigation strategies and recovery of dechlorination activities

In addition to relying on community members for providing corrinoids and nutrients, *Dhc* in microbial communities also requires other organisms to scavenge trace oxygen, to remove carbon monoxide it produces but cannot tolerate [63], and potentially, to curb toxic effects caused by N_2O. The *Dhc*-containing SDC-9 consortium with one-time addition of 100 µM N_2O recovered dechlorination capability soon after the consumption of amended N_2O, suggesting a detoxification role of N_2O reducers for *Dhc* in SDC-9 consortium. In

anoxic environments, anaerobic organisms such as methanogens, acetogens and OHRB with corrinoid-dependent enzyme systems need to maintain super-reduced Co(I)-corrinoids for function [64]. Co(I)-corrinoids oxidation by molecular oxygen or N_2O leads to the formation of inactive Co(II)-corrinoid [34,65]. To compensate the function loss of corrinoid-dependent enzyme systems caused by this oxidation reaction, organisms developed diverse defense strategies. Homoacetogenic bacteria such as *Acetobacterium woodii* employ an activating enzyme to catalyze the reduction of inactivate Co(II) back to catalytically active Co(I)-corrinoids at the expense of ATP [65]. Other organisms such as *Paracoccus denitrificans* strain PD1222 and *Escherichia coli* up-regulate MetE to relieve the toxicity caused by N_2O [53,54]. These findings are in accordance with the observations that PCE-grown *Geo* strain SZ in presence of 100 µM N_2O completely lost expression of *metH* but the organism was still able to maintain growth via up-regulation of *metE* transcription.

Genomic analysis showed that *Dhc* lack *metE*/*metH* genes and no clear evidence of possessing activating enzymes have been found in *Dhc* RDase systems [66]. Therefore, *Dhc* in the environment must rely on N_2O reducers for alleviating the N_2O toxicity. In turn, *Dhc* potentially promotes the growth of N_2O reducers by consuming chlorinated solvents that can be toxic to N_2O reducers. Introduction of *P.* strain DCP-Ps1 harboring clade I NosZ restored the growth and dechlorination activities of both N_2O-inhibited *Dhc* strain BAV1 and *Geo* strain SZ. The experimental results confirmed the reversibility of N_2O inhibition and also

suggested that N_2O reducers play an important role for removing toxic N_2O and enabling reductive dechlorination. Recently, phylogenetically diverse organisms possessing clade II NosZ have been found widely distributed in various environments [37,38]. Whether these widespread N_2O reducers have a detoxification role for alleviating N_2O inhibition on corrinoid-dependent organisms is unclear. Findings reported here showed that clade II N_2O reducer (i.e., *Adehal* strain 2CP-C) was able to consume low concentrations of N_2O (i.e., 30 or 100 µM) within 2 days, much faster than *P* strain DCP-Ps1 (i.e., 3 and 5 days for 30 and 100 µM N_2O, respectively). As a result, a much shorter incubation time was required for *Adehal* strain 2CP-C than for *P* strain DCP-Ps1 before TCE dechlorination resumed in N_2O-inhibited *Geo* strain SZ cultures. Prior work showed that clade II NosZ exhibit one to two orders of magnitude higher affinities to N_2O [67,68], consistent with the observed higher efficiency of *Adehal* strain 2CP-C for restoring dechlorination activity of N_2O-inhibited *Geo* strain SZ. Together, these findings demonstrated the reversibility of N_2O inhibition on bacterial reductive dechlorination, and applicable approaches (such as maintaining N_2O-reducing capability) must be exploited to achieve and sustain desirable reductive dechlorination rates at sites impacted with chlorinated solvents and elevated N_2O concentrations.

4.6 Acknowledgement

I thank Fadime Murdoch for assistance with molecular analysis and Robert Murdoch for help with the analyses of 16S amplicon sequencing data, Amanda Lee for assistance with the metabolomics works and Paul Hatzinger at APTIM for providing SDC-9 consortium. I also thank Gao Chen for suggestions and contributions on experiments and manuscript preparation.

4.7 References

(1) Adrian, L.; Löffler, F. E., *Organohalide-respiring bacteria*. Springer: Berlin Heidelberg: 2016.

(2) Schmidt, K. R.; Tiehm, A., Natural attenuation of chloroethenes: identification of sequential reductive/oxidative biodegradation by microcosm studies. *Water Sci Technol* **2008,** *58* (5), 1137-1145.

(3) Amaral, H. I.; Aeppli, C.; Kipfer, R.; Berg, M., Assessing the transformation of chlorinated ethenes in aquifers with limited potential for natural attenuation: added values of compound-specific carbon isotope analysis and groundwater dating. *Chemosphere* **2011,** *85* (5), 774-781.

(4) Dugat-Bony, E.; Biderre-Petit, C.; Jaziri, F.; David, M. M.; Denonfoux, J.; Lyon, D. Y.; Richard, J. Y.; Curvers, C.; Boucher, D.; Vogel, T. M.; Peyretaillade, E.; Peyret, P., *In situ* TCE degradation mediated by complex dehalorespiring communities during biostimulation processes. *Microb Biotechnol* **2012,** *5* (5), 642-653.

(5) Tillotson, J. M.; Borden, R. C., Rate and extent of chlorinated ethene removal at 37 ERD sites. *J Environ Eng* **2017,** *143* (8), 04017028.

(6) Löffler, F. E.; Edwards, E. A., Harnessing microbial activities for environmental cleanup. *Curr Opin Biotechnol* **2006,** *17* (3), 274-284.

(7) Löffler, F. E.; Yan, J.; Ritalahti, K. M.; Adrian, L.; Edwards, E. A.; Konstantinidis, K. T.; Müller, J. A.; Fullerton, H.; Zinder, S. H.; Spormann, A. M., *Dehalococcoides mccartyi gen. nov., sp. nov.*, obligately organohalide-respiring anaerobic bacteria relevant to halogen cycling and bioremediation, belong to a novel bacterial class, *Dehalococcoidia classis nov.*, order *Dehalococcoidales ord. nov.* and family *Dehalococcoidaceae fam. nov*., within the phylum *Chloroflexi*. *Int J Syst Evol Microbiol* **2013,** *63* (2), 625-635.

(8) Yang, Y.; Higgins, S. A.; Yan, J.; Simsir, B.; Chourey, K.; Iyer, R.; Hettich, R. L.; Baldwin, B.; Ogles, D. M.; Löffler, F. E., Grape pomace compost harbors organohalide-respiring Dehalogenimonas species with novel reductive dehalogenase genes. *ISME J* **2017,** *11* (12), 2767-2780.

(9) Sung, Y.; Fletcher, K. E.; Ritalahti, K. M.; Apkarian, R. P.; Ramos-Hernández, N.; Sanford, R. A.; Mesbah, N. M.; Löffler, F. E., *Geobacter lovleyi* sp. nov. strain SZ, a novel metal-reducing and tetrachloroethene-dechlorinating bacterium. *Appl Environ Microbiol* **2006,** *72* (4), 2775-2782.

(10) Fincker, M.; Spormann, A. M., Biochemistry of catabolic reductive dehalogenation. *Annu Rev Biochem* **2017,** *86*, 357-386.

(11) Yi, S.; Seth, E. C.; Men, Y. J.; Stabler, S. P.; Allen, R. H.; Alvarez-Cohen, L.; Taga, M. E., Versatility in corrinoid salvaging and remodeling pathways supports corrinoid-dependent metabolism in Dehalococcoides mccartyi. *Appl Environ Microbiol* **2012,** *78* (21), 7745-7752.

(12) Yan, J.; Im, J.; Yang, Y.; Löffler, F. E., Guided cobalamin biosynthesis supports *Dehalococcoides mccartyi* reductive dechlorination activity. *Philos Trans R Soc Lond B Biol Sci* **2013,** *368* (1616), 20120320.

(13) Hug, L. A.; Edwards, E. A., Diversity of reductive dehalogenase genes from environmental samples and enrichment cultures identified with degenerate primer PCR screens. *Front Microbiol* **2013,** *4*, 1-16.

(14) Yan, J.; Ritalahti, K. M.; Wagner, D. D.; Löffler, F. E., Unexpected specificity of interspecies cobamide transfer from *Geobacter spp*. to organohalide-respiring *Dehalococcoides mccartyi* strains. *Appl Environ Microbiol* **2012,** *78* (18), 6630-6636.

(15) Zhang, Y.; Rodionov, D. A.; Gelfand, M. S.; Gladyshev, V. N., Comparative genomic analyses of nickel, cobalt and vitamin B_{12} utilization. *BMC Genomics* **2009,** *10* (1), 78.

(16) Johnson, D. R.; Nemir, A.; Andersen, G. L.; Zinder, S. H.; Alvarez-Cohen, L., Transcriptomic microarray analysis of corrinoid responsive genes in *Dehalococcoides ethenogenes* strain 195. *FEMS Microbiol Lett* **2009,** *294* (2), 198-206.

(17) Men, Y.; Seth, E. C.; Yi, S.; Crofts, T. S.; Allen, R. H.; Taga, M. E.; Alvarez-Cohen, L., Identification of specific corrinoids reveals corrinoid modification in dechlorinating microbial communities. *Environ Microbiol* **2014,** *17* (12), 4873-4884.

(18) Men, Y.; Seth, E. C.; Yi, S.; Allen, R. H.; Taga, M. E.; Alvarez-Cohen, L., Sustainable growth of *Dehalococcoides mccartyi* 195 by corrinoid salvaging and remodeling in defined lactate-fermenting consortia. *Appl Environ Microbiol* **2014,** *80* (7), 2133-41.

(19) Men, Y.; Lee, P. K.; Harding, K. C.; Alvarez-Cohen, L., Characterization of four TCE-dechlorinating microbial enrichments grown with different cobalamin stress and methanogenic conditions. *Appl Microbiol Biotechnol* **2013,** *97* (14), 6439-6450.

(20) Yan, J.; Bi, M.; Bourdon, A. K.; Farmer, A. T.; Wang, P. H.; Molenda, O.; Quaile, A. T.; Jiang, N.; Yang, Y.; Yin, Y.; Şimşir, B.; Campagna, S. R.; Edwards, E. A.; Löffler, F. E., Purinyl-cobamide is a native prosthetic group of reductive dehalogenases. *Nat Chem Biol* **2018,** *14* (1), 8-14.

(21) Yin, Y.; Yan, J.; Chen, G.; Murdoch, F. K.; Pfisterer, N.; Löffler, F. E., Nitrous oxide is a potent inhibitor of bacterial reductive dechlorination. *Environ Sci Technol* **2018,** *53* (2), 692-701.

(22) Zumft, W. G., Cell biology and molecular basis of denitrification. *Microbiol Mol Biol Rev* **1997,** *61* (4), 533-616.

(23) Thomson, A. J.; Giannopoulos, G.; Pretty, J.; Baggs, E. M.; Richardson, D. J., Biological sources and sinks of nitrous oxide and strategies to mitigate emissions. *Philos Trans R Soc Lond B Biol Sci* **2012,** *367* (1593), 1157-1168.

(24) Zhu, X.; Burger, M.; Doane, T. A.; Horwath, W. R., Ammonia oxidation pathways and nitrifier denitrification are significant sources of N_2O and NO under low oxygen availability. *Proc Natl Acad Sci USA* **2013,** *110* (16), 6328-6333.

(25) Daims, H.; Lücker, S.; Wagner, M., A new perspective on microbes formerly known as nitrite-oxidizing bacteria. *Trends Microbiol* **2016,** *24* (9), 699-712.

(26) Tian, H.; Yang, J.; Xu, R.; Lu, C.; Canadell, J. G.; Davidson, E. A.; Jackson, R. B.; Arneth, A.; Chang, J.; Ciais, P.; Gerber, S.; Ito, A.; Joos, F.; Lienert, S.; Messina, P.; Olin, S.; Pan, S.; Peng, C.; Saikawa, E.; Thompson, R. L.; Vuichard, N.; Winiwarter, W.; Zaehle, S.; Zhang, B., Global soil nitrous oxide emissions since the preindustrial era estimated by an ensemble of terrestrial biosphere models: Magnitude, attribution, and uncertainty. *Glob Chang Biol* **2018**, 25(2), 640-659.

(27) Voigt, C.; Marushchak, M. E.; Lamprecht, R. E.; Jackowicz-Korczynski, M.; Lindgren, A.; Mastepanov, M.; Granlund, L.; Christensen, T. R.; Tahvanainen, T.; Martikainen, P. J.; Biasi, C., Increased nitrous oxide emissions from Arctic peatlands after permafrost thaw. *Proc Natl Acad Sci USA* **2017,** *114* (24), 6238-6243.

(28) Griffis, T. J.; Chen, Z.; Baker, J. M.; Wood, J. D.; Millet, D. B.; Lee, X.; Venterea, R. T.; Turner, P. A., Nitrous oxide emissions are enhanced in a warmer and wetter world. *Proc Natl Acad Sci USA* **2017,** *114* (45), 12081-12085.

(29) Hazra, A. B.; Han, A. W.; Mehta, A. P.; Mok, K. C.; Osadchiy, V.; Begley, T. P.; Taga, M. E., Anaerobic biosynthesis of the lower ligand of vitamin B_{12}. *Proc Natl Acad Sci USA* **2015,** *112* (34), 10792-10797.

(30) Stupperich, E.; Eisinger, H.-J.; Schurr, S., Corrinoids in anaerobic bacteria. *FEMS Microbiol Rev* **1990,** *7* (3-4), 355-359.

(31) He, J.; Holmes, V. F.; Lee, P. K.; Alvarez-Cohen, L., Influence of vitamin B_{12} and cocultures on the growth of Dehalococcoides isolates in defined medium. *Appl Environ Microbiol* **2007,** *73* (9), 2847-2853.

(32) Banks, R. G. S.; Henderson, R. J.; Pratt, J. M., Reactions of gases in solution. Part III. Some reactions of nitrous oxide with transition-metal complexes. *J Chem Soc Sec A* **1968,** (0), 2886-2889.

(33) Blackburn, R.; Kyaw, M.; Swallow, A. J., Reaction of cob(I)alamin with nitrous oxide and cob(III)alamin. *J Chem Soc, Faraday Trans I* **1977,** *73* (0), 250-255.

(34) Drummond, J. T.; Matthews, R. G., Nitrous oxide inactivation of cobalamin-dependent methionine synthase from *Escherichia coli*: characterization of the damage to the enzyme and prosthetic group. *Biochemistry* **1994,** *33* (12), 3742-3750.

(35) Drummond, J. T.; Matthews, R. G., Nitrous oxide degradation by cobalamin-dependent methionine synthase: characterization of the reactants and products in the inactivation reaction. *Biochemistry* **1994,** *33*, 3732-3741.

(36) Banger, K.; Tian, H.; Lu, C., Do nitrogen fertilizers stimulate or inhibit methane emissions from rice fields? *Glob Chang Biol* **2012,** *18* (10), 3259-3267.

(37) Sanford, R. A.; Wagner, D. D.; Wu, Q.; Chee-Sanford, J. C.; Thomas, S. H.; Cruz-Garcia, C.; Rodriguez, G.; Massol-Deya, A.; Krishnani, K. K.; Ritalahti, K. M.; Nissen, S.; Konstantinidis, K. T.; Löffler, F. E., Unexpected nondenitrifier nitrous oxide reductase gene diversity and abundance in soils. *Proc Natl Acad Sci USA* **2012,** *109* (48), 19709-19714.

(38) Hallin, S.; Philippot, L.; Löffler, F. E.; Sanford, R. A.; Jones, C. M., Genomics and Ecology of Novel N2O-Reducing Microorganisms. *Trends Microbiol* **2018,** *26* (1), 43-55.

(39) Jurado, A.; Borges, A. V.; Brouyere, S., Dynamics and emissions of N_2O in groundwater: A review. *Sci Total Environ* **2017,** *584*, 207-218.

(40) Yan, J.; Şimşir, B.; Farmer, A. T.; Bi, M.; Yang, Y.; Campagna, S. R.; Löffler, F. E., The corrinoid cofactor of reductive dehalogenases affects dechlorination rates and extents in organohalide-respiring *Dehalococcoides mccartyi*. *ISME J* **2016,** *10* (5), 1092-1101.

(41) Wolin, E. A.; Wolin, M. J.; Wolfe, R. S., Formation of methane by bacterial extracts. *J Biol Chem* **1963,** *238* (8), 2882-2886.

(42) Sander, R., Compilation of Henry's law constants (version 4.0) for water as solvent. *Atmos Chem Physics* **2015,** *15* (8), 4399-4981.

(43) Stupperich, E.; Steiner, I.; Rühlemann, M., Isolation and analysis of bacterial cobamides by high-performance liquid chromatography. *Analytical Biochem* **1986,** *155* (2), 365-370.

(44) Bennett, B. D.; Yuan, J.; Kimball, E. H.; Rabinowitz, J. D., Absolute quantitation of intracellular metabolite concentrations by an isotope ratio-based approach. *Nat Protoc* **2008,** *3* (8), 1299-1311.

(45) Lu, W.; Clasquin, M. F.; Melamud, E.; Amador-Noguez, D.; Caudy, A. A.; Rabinowitz, J. D., Metabolomic analysis via reversed-phase ion-pairing liquid chromatography coupled to a stand alone orbitrap mass spectrometer. *Anal Chem* **2010,** *82* (8), 3212-3221.

(46) Rabinowitz, N. C.; Willmore, B. D. B.; King, A. J.; Schnupp, J. W. H., Constructing noise-invariant representations of sound in the auditory pathway. *PLoS Biol* **2013,** *11* (11), e1001710.

(47) Yoon, S.; Cruz-García, C.; Sanford, R.; Ritalahti, K. M.; Löffler, F. E., Denitrification versus respiratory ammonification: environmental controls of two competing dissimilatory NO_3^-/NO_2^- reduction pathways in *Shewanella loihica* strain PV-4. *ISME J* **2015,** *9* (5), 1093-1104.

(48) Ritalahti, K. M.; Amos, B. K.; Sung, Y.; Wu, Q.; Koenigsberg, S. S.; Löffler, F. E., Quantitative PCR targeting 16S rRNA and reductive dehalogenase genes simultaneously monitors multiple *Dehalococcoides strains*. *Appl Environ Microbiol* **2006,** *72* (4), 2765-2774.

(49) Ritalahti, K.; Cruz-García, C.; Padilla-Crespo, E.; Hatt, J.; Löffler, F. E, RNA extraction and cDNA analysis for quantitative assessment of biomarker transcripts in groundwater. *Handbook of Hydrocarbon and Lipid Microbiology* **2010**, 3671-3685.

(50) Kearse, M.; Moir, R.; Wilson, A.; Stones-Havas, S.; Cheung, M.; Sturrock, S.; Buxton, S.; Cooper, A.; Markowitz, S.; Duran, C.; Thierer, T.; Ashton, B.; Meintjes, P.; Drummond, A., Geneious Basic: an integrated and extendable desktop software platform for the organization and analysis of sequence data. *Bioinformatics* **2012,** *28* (12), 1647-1649.

(51) Ye, J.; Coulouris, G.; Zaretskaya, I.; Cutcutache, I.; Rozen, S.; Madden, T. L., Primer-BLAST: A tool to design target-specific primers for polymerase chain reaction. *BMC Bioinformatics* **2012,** *13* (1), 134.

(52) Karlen, Y.; McNair, A.; Perseguers, S.; Mazza, C.; Mermod, N., Statistical significance of quantitative PCR. *BMC Bioinformatics* **2007,** *8* (1), 131.

(53) Sullivan, M. J.; Gates, A. J.; Appia-Ayme, C.; Rowley, G.; Richardson, D. J., Copper control of bacterial nitrous oxide emission and its impact on vitamin B_{12}-dependent metabolism. *Proc Natl Acad Sci USA* **2013,** *110* (49), 19926-19931.

(54) Matthews, R. G., Cobalamin- and corrinoid-dependent enzymes. *Met Ions Life Sci* **2009,** *6*, 53-114.

(55) Klüber, H. D.; Conrad, R., Inhibitory effects of nitrate, nitrite, NO and N_2O on methanogenesis by *methanosarcina barkeri* and *Methanobacterium bryantii*. *FEMS Microbiol Ecol* **1998,** *25*, 331-339.

(56) Klüber, H. D.; Conrad, R., Effects of nitrate, nitrite, NO and N_2O on methanogenesis and other redox processes in anoxic rice field soil. *FEMS Microbiol Ecol* **1998,** *25* (3), 301-318.

(57) Atashgahi, S.; Lu, Y.; Zheng, Y.; Saccenti, E.; Suarez-Diez, M.; Ramiro-Garcia, J.; Eisenmann, H.; Elsner, M.; A, J. M. S.; Springael, D.; Dejonghe, W.; Smidt, H., Geochemical and microbial community determinants of reductive dechlorination at a site biostimulated with glycerol. *Environ Microbiol* **2017,** *19* (3), 968-981.

(58) Balderston, W. L.; Payne, W. J., Inhibition of methanogenesis in salt marsh sediments and whole-cell suspensions of methanogenic bacteria by nitrogen oxides. *Appl Environ Microbiol* **1976,** *32* (2), 264-269.

(59) Lankadurai, B. P.; Wolfe, D. M.; Simpson, A. J.; Simpson, M. J., ^{1}H NMR-based metabolomic observation of a two-phased toxic mode of action in *Eisenia fetida* after sub-lethal phenanthrene exposure. *Environ Chem* **2011,** *8* (2), 105-114.

(60) Mashego, M. R.; Rumbold, K.; De Mey, M.; Vandamme, E.; Soetaert, W.; Heijnen, J. J., Microbial metabolomics: past, present and future methodologies. *Biotechnol Lett* **2007,** *29* (1), 1-16.

(61) Hou, Y.; Braun, D. R.; Michel, C. R.; Klassen, J. L.; Adnani, N.; Wyche, T. P.; Bugni, T. S., Microbial strain prioritization using metabolomics tools for the discovery of natural products. *Analyt Chem* **2012,** *84* (10), 4277-4283.

(62) Tang, J., Microbial metabolomics. *Curr Genomics* **2011,** *12* (6), 391-403.

(63) Atashgahi, S.; Haggblom, M. M.; Smidt, H., Organohalide respiration in pristine environments: implications for the natural halogen cycle. *Environ Microbiol* **2018,** *20* (3), 934-948.

(64) Richter, N.; Zepeck, F.; Kroutil, W., Cobalamin-dependent enzymatic O-, N-, and S-demethylation. *Trends Biotechnol* **2015,** *33* (7), 371-373.

(65) Farnberger, J. E.; Richter, N.; Hiebler, K.; Bierbaumer, S.; Pickl, M.; Skibar, W.; Zepeck, F.; Kroutil, W., Biocatalytic methylation and demethylation via a shuttle catalysis concept involving corrinoid proteins. *Commun Chem* **2018,** *1* (1), 82.

(66) Zhuang, W. Q.; Yi, S.; Bill, M.; Brisson, V. L.; Feng, X.; Men, Y.; Conrad, M. E.; Tang, Y. J.; Alvarez-Cohen, L., Incomplete Wood-Ljungdahl pathway facilitates one-carbon metabolism in organohalide-respiring Dehalococcoides mccartyi. *Proc Natl Acad Sci USA* **2014,** *111* (17), 6419-6424.

(67) Yoon, S.; Nissen, S.; Park, D.; Sanford, R. A.; Löffler, F. E., Nitrous oxide reduction kinetics distinguish bacteria harboring Clade I NosZ from those harboring Clade II NosZ. *Applied and Environmental Microbiology* **2016,** *82* (13), 3793-3800.

(68) Suenaga, T.; Riya, S.; Hosomi, M.; Terada, A., Biokinetic characterization and activities of N_2O-reducing bacteria in response to various oxygen levels. *Frontiers in Microbiology* **2018,** *9*(13), 697.

4.7 Appendix

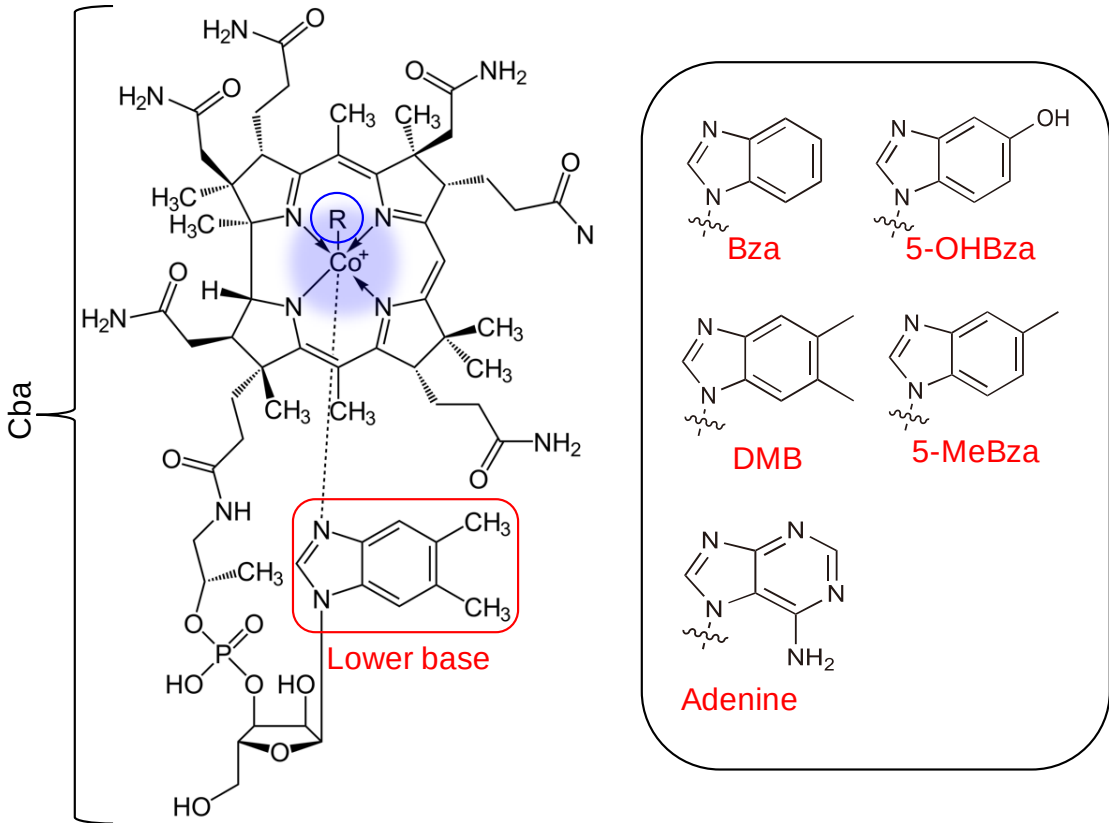


Figure 4.1. Corrinoids with the listed lower bases identified in this study. The structure of cobalamin (i.e., vitamin B_{12}) is shown as the example. In the case of cobalamin, the lower base in cobalamin is 5, 6-dimethylbenzimidazole (DMB) and the upper ligand is cyanide. The R group (i.e., upper ligand) can be a methyl or adenosyl group, etc. Bza, benzimidazole; 5-OHBza, 5-hydroxybenzimidazole; 5-MeBza, 5-methylbenzimidazole.

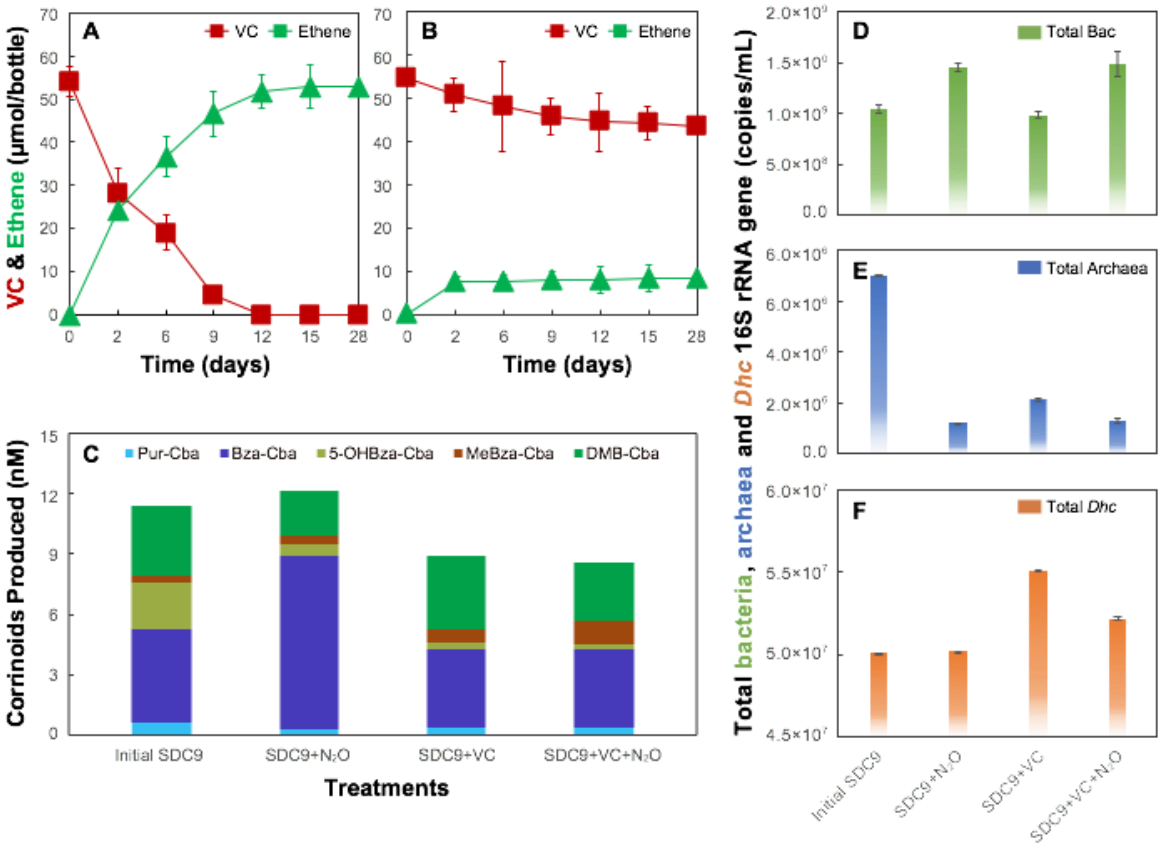


Figure 4.2. Effect of N_2O on reductive dechlorination of VC in *Dhc*-containing SDC-9 consortium. VC reductive dechlorination in SDC-9 without N_2O **(A)** and in the presence of 100 μM N_2O **(B)**. **(C)** Corrinoid yields profiles of SDC-9. Enumeration of total Bacteria **(D),** total Archaea **(E)** and total *Dhc* **(F)** 16S rRNA at the end of growth experiments.

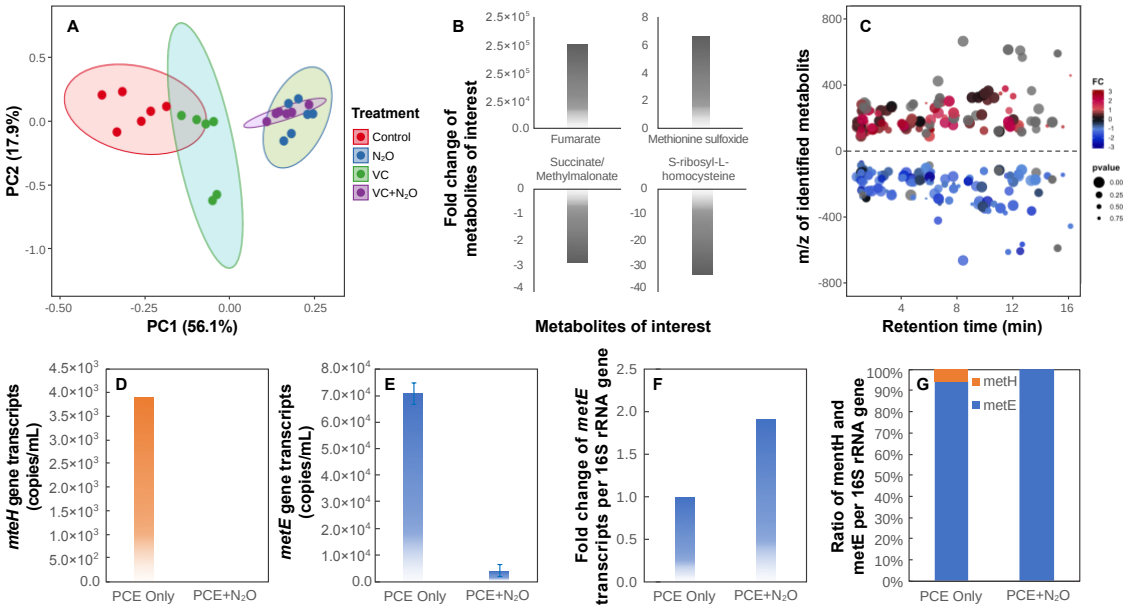


Figure 4.3. Metabolic responses of SDC-9 to N_2O inhibition (A), (B) and (C) & transcription change of *metH/metE* in *Geo* strain SZ (D), (E), (F) and (G). **(A)** PCA plot using all identified metabolites in SDC-9 consortium with triplicate cultures and duplicate injections. **(B)** Relative abundances of selected metabolites involved in corrinoid-dependent enzymes in VC-dechlorinating VS 100 µM N_2O inhibited SDC-9. **(C)** Cloud Plot of identified metabolites in VC-dechlorinating VS 100 µM N_2O inhibited SDC-9: data show fold changes and p-values of the identified metabolites along the LC-MS trace using retention time and m/z. **(D)**, **(E)**, **(F)** and **(G)** show average transcriptions of *metH* **(D)**, *metE* **(E),** relative fold change of *metE* normalized to 16S rRNA gene **(F)** and calculated ratio of *metE/metH* **(G)** after normalized to 16S rRNA gene in PCE dechlorinating *Geo* strain SZ cultures with and without 100 µM N_2O.

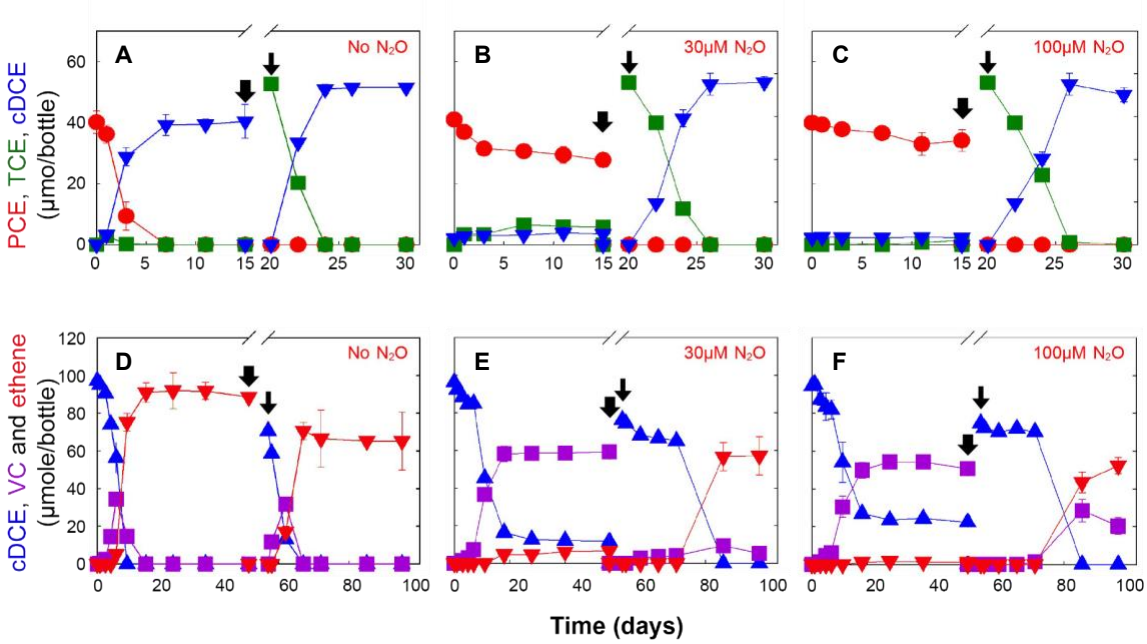


Figure 4.4. Recovery of dechlorination activity after replacing N_2O with N_2/CO_2 (80/20) and respike electron donor/acceptors in N_2O-inhibited *Geo* strain SZ (A), (B), and **(C),** and *Dhc* strain BAV1 **(D), (E),** and **(F).** Thick arrows indicate the time points to flush out N_2O; Thin arrows indicate the time points to respike electron donor/acceptors.

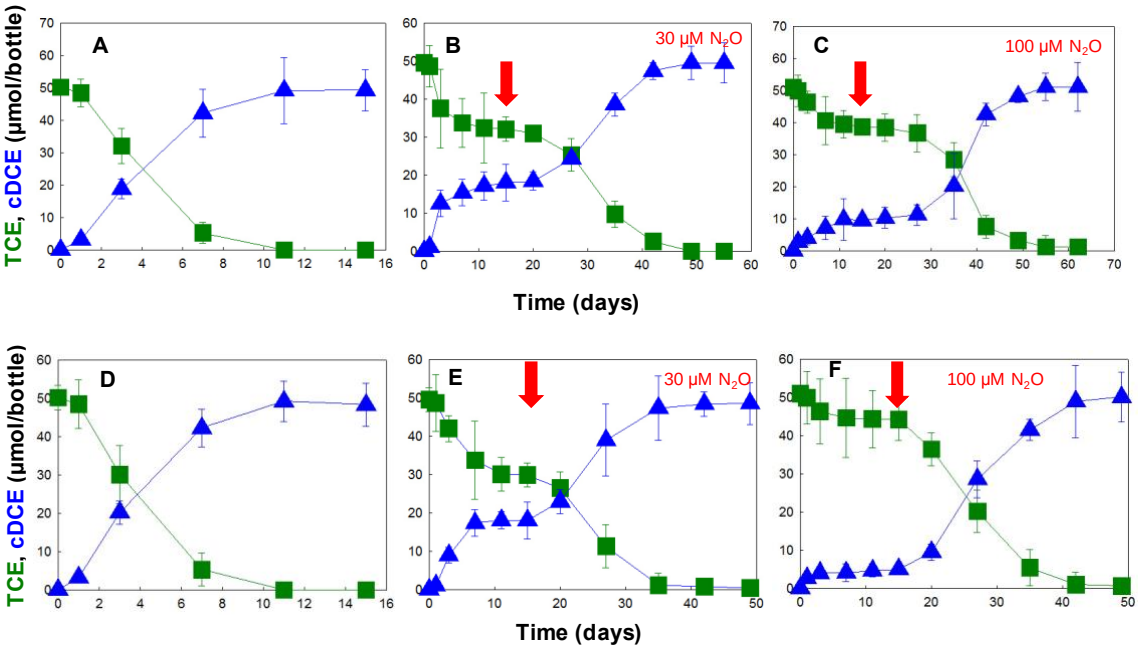


Figure 4.5. Recovery of TCE dechlorination activity of *Geo* strain SZ after introducing clade I (*P* strain DCP-Ps1) and clade II (*A* strain 2CP-C) N_2O reducers. *Geo* strain SZ grown with TCE as electron acceptor and with N_2O at the concentrations of 0 μM **(A)** and **(D)**, 30 μM **(B)** and **(E)**, 100 μM **(C) and (F)**. Red arrows indicate the time points to introduce corresponding N_2O reducers.

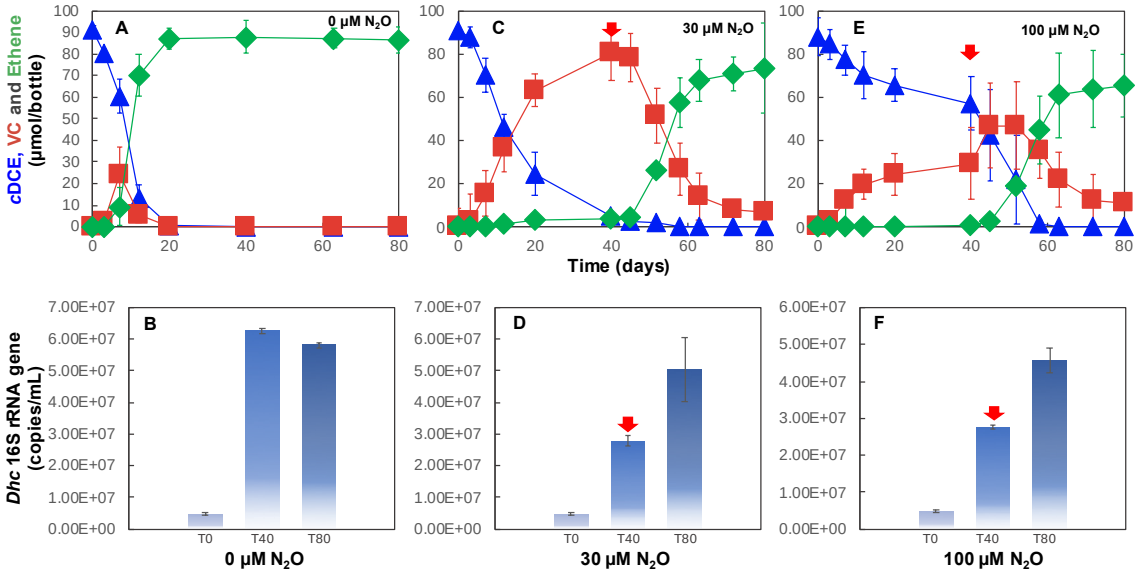


Figure 4.6. Recovery of *c*DCE dechlorination activity of *Dhc* strain BAV1 after introducing clade I (*P* strain DCP-Ps1) N_2O reducers. *Dhc* strain BAV1 grown with *c*DCE and with N_2O at the concentrations of 0 μM **(A)**, 30 μM **(C)**, 100 μM (E). *Dhc* 16S rRNA gene yields before and after the introduction of *P* strain DCP-Ps1. Red arrows indicate the time points to introduce *P* strain DCP-Ps1.

Table 4.1. Primers and Probes used in this study

Target DNA	Primer and Probe sets	Sequence (5' – 3')
Geobacter 16S rRNA gene	Geo_16S810F	CGATGAGWACTAGGTGTTGCGG
	Geo_16S884R	CTTCCCAGGCGGAGWACTTAATGC
	Geo_16S834P	FAM-ATTGACCCCTGCAGTGCC-MGB
Geobacter metE gene	metE_Geo_SZ817F	TCCATCCGTGGCAAGGTTATC
	metE_Geo_SZ953qR	TGTTCGACAAAGCCGTCAGT
	metE_Geo_SZ_953qP	FAM-CTTGGTCTGTTCACCATCGCT-MGB
Geobacter metE gene	metH_GeoSZ_195F	TGGCGCTGATATTGTAGAGACC
	metH_GeoSZ_292qR	CGGCCTTGTTCAGTTCAAAGAC
	metH-GeoSZ-243qP	FAM-ACTGGCTGAATATGGCCTTGC-MGB
Total Bacteria 16S rRNA gene	Bac_1055YF	ATGGYTGTCGTCAGCT
	Bac_1392R	ACGGGCGGTGTGTAC
	Bac_1115_P	FAM-CAACGAGCGCAACCC-MGB
Total Archaea16S rRNA gene	Mtgen_835F	GGGRAGTACGKYCGCAAG
	Mtgen_918R	GAVTCCAATTRARCCGCA
	Mtgen_831_P	FAM-CCAATTCCTTTAAGTTTCA-MGB
Luciferase control mRNA	Luc_refF	TACAACACCCCAACATCTTCGA
	Luc_refR	GGAAGTTCACCGGCGTCAT
	Luc_refqP	FAM-TGGCAGGTCTTCCCGA-MGB

CHAPTER FIVE:
SUMMARY AND CONCLUSION

The massive perturbation of global N cycle as a result of intensive application of N fertilizers as well as fossil-fuel combustion has enabled human to largely increase food and fuel production, while has also led to a series of precedent environmental problems, including increased N_2O production. Anthropogenic activities introduce around 6.8 Tg N_2O yr^{-1} on global scale and the increasing food and fuel demand by growing world population will further boost the use of N fertilizers and eventually, the production and emission of N_2O. However, knowledge of the regulations of N_2O emissions and its impact on bacterial cellular metabolism are limited. N_2O is generally considered chemically inert without toxicity to microorganisms, and is either released to the atmosphere or further reduced by microorganisms harboring NosZ; however, research conducted in the 1960s demonstrated that N_2O abiotically reacts with certain transition metal complexes including reduced corrinoids such as Co(I) corrinoid. Corrinoid-dependent enzyme systems play key roles in biology, and are essential in the majority of living organisms, including humans. As N_2O concentrations in watersheds and groundwater aquifers continue to rise, its inhibition of enzyme-catalyzed metabolic steps that involve the Co(I) supernucleophile will likely also increase. Therefore, I proposed to investigate the impact of N_2O with organohalide-respiring bacteria (OHRB) and methanogenic archaea (methanogen), two groups of strict corrinoid-dependent microorganisms that have important roles in global Cl and C cycling.

In chapter two, detailed work examining the impact of N_2O on OHRB are presented. OHRB are keystone bacteria responsible for reductive dechlorination of the widespread chlorinated contaminants such as PCE and TCE. Nearly all OHRB have strictly requirement for corrinoid to synthesize functional reductive dehalogenases (RDases). Efforts of this work demonstrate that micromolar levels of N_2O inhibit bacterial reductive dechlorination activity and provide an explanation for the stalled reductive dechlorination practices observed at bioremediation sites. The determined inhibitory constant (K_I) values of N_2O for key dechlorination steps (i.e., PCE-to-cDCE, cDCE-to-VC and VC-to-ethene, respectively) therefore can be used for evaluating the bioremediation potential at sites where N_2O accumulations also occur.

Chapter three examines the negative feedback of N_2O on CH_4 production since all known methanogens require the involvement of Co(I) supernucleophile for central metabolism (i.e., methyl transfer) and energy conservation. Evidences presented in this study demonstrated that micromolar levels of N_2O exhibit potent inhibitory effect for major methanogenic pathways, revealing an overlooked feedback loop between N_2O and CH_4, two important greenhouse gases contributing to climate change. Kinetic analyses revealed that CH_4 production from acetate (i.e., acetoclastic methanogenesis pathway), the major methanogenic substrate in nature, was most sensitive to 20 μM levels of N_2O, suggesting a potent negative effect of N_2O for microbial CH_4 production. Results therefore indicate that the inhibitory effect of N_2O for microbial CH_4 production

should not be ignored, particularly at conditions where high content of both bio-accessible C and N exist.

Chapter four explores the metabolic response of dechlorinating microbial communities in presence of N_2O stress. The results showed that N_2O exerts negative impacts on corrinoid metabolism, as well as the metabolome profile of microbial dechlorinating community. Further efforts investigating the reversibility of N_2O toxicity on OHRB showed that through introducing clade I or clade II N_2O reducers, the dechlorination activities of N_2O-inhibited OHRB can be recovered, corroborated the reversibility of N_2O toxicity and suggests a potentially unrecognized detoxification role of the phylogenetically diverse organisms with the capacity of N_2O reduction.

Findings of this dissertation work revealed an overlooked negative feedback of N_2O on corrinoid-dependent methanogenesis and bacterial organohalide respiration. Many microbial processes with large impacts on C and nutrient cycling, as well as contaminant transformation, strictly depend on corrinoid-dependent enzyme systems to catalyze key reactions. Considering that the anthropogenic N input into the environment will continue to intensify on a global scale, N_2O accumulation in watersheds and groundwater resources will increase as a result of disrupted balance between microbial production and consumption. Knowledge about the effects of N_2O on corrinoid-dependent enzyme system that are crucial for biogeochemical cycling must not be ignored in order to obtain system-level understanding of key nutrient cycles in soils,

sediments, watersheds, and aquifers. Therefore, more efforts investigating the impacts of the ever-increasing N_2O will provide valuable information for successful contaminated-site cleanup and climate change prediction and mitigation.

VITA

Yongchao Yin was born in Handan City, Hebei Province, China, on January 8, 1987. He grew up and attended high school at Handan until 2007. He then left home and moved to Ganzhou City, Jiangxi Province to attend college at Jiangxi University of Science and Technology (JXUST). After receiving his bachelor degree of Environmental Engineering at JXUST in 2011, Yongchao then moved to Shenyang beginning to pursue his Master's degree in Environmental Science at Institute of Applied Ecology, Chinese Academy of Sciences (IAE-CAS) under the guidance of Prof. Dr. Yufang Song. During his time at IAE-CAS, Yongchao was deeply influenced by Dr. Yufang Song: her passion towards research and life, her excellent research and teaching skills. Upon completing his Master's degree in 2014, Yongchao came to the US and entered the graduate school in the Department of Microbiology, University of Tennessee, Knoxville to pursue a PhD degree in microbiology under the guidance of Prof. Dr. Frank Loeffler. Yongchao is very grateful for the 5 years education he received from UTK and the life experience he had in Knoxville. Upon completion of his doctoral thesis, Yongchao plans to continue his research career in academia.